



TECHNISCHE
UNIVERSITÄT
WIEN

D I S S E R T A T I O N

Geometric analysis of multi-scale solutions in regularized models of microstructures and touchdown phenomena in MEMS

ausgeführt zum Zwecke der Erlangung des akademischen Grades
eines Doktors der Naturwissenschaften unter der Leitung von

Prof. Dr. Peter Szmolyan

E101 – Institut für Analysis und Scientific Computing, TU Wien

eingereicht an der Technischen Universität Wien
Fakultät für Mathematik und Geoinformation

von

Dott.mag. Annalisa Iuorio

Matrikelnummer: 1329681

Wiedner Hauptstrasse 8-10

1040 Wien

Diese Dissertation haben begutachtet:

1. **Prof. Dr. Alan Lindsay**

Dept. of Applied & Computational Math & Statistics, University of Notre Dame

2. **Prof. Dr. Nikola Popović**

School of Mathematics and Maxwell Institute of Math. Sciences, University of Edinburgh

3. **Prof. Dr. Peter Szmolyan**

Institute for Analysis and Scientific Computing (E101), TU Wien

Wien, am 25.01.2018

Kurzfassung

Die Analyse qualitativer Eigenschaften von nichtlinearen partiellen Differentialgleichungen (PDEs) durch Methoden aus der Theorie dynamischer Systeme ist ein aktives Forschungsgebiet. Ein wichtiges Thema dabei ist die Analyse der Existenz, Stabilität und Verzweigung von speziellen Lösungen, die wesentliche Merkmale der zu untersuchenden PDE enthalten. Insbesondere für PDEs mit singulären Störungen oder Singularitäten hat sich dabei eine Kombination aus Methoden aus der Theorie dynamischer Systeme, Methoden der singulären Störungstheorie und numerischen Berechnungen als sehr effektiv erwiesen.

Dieses Projekt befasst sich mit zwei Problemen dieser Art, die neuartige Multiskalenmerkmale aufweisen. Im ersten Problem untersuchen wir die Euler-Lagrange-Gleichung der Regularisierung eines nichtkonvexen Variationsproblems, das als einfaches mathematisches Modell für Mikrostrukturen in Formgedächtnislegierungen auftritt. Für dieses singular gestörte Hamiltonische System beweisen wir die Existenz einer Klasse von periodischen Lösungen und untersuchen ihre Abhängigkeit von den wesentlichen Parametern durch asymptotische Methoden und numerische Fortsetzung. Das Ziel ist ein besseres Verständnis der Struktur von minimierenden Lösungen und ihres ungewöhnlichen Skalierungsverhaltens. Mittels numerischer Pfadverfolgung werden zusätzlich neue Typen von Lösungen gefunden.

Das zweite Problem betrifft die Asymptotik und Verzweigung von stationären Lösungen eines Modells für mikroelektromechanische Systeme (MEMS). Dieses Modell wurde kürzlich als Regularisierung eines einfacheren Modells vorgeschlagen, von dem bekannt ist, dass es in endlicher Zeit Singularitäten entwickelt. Für dieses Problem wird das numerisch berechnete Verzweigungsdiagramm erklärt, indem die Interaktion des Regularisierungsterms mit der für das Touchdown-Phänomen verantwortlichen Singularität im Detail untersucht wird. Dabei wird die Blow-up-Methode verwendet, um die Dynamik in der Nähe der Singularität

zu analysieren und rigorose Ergebnisse zu erhalten, welche die bereits existierende formale Asymptotik und Numerik beweisen und ergänzen. Ein zentraler Aspekt dabei ist die Untersuchung einer speziellen Sattel-Knoten Verzweigung, deren numerische Untersuchung aufgrund ihres singulären Charakters sehr schwierig ist.

Diese neuartige Erweiterung der Blow-up-Methode zur Analyse von Randwertproblemen und singulären Grenzwerten in Verzweigungsproblemen hat das Potential auch in anderen Zusammenhängen von Nutzen zu sein.

Abstract

The analysis of qualitative properties of nonlinear PDEs by dynamical systems methods is an active area of research. A major issue is the analysis of the existence, stability and bifurcation of special solutions which capture crucial features of the PDE. In particular for PDEs involving singular perturbations or singularities a combination of dynamical systems methods, singular perturbation methods and numerical computation has proven to be very effective.

This project is concerned with two problems of this kind exhibiting novel multi-scale features. In the first problem we study the Euler-Lagrange equation of the regularization of a non-convex variational problem arising as a toy model for microstructures in shape memory alloys. For this singularly perturbed Hamiltonian system we prove the existence of a class of periodic solutions and study their dependence on the main parameters by asymptotic methods and numerical continuation. The goal is to obtain a better understanding of the structure of minimizers and their unusual scaling behavior. Novel solutions via numerical path following are also discovered.

The second problem is concerned with the asymptotics and bifurcations of steady state solutions of a model for Micro-Electro Mechanical Systems (MEMS). This model has recently been proposed as a regularization of a more basic model, that is known to develop singularities in finite time.

We analyze the structure of steady state solutions close to touchdown and their bifurcation diagram as the regularization parameter tends to zero. By means of geometric singular perturbation theory and blow-up techniques, we give a rigorous analysis of the bifurcation curve and its singular limit. The numerically computed bifurcation diagram is explained by resolving the interaction of the regularizing term with the main singularity leading to

the touchdown phenomenon. In particular, we use the blow-up method to analyze the dynamics in proximity of the singularity and obtain rigorous results complementing existing formal asymptotics and numerics. An important part of the analysis deals with a special saddle-node bifurcation point which, due to its singular nature, is very hard to obtain even numerically.

This novel extension of the blow-up method to the analysis of boundary value problems and singular limits in bifurcation diagrams is expected to be useful in other contexts as well.

Acknowledgements

At the end of this experience, when the stress of the final steps is over and you start summing up everything from the beginning, you realize how lucky you are having had amazing people by your side and how crucial they have been in the realization of this project. Each of them deserves a special acknowledgement.

First of all, I would like to thank my supervisor Peter Szmolyan, for leading me in the discovery of the beautiful and yet challenging world of slow-fast systems and for being there for me every step of the way (especially in moments of distress!) Thank you for your patience and support, and thank you for pointing my attention towards problems with such rich dynamics. You have been a great mentor.

Then, I would like to thank my “inofficial” co-advisors Christian Kühn and Nikola Popović. Christian, your book was the first taste of multiple time scale systems I had, and it was the best I could have possibly had. Our discussions and our work together have always been extremely stimulating, and I’m happy we kept our collaboration even after your successful transfer. Nikola, you made my stay in Edinburgh the best I could have possibly imagined. You have been and still are a great teacher and friend to me. Your expertise and support helped me through the good (mostly) and the bad (just a few) times :)

A special thanks goes to Ansgar Jüngel and all the faculty of the doctoral school, for giving me the possibility to be the coordinator of the DK. It is a true honour to be part of it.

Thanks to the secretaries and all the scientific staff for their support and kindness. You make every problem solvable.

I would also like to acknowledge the support of TU Wien through the Austrian Science Fund (FWF) under grant W1245.

And now, the colleagues, with whom I’ve shared this experience from the beginning. First

of all, thanks to my colleague and friend Kirian. You have been the best officemate I could have hoped for, and way more than that. Thank you for all the chats, the events organized together, the “TUesday salads”, simply for making every day at the university wonderful. I’ll miss our office so much.

Thanks to Dominik and Angelika for the great time spent together, especially our “jour fixe” :) Thank you for your friendship and for letting me have a closer look at the “austrian lifestyle”. You are one of the reasons why I liked being here so much :)

Thank you to the sixth floor, Tobias, Stefan, Bea, Giacomo, Franz, and Ilona for sharing our everyday life and making even the hard days lighter :) Special thanks to Frau Schweigler for helping me with any little bureaucratic issue in the best, fastest, kindest way, and to Prof. Arnold, for making me feel part of his workgroup too :)

Thanks to my precious “Mädls” Karolina, Polina, Anita and Lara. We are quite different, but our differences turned out to be an inspiration for all of us. You made me go beyond my limits and have always been there for me. I’m truly happy to have friends like you :)

Thank you to all the new DK/SFB group for having brought new life (and challenges!) to ours. Special thanks to Matteo for the help and support without which all of this would be way harder! I really couldn’t have been luckier :)

Thank you to all the incredible people I met during my traveling, in particular Martina, Stefano, Frits and all the Edinburgh group. Research has been much more fun and inspiring with you around, and you really made me feel at home even when I was far away from it.

And now the family, the one I was lucky enough to have and the one I was lucky enough to build with time.

Thanks to my parents, for being much stronger and braver than I could have possibly imagined. You overcame all the difficulties and turned them into chances to do things you’d never thought to do. You supported me and helped me always, no matter the distance. You are, and always will be, my rocks.

Thanks to my lifetime friends, in particular to Valentina, Giuliana, Raf and Chiara for our friendship that distance simply made stronger. Thank you for our Skype calls, our laughs and our never ending conversations. I wouldn’t be who I am without you. Special thanks to Filippo, for pushing me out of my comfort zone. This adventure would have probably

never started without you. Thank you for making me take the first real jump of my life. Finally, thank you Stefano, for providing me a “cane” to help me go faster and steadier, (metaphorically and sometimes literally!), whenever I needed. Thank you for dancing through life with me. You make me happy every single day.

As strange as this might seem, my last thanks goes to Vienna, Edinburgh, and Naples, for always making me feel I belong. Because of you my heart might be a bit spread around the world, but in each of you I found another piece of myself.

Contents

1	Introduction	1
1.1	Fast-Slow Systems	1
1.1.1	Terminology	1
1.1.2	Fenichel Theory	2
1.1.3	Exchange Lemma	5
1.2	Blow-up Method	9
1.4	Thesis Overview	13
1.4.1	Structure	13
1.4.2	Main Results	14
2	Geometry and numerical continuation of multiscale orbits in a nonconvex variational problem	15
2.1	Introduction	15
2.2	The Euler-Lagrange equation as a fast-slow system	18
2.2.1	The Reduced Problem	21
2.2.2	The Layer Problem	23
2.2.3	Singular Fast-Slow Periodic Orbits	25
2.3	Numerical Continuation	29
2.3.1	Construction of the starting orbit	30
2.3.2	Continuation in μ	32
2.3.3	Continuation in ε	33
2.3.4	Period scaling	35
2.4	Conclusion & Outlook	38

3 Singular perturbation analysis of a regularized MEMS model	42
3.1 Introduction	42
3.2 Dynamical Systems Formulation	48
3.3 Geometric Desingularization (“Blow-Up”)	54
3.3.1 Dynamics in chart K_1	57
3.3.2 Dynamics in chart K_2	58
3.4 Analysis of the Bifurcation Diagram	58
3.4.1 Region \mathcal{R}_1	64
3.4.2 Region \mathcal{R}_2	77
3.4.3 Region \mathcal{R}_3	87
3.5 Logarithmic switchbacks	95
3.5.1 Dynamics in chart K_1	96
3.5.2 Dynamics in chart K_2	101
3.6 Discussion and Outlook	103
Bibliography	105
Curriculum Vitae	113

1 Introduction

1.1 Fast-Slow Systems

Most of the results presented in this thesis rely on the geometric theory of multiple time scale dynamical systems. These systems are characterized by the fact that the dynamics occur on several (usually two) time-scales, *fast* and *slow*; hence their definition as “*fast-slow systems*”. They play a crucial role for example in asymptotic analysis, in particular in the field of matched asymptotic expansions. In the last few decades, geometric techniques to analyze these systems have developed increasingly, leading to Geometric Singular Perturbation Theory (GSPT) [35]. In the following, we give a more precise definition of their general structure and show how GSPT leads to the analysis of their solutions.

1.1.1 Terminology

A general formulation of fast-slow systems can be given as follows.

Definition 1.1.1. A (m, n) -**fast-slow system** is a system of ordinary differential equations of the form

$$\begin{aligned}\varepsilon \dot{x} &= f(x, y, \eta, \varepsilon), \\ \dot{y} &= g(x, y, \eta, \varepsilon),\end{aligned}\tag{1.1}$$

where $\dot{} = \frac{d}{dt}$, $f : \mathbb{R}^m \times \mathbb{R}^n \times \mathbb{R}^p \times \mathbb{R} \rightarrow \mathbb{R}^m$, $g : \mathbb{R}^m \times \mathbb{R}^n \times \mathbb{R}^p \times \mathbb{R} \rightarrow \mathbb{R}^n$, $\eta \in \mathbb{R}^p$ are system parameters and $0 < \varepsilon \ll 1$. Moreover, $x \in \mathbb{R}^m$ are defined as the **fast variables**, while $y \in \mathbb{R}^n$ are defined as the **slow variables**.

Introducing $t = \tau/\varepsilon$, $' = \frac{d}{dt}$ leads to the equivalent formulation

$$\begin{aligned}x' &= f(x, y, \eta, \varepsilon), \\y' &= \varepsilon g(x, y, \eta, \varepsilon).\end{aligned}\tag{1.2}$$

As for the time variables, t and τ are referred to as **fast time scale** and **slow time scale**, respectively.

A key role is played by a small parameter $0 < \varepsilon \ll 1$, involved in the equations as well as in the time rescaling. Considering in fact the limit $\varepsilon \rightarrow 0$ in (1.1) yields

$$\begin{aligned}0 &= f(x, y, \eta, 0), \\ \dot{y} &= g(x, y, \eta, 0),\end{aligned}\tag{1.3}$$

i.e., a differential-algebraic equation (DAE) called **slow subsystem** or equivalently **reduced problem**. This represents the flow of the slow variables y (“**slow flow**”) on the geometric object (called **critical manifold**) determined by the algebraic constraint $0 = f(x, y, \eta, 0)$.

Letting $\varepsilon \rightarrow 0$ in (1.2) leads instead to

$$\begin{aligned}x' &= f(x, y, \eta, 0), \\y' &= 0,\end{aligned}\tag{1.4}$$

called **fast subsystem** or **layer problem**. This corresponds to the flow of the fast variables x (“**fast flow**”) on “layers” of constant y -values.

The idea on which Geometric Singular Perturbation Theory is based is the following: investigating the reduced and the layer problem, a singular orbit for the full problem can be constructed. Important tools such as Fenichel Theory [22] and the Exchange Lemmas [71, 72] can then guarantee, under some conditions, the persistence of these results for $0 < \varepsilon \ll 1$. In the following, we examine them in more detail.

1.1.2 Fenichel Theory

In its broadest sense, Fenichel’s theory includes a variety of results regarding the perturbation of normally hyperbolic invariant manifolds. As our main focus relies on fast-slow

systems, however, we are going to focus our attention on its application in this field. The main theorem we are going to present is in fact concerned with perturbations of the critical manifold arising in the study of the reduced problem.

We briefly recall some basic definitions and assumptions:

- The critical manifold C_0 is defined as (cf. (1.3))

$$C_0 = \{(x, y) \in \mathbb{R}^{m+n} : f(x, y, \eta, 0) = 0\}. \quad (1.5)$$

- A subset $S \subset C_0$ is called **normally hyperbolic** if the $m \times m$ matrix $(D_x f)(p, \eta, 0)$ of first partial derivatives with respect to the fast variables has no eigenvalues with zero real part for all $p \in S$, or equivalently, if and only if for each $p = (x^*, y^*) \in S$ we have that x^* is a hyperbolic equilibrium point of $x' = f(x, y^*, \eta, 0)$.
- The minimum requirement for S is compactness; usually we will deal with smooth manifolds.
- A normally hyperbolic subset $S \subset C_0$ is called **attracting** if all eigenvalues of $(D_x f)(p, 0)$ have negative real part for $p \in S$; similarly, S is called **repelling** if all eigenvalues have positive real part. If S is normally hyperbolic and neither attracting nor repelling, it is said to be of **saddle-type**.
- The **Hausdorff distance** between two nonempty sets $V, W \subset \mathbb{R}^{m+n}$ is defined as follows:

$$d_H(V, W) := \max \left\{ \sup_{v \in V} \inf_{w \in W} \|v - w\|, \sup_{w \in W} \inf_{v \in V} \|v - w\| \right\}.$$

The main result of GSPT is the following:

Theorem 1.1.2 (Fenichel's theorem [22]). *Suppose $S = S_0$ is a compact normally hyperbolic submanifold (possibly with boundary) of the critical manifold C_0 of (1.1) and that $f, g \in C^r (r < \infty)$. Then for $\varepsilon > 0$ sufficiently small, the following hold:*

- (F1) *There exists a locally invariant manifold S_ε diffeomorphic to S_0 . Local invariance means that trajectories can enter or leave S_ε only through its boundaries.*
- (F2) *S_ε has Hausdorff distance $\mathcal{O}(\varepsilon)$ (as $\varepsilon \rightarrow 0$) from S_0 .*

(F3) The flow on S_ε converges to the slow flow as $\varepsilon \rightarrow 0$.

(F4) S_ε is C^r -smooth.

(F5) S_ε is hyperbolic and has the same stability properties with respect to the fast variables as S_0 (attracting, repelling, or saddle-type).

(F6) S_ε is usually not unique. In regions that remain at a fixed distance from ∂S_ε , all manifolds satisfying (F1)-(F5) lie at a Hausdorff distance $\mathcal{O}(e^{-K/\varepsilon})$ from each other for some $K > 0, K = \mathcal{O}(1)$.

Note that all asymptotic notation refers to $\varepsilon \rightarrow 0$. Similar conclusions as for S_0 hold locally for its stable and unstable manifolds:

$$W_{\text{loc}}^s(S_0) = \bigcup_{p \in S_0} W_{\text{loc}}^s(p), \quad W_{\text{loc}}^u(S_0) = \bigcup_{p \in S_0} W_{\text{loc}}^u(p),$$

where we view points $p \in S_0$ as equilibria of the fast subsystem. These manifolds also persist for $\varepsilon > 0$ sufficiently small: there exist local stable and unstable manifolds $W_{\text{loc}}^s(S_\varepsilon)$ and $W_{\text{loc}}^u(S_\varepsilon)$, respectively, for which conclusions (F1)-(F6) hold if we replace S_ε and S_0 by $W_{\text{loc}}^s(S_\varepsilon)$ and $W_{\text{loc}}^s(S_0)$ (or similarly by $W_{\text{loc}}^u(S_\varepsilon)$ and $W_{\text{loc}}^u(S_0)$).

Theorem 1.1.2 is at the core of Geometric Singular Perturbation Theory, which however comprises also another large variety of geometric methods. It is often known also as Tikhonov theorem [74]; he proved in addition that every solution starting sufficiently close to a compact attracting normally hyperbolic submanifold $S \subset C_0$ approaches S in a slow time $\mathcal{O}(\varepsilon |\log \varepsilon|)$ and then stays $\mathcal{O}(\varepsilon)$ -close to S . The manifold S_ε cited in Theorem 1.1.2 is called a **slow manifold**; often it is referred to also as “the” slow manifold C_ε as, although formally incorrect, all possible choices lie $\mathcal{O}(e^{-K/\varepsilon})$ -close, hence making it irrelevant which choice is made.

It is finally important to indicate that the dynamics of a fast-slow system near a critical manifold can be significantly simplified through a certain coordinate change:

Theorem 1.1.3 (Fenichel Normal Form [22]). *Suppose the origin $0 \in C$ is a normally hyperbolic point with m_s stable and m_u unstable fast directions. Then there exists a smooth*

invertible coordinate change $(x, y) \mapsto (a, b, v) \in \mathbb{R}^{m_s+m_u+n}$ so that a fast-slow system (1.2) can be written as:

$$\begin{aligned} a' &= \Lambda(a, b, v, \varepsilon)a, \\ b' &= \Gamma(a, b, v, \varepsilon)b, \\ v' &= \varepsilon(m(v, \varepsilon) + H(a, b, v, \varepsilon)ab), \end{aligned} \tag{1.6}$$

where Λ, Γ are matrix-valued functions and H is bilinear and given in coordinates by

$$H_i(a, b, v, \varepsilon)ab = \sum_{r=1}^{m_s} \sum_{s=1}^{m_u} H_{irs} a_r b_s. \tag{1.7}$$

1.1.3 Exchange Lemma

In the following, we are often going to face the issue of tracking invariant manifolds in phase space. A crucial tool to perform this task is the Exchange Lemma, initially proved by Jones and Kopell [36]: roughly speaking, it guarantees that some parts of a manifold which enters a neighbourhood of the slow manifold by intersecting its stable foliation will exit along its unstable foliation after the slow drift. This tool is extremely useful in many situations, such as the persistence of periodic orbits constructed with both fast and slow pieces in the singular limit $\varepsilon = 0$ after ε is activated. Suppose for example (as we will see in Chapter 2) that a periodic orbit in the singular limit is found by connecting two slow pieces with two heteroclinic orbits of the fast subsystem. As the heteroclinic connections in the singular limit occur by means of a transversal intersection between the stable and unstable manifolds of the slow pieces, the persistence of the periodic orbit for $0 < \varepsilon \ll 1$ is guaranteed not only when the transversality condition is preserved (result guaranteed by Fenichel's theorem 1.1.2), but also when the fast flow approaching the slow manifold close to its stable foliation leaves it along its unstable foliation. This is where the Exchange Lemma plays its fundamental role. Its importance applies however not only to periodic orbits, but also to more general scenarios, as we see in Chapter 3. There, we obtain a global transversal intersection as follows: a boundary manifold is proved to intersect the stable foliation of the slow manifold transversely. As the flow leaves again the slow manifold close to its unstable foliation thanks to the Exchange Lemma, and as the unstable foliation

intersects the other boundary manifold again transversely, we have an overall transverse intersection.

We illustrate the main statements of the Exchange Lemmas in the following. To this aim, we first need to recall some important concepts.

Definition 1.1.4. Two manifolds M_1 and M_2 are **transversal** (or **intersect transversely**) in \mathbb{R}^N if the tangent spaces $T_p M_1$ and $T_p M_2$ span $T_p \mathbb{R}^N \cong \mathbb{R}^N$ at each point $p \in M_1 \cap M_2$.

The general framework we consider here is the fast-slow system

$$\begin{aligned}\varepsilon \dot{x} &= f(x, y, \varepsilon), \\ \dot{y} &= g(x, y, \varepsilon),\end{aligned}\tag{1.8}$$

where we included the eventual parameters $\eta \in \mathbb{R}^p$ of the system in the slow variables (it suffices to include the equations $\dot{\eta} = 0$ and relabel the variables to suitably-indexed y coordinates). Assume S_0 is a compact normally hyperbolic submanifold of the critical manifold C_0 . According to Theorem 1.1.3, we can apply a change of variables to convert System (1.8) near S_0 into Fenichel normal form:

$$\begin{aligned}a' &= \Lambda(a, b, y, \varepsilon)a, \\ b' &= \Gamma(a, b, y, \varepsilon)b, \\ y' &= \varepsilon(h(y, \varepsilon) + H(a, b, y, \varepsilon)(a, b)),\end{aligned}\tag{1.9}$$

with $a \in \mathbb{R}^k$, $b \in \mathbb{R}^l$, $y \in \mathbb{R}^n$ and $k + l = m$; H is a bilinear-form valued function which can be explicitly written as

$$y'_i = \varepsilon \left(h_i(y, \varepsilon) + \sum_{u=1}^k \sum_{s=1}^l H_{ius} a_u b_s \right);$$

Λ and Γ are matrix-valued functions defined by separating the fast unstable and stable directions. The manifold S_0 is now represented by $\{a = 0, b = 0\}$ and, as it is normally hyperbolic by assumption, there exist $\lambda_0 > 0$, $\gamma_0 < 0$ such that for any λ_i eigenvalue of $\Lambda(0, 0, y, 0)$ or any γ_i eigenvalue of $\Gamma(0, 0, y, 0)$ the following holds:

$$\operatorname{Re} \lambda_i > \lambda_0 > 0, \quad \operatorname{Re} \gamma_i < \gamma_0 < 0$$

in a region

$$\mathcal{B} = \{(a, b, y) : \|a\| < \delta, \|b\| < \delta, y \text{ in a compact region}\} \quad (1.10)$$

with δ sufficiently small. For ε positive and small Equation (1.9) still applies; $\lambda_\varepsilon > 0$ and $\gamma_\varepsilon < 0$ correspond now to the weak unstable and weak stable eigenvalues near S_ε respectively. The stable and unstable manifolds of S_ε are hence given by

$$W^s(S_\varepsilon) = \{a = 0\}, \quad W^u(S_\varepsilon) = \{b = 0\}, \quad (1.11)$$

respectively. Equation (1.9) can be furtherly modified with the non-restrictive assumption that the slow flow is pointing in the y_1 -direction¹:

$$\begin{aligned} a' &= \Lambda(a, b, y, \varepsilon)a, \\ b' &= \Gamma(a, b, y, \varepsilon)b, \\ y' &= \varepsilon(U + H(a, b, y, \varepsilon)(a, b)), \end{aligned} \quad (1.12)$$

with $U = (1, 0, \dots, 0)^T$.

We introduce now the invariant manifold M we aim to track: we assume it is $(k + 1)$ -dimensional for sake of simplicity, but the following results can be extended to the general case as well. Suppose M intersects the boundary $\{b = \delta\}$ of region \mathcal{B} at some point q ; if q is sufficiently close to the stable manifold $W^s(S_\varepsilon)$, a trajectory starting at q will stay close to S_ε for a time $\mathcal{O}(1/\varepsilon)$ with respect to the fast time scale t . In particular, the following lemma provides estimates on the fast coordinates (a, b) :

Lemma 1.1.5 ([46]). *Let us consider System (1.12). There exist constants $c_a, c_b, K > 0$ such that for $s \leq t$ the following results hold:*

$$(R1) \quad \|b(t)\| \leq c_b \|b(s)\| e^{\gamma_0(t-s)}$$

$$(R2) \quad \|a(t)\| \leq c_a \|a(s)\| e^{\lambda_0(t-s)}$$

$$(R3) \quad \left\| \int_s^t a(\sigma) d\sigma \right\| \leq K \quad (\text{independent of } \varepsilon, s, t)$$

as long as a trajectory remains in \mathcal{B} .

¹This hypothesis applies particularly to the contexts we deal with later, as we often have $n = 1$.

To follow a trajectory inside \mathcal{B} , we use the following observation: as M is invariant, trajectories that start at $q \in M \cap \{\|b\| = \delta\}$ have to remain inside M . Therefore, a neighbourhood of q in M can be followed under the flow in (1.12) as shown by the C^0 -Exchange Lemma:

Theorem 1.1.6 (C^0 -Exchange Lemma [36, 46]). *Let us consider System (1.12). Let M be a $(k + 1)$ -dimensional invariant manifold, $\bar{q} \in M \cap \{\|a\| = \delta\}$ be the exit point of a trajectory starting at $q \in M \cap \{\|b\| = \delta\}$ that spends a time t that is $\mathcal{O}(1/\varepsilon)$ in \mathcal{B} . Let V be a neighborhood of q in M . If V is sufficiently small then the image of V under the time t map is close to*

$$\{\|a\| = \delta, y_i - y_i(0) = 0, i > 1\}$$

in the C^0 -norm where $y_i(0)$ denotes the y -coordinates of q .

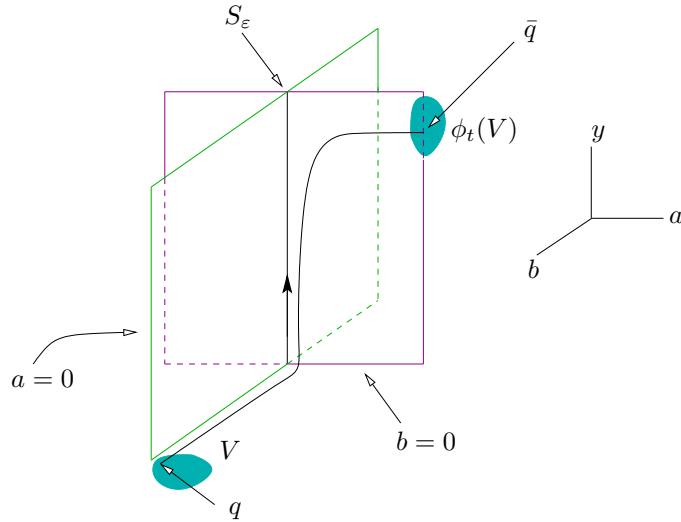


Figure 1.1: Schematic representation of the situation described in the C^0 -Exchange Lemma 1.1.6: $\phi_t(V)$ (light cyan) indicates the image of region V (light cyan) near the exit point \bar{q} , which is very close to the unstable manifold $W^u(S_\varepsilon) = \{\|b\| = 0\}$ (magenta). All coordinates y_i with $i > 1$ have been here suppressed.

If we aim to use the C^0 -Exchange Lemma to prove the persistence of a transversality condition between two manifolds for $\varepsilon > 0$ small, however, we soon realize that this is not

possible: we have in fact no information about the part of the tangent spaces of M in the center directions, as every trajectory exits near \bar{q} almost tangent to the unstable manifold $W^u(S_\varepsilon)$. That's where the C^0 label comes from: Theorem 1.1.6 gives accurate information about the location of the manifold M itself, but does not provide enough details about its tangent spaces. This “ C^1 ”-information is instead given by the following:

Theorem 1.1.7 (C^1 -Exchange Lemma [36, 46]). *Let us consider System (1.12). Let M be a $(k + 1)$ -dimensional invariant manifold. Assume $M \cap \{\|b\| = \delta\}$ intersects $\{a = 0\}$ transversely. Let $\bar{q} \in M \cap \{\|a\| = \delta\}$ be the exit point of a trajectory starting at $q \in M \cap \{\|b\| = \delta\}$ that spends a time $t = \mathcal{O}(1/\varepsilon)$ in \mathcal{B} . Let V be a neighborhood of q in M . The image of V under the time t map is close in the C^1 -norm to*

$$\{\|a\| = \delta, y_i - y_i(0) = 0, i > 1\},$$

where $y_i(0)$ denotes the y -coordinates of q . In particular M is C^1 -close to $\{\|a\| = \delta, y_i - y_i(0) = 0, i > 1\}$ near \bar{q} .

1.2 Blow-up Method

Another powerful tool we are going to use is the blow-up method. This technique was introduced to singular perturbation problems by Dumortier and Roussarie [20, 21]; further details on weighted blow-ups can be found in [11, 61, 10, 9]. Other important results concerning the blow-up analysis of the fold point have been reached by Krupa, Szmolyan, and van Gils [44, 45, 80]. Interesting overviews of the method are available in [4, 46]. The method allows us to analyze the dynamics of a system close to degenerate equilibria by constructing a vector field with hyperbolic singularities out of the original one. A degenerate equilibrium is an equilibrium with a nilpotent linearization, *i.e.*, with a zero eigenvalue of multiplicity greater than two. Such degenerate equilibria arise if hyperbolic directions are split off by means of a center manifold reduction. They also appear as points of critical manifolds where normal hyperbolicity is lost.

The idea behind this method is to “blow” the degenerate equilibrium “up” to a higher dimensional structure and then study the dynamics in blown-up space. This procedure

can be repeated as long as non-hyperbolic points are present; Dumortier [21] has shown that, in the case of planar systems, the number of blow-ups necessary to desingularize a non-hyperbolic point is finite if the vector field satisfies the Lojasiewicz inequality.

We focus our attention here on the **quasihomogeneous blow-up**, which we use in the second part of the thesis. For more background on other types of blow-up, we refer to [46, 20].

Definition 1.2.1. Consider a C^∞ -vector field F on \mathbb{R}^n . Without loss of generality, let us assume that the origin is a degenerate equilibrium point ($F(0) = 0$). Let $a_i \in \mathbb{N}$ for $i = 1, \dots, n$. The **quasihomogeneous blow-up** φ with weights a_1, \dots, a_n corresponds to the coordinate transformation:

$$\begin{aligned} \varphi: S^{n-1} \times I &\longrightarrow \mathbb{R}^n, \\ (\bar{z}_1, \dots, \bar{z}_n, r) &\longmapsto (r^{a_1} \bar{z}_1, \dots, r^{a_n} \bar{z}_n), \end{aligned} \tag{1.13}$$

where I is an interval in \mathbb{R} with $0 \in I$ and $\sum_{k=1}^n \bar{z}_k^2 = 1$. The **quasihomogeneous blow-up** \hat{F} of the vector field F is defined by

$$\hat{F}(\bar{z}_1, \dots, \bar{z}_n, r) = (D\varphi_{(\bar{z}_1, \dots, \bar{z}_n, r)}^{-1} \circ F \circ \varphi)(\bar{z}_1, \dots, \bar{z}_n, r) \tag{1.14}$$

for $r \neq 0$ and by the continuous extension of (1.14) to $r = 0$. From a geometric viewpoint, the quasihomogeneous blow-up can be interpreted as follows: the nonhyperbolic point is replaced by the sphere in blown-up space. $\varphi^{-1}(0) = S^{n-1} \times \{0\}$ is also known as the *singular locus*. Since \hat{F} vanishes for $r = 0$, it is necessary to divide out a suitable factor of r^k (*i.e.*, suitably rescale time) to obtain a nontrivial flow on the sphere S^{n-1} . We define the **(rescaled) quasihomogeneous blow-up** by $\bar{F} = \frac{1}{r^k} \hat{F}$.

The weights a_1, \dots, a_n in the blow-up transformation have to be chosen such that dividing out such a factor r^k is *i*) possible and *ii*) leads to a flow on the sphere which captures the essential dynamics. The dynamics in blown-up space can be conveniently studied in charts $K_i, i = 1, \dots, n$, where one of the blow-up variables $\bar{\cdot}$ is kept fixed and equal to 1. A new coordinate system is then introduced on each chart through local maps μ_i such that $\varphi = K_i \circ \mu_i$. For sake of clarity, we introduce the normal form of a fold in planar fast-slow

systems as an example. For the analysis of the generic fold in planar fast-slow systems we refer to Krupa and Szmolyan [44, 45].

Example 1.3 ([46]). Let us consider the following fast-slow system:

$$\begin{aligned}x' &= x^2 - y, \\y' &= -\varepsilon, \\ \varepsilon' &= 0,\end{aligned}\tag{1.15}$$

which has been extended to a three-dimensional system by adding the trivial equation for ε . The origin is a degenerate equilibrium of this system. The vector field defined by (1.15) will be denoted by F . Introducing the space $B_0 := S^2 \times [0, r_0]$ for some $r_0 > 0$, we can define the blow-up map $\varphi : B_0 \rightarrow \mathbb{R}^3$ as the map which induces a vector field \bar{F} by $\varphi_*(\bar{F}) = F$. Denoting the coordinates on S^2 with $(\bar{x}, \bar{y}, \bar{\varepsilon})$ and the one on $[0, r_0]$ by \bar{r} and applying Definition 1.2.1, the quasihomogeneous blow-up in (1.13) corresponds to

$$\varphi(\bar{x}, \bar{y}, \bar{\varepsilon}, \bar{r}) = (\bar{r}^{a_1} \bar{x}, \bar{r}^{a_2} \bar{y}, \bar{r}^{a_3} \bar{\varepsilon}),\tag{1.16}$$

where the coefficients (a_1, a_2, a_3) need to be determined. Typically the weights can be determined efficiently if one considers the ε -dependent rescaling of x and y which is obtained by setting $\bar{\varepsilon} = 1$ in (1.16). This gives

$$x = r^{a_1} \tilde{x}, \quad y = r^{a_2} \tilde{y}, \quad \varepsilon = r^{a_3}.$$

Plugging this into (1.15) gives

$$\begin{aligned}r^{a_1} \tilde{x}' &= r^{2a_1} \tilde{x}^2 - r^{a_2} \tilde{y}, \\r^{a_2} \tilde{y}' &= r^{a_3}.\end{aligned}$$

It is easy to see that the choice

$$a_1 = 1, \quad a_2 = 2, \quad a_3 = 3$$

leaves a common factor r on the right-hand side, which can then be divided out. Hence the blow-up transformation has the form

$$\varphi(\bar{x}, \bar{y}, \bar{\varepsilon}, \bar{r}) := (\bar{r} \bar{x}, \bar{r}^2 \bar{y}, \bar{r}^3 \bar{\varepsilon}).\tag{1.17}$$

The blow-ups induced from the charts K_i and the blow-up φ are then

$$\text{for } K_1 (\bar{y} = 1) : \quad x = r_1 x_1, \quad y = r_1^2, \quad \varepsilon = r_1^3 \varepsilon_1, \quad (1.18a)$$

$$\text{for } K_2 (\bar{\varepsilon} = 1) : \quad x = r_2 x_2, \quad y = r_2^2 y_2, \quad \varepsilon = r_2^3, \quad (1.18b)$$

$$\text{for } K_3 (\bar{x} = 1) : \quad x = r_3, \quad y = r_3^2 y_3, \quad \varepsilon = r_3^3 \varepsilon_3. \quad (1.18c)$$

A schematic representation can be found in Figure 1.2.

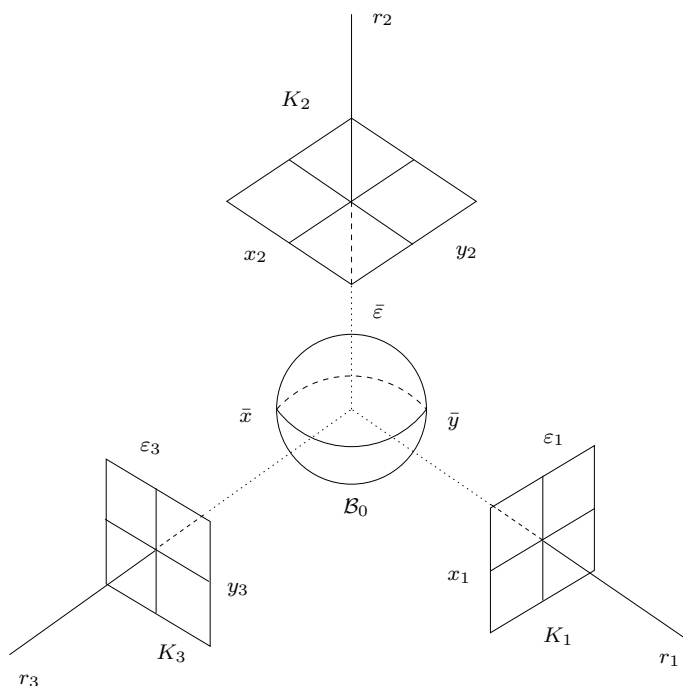


Figure 1.2: Homogeneous blow-up of a nonhyperbolic point in \mathbb{R}^3 ; charts $K_i, i = 1, \dots, n$ are also displayed.

For illustration, we work out the equations in chart K_2 to show how System (1.15) can be desingularized by dividing out a power of r . Rewriting Equations (1.15) by means of the coordinate transformation in (1.18b) we have

$$\begin{aligned} x_2' &= r_2(x_2^2 - y_2), \\ y_2' &= -r_2, \\ r_2' &= 0. \end{aligned} \quad (1.19)$$

Dividing out the common factor r_2 from the right-hand sides we finally get the desingularized system:

$$\begin{aligned}x_2' &= x_2^2 - y_2, \\y_2' &= -1, \\r_2' &= 0,\end{aligned}\tag{1.20}$$

which plays a key role in the analysis of the generic planar singularly perturbed fold point.

To summarize, the main steps to follow when analyzing the dynamics close to a degenerate point with the blow-up method are the following:

1. Determine a suitable map φ to desingularize the degenerate point, *i.e.*, find the “right” weights in (1.13);
2. Use suitable charts to express the blow-up in local coordinates;
3. Investigate the local dynamics in the charts and their overlap by using the transition maps κ_{ij} ;
4. Combine the results from the charts to analyze the full dynamics in the blown-up space;
5. “Blow-down” to the original phase space via the blow-up map φ in (1.13).

The third and the fourth step can be carried out only if one obtains a desingularized problem on the sphere, which both captures the essential behaviour and can be analysed. In simple scenarios, finding the weights is often straightforward (as we have seen in Example 1.3), but in general this is a highly nontrivial problem.

1.4 Thesis Overview

1.4.1 Structure

The results presented in this Thesis are concerned with the two main projects I have been working on during my Ph.D. Though the main definitions are presented in this introductory Section, some basic definitions might be repeated throughout the text, as both Chapters 2

and 3 are meant as independent readings; we hope, however, the reader might consider this mostly helpful.

1.4.2 Main Results

Here we present the main results of the thesis:

1. Chapter 2 is devoted to the analysis of a nonconvex variational problem by means of GSPT. We prove the existence of a class of periodic solutions and study their dependence on the main parameters by asymptotic methods and numerical continuation. In particular, the Hamiltonian structure of the fast-slow system corresponding to the Euler-Lagrange equation associated to the minimization functional allows us to prove existence of periodic solutions on hypersurfaces with fixed Hamiltonian value. Numerical continuation with respect to the main system parameters is then carried out with AUTO [18], after having constructed a starting orbit with the Slow-Manifolds-of-Saddle-Type (SMST) algorithm [27]. The results confirm the analytical predictions and open up new possible scenarios.
2. Chapter 3 is focused on the analysis of a model arising in Micro-Electro-Mechanical-Systems (MEMS). In particular, we investigate the multi-scale structure of the steady-state solutions to a second order PDE and perform a detailed asymptotic resolution of the structure of the corresponding bifurcation diagram. Rewriting the boundary value problem in a dynamical system formulation and applying a combination of GSPT and blow-up methods allows us to explain the numerically computed bifurcation diagrams by resolving the interaction of a regularizing term with the main singularity leading to the touchdown phenomenon. The existence of a new bifurcation branch, observed in the original model formulation, is here explained and resolved both in the singular limit $\varepsilon = 0$ and for ε positive and sufficiently small. This extended use of the blow-up method also leads to the analytical computation of a the saddle-node bifurcation point, so far accessible only numerically.

2 Geometry and numerical continuation of multiscale orbits in a nonconvex variational problem

2.1 Introduction

The minimization problem we consider is to find

$$\min_{u \in U} \left\{ \mathcal{I}^\varepsilon(u) := \int_0^1 (\varepsilon^2 u_{XX}^2 + W(u_X) + u^2) \, dX \right\}, \quad (2.1)$$

where U is a space containing all sufficiently regular functions $u : [0, 1] \rightarrow \mathbb{R}$ of the spatial variable $X \in [0, 1]$, $0 < \varepsilon \ll 1$ is a small parameter, $u_X = \frac{\partial u}{\partial X}$, $u_{XX} = \frac{\partial^2 u}{\partial X^2}$, and the function W is a symmetric, double well potential; in particular, here W is chosen as

$$W(u_X) = \frac{1}{4}(u_X^2 - 1)^2. \quad (2.2)$$

This model arises in the context of coherent solid-solid phase transformation to describe the occurrence of simple laminate microstructures in one-space dimension. Simple laminates are defined as particular structures where two phases of the same material (e.g., austenite/martensite) simultaneously appear in an alternating pattern [59]. This situation is shown schematically in Figure 2.1(a). These and related structures have been intensively studied both in the context of geometrically linear elasticity [38, 39, 69] and in the one of fully nonlinear elasticity [1, 2, 5, 6, 8, 19, 62, 65, 75, 76]. A comparison between these two approaches is given by Bhattacharya [7]. We focus here on the one-dimensional case starting from the work of Müller [58], but a 2D approach has also been proposed [40, 25, 33]. An alternative choice of the functional W which sensibly simplifies energy calculations for

equilibria has been recently adopted by Yip [83]. The same functional with more general boundary conditions has been treated by Vainchtein et al [79]. In all these cases, very significant theoretical and experimental advances have been reached. Nevertheless, many interesting features concerning the asymptotics and dynamics of these problems can still be explored.

We start from the one-dimensional model (2.1)-(2.2) analyzed by Müller and introduce a different approach based on geometric singular perturbation theory [35, 46] which allows us to better understand the critical points of the functional \mathcal{I}^ε and to obtain an alternative method eventually able to handle more general functionals.

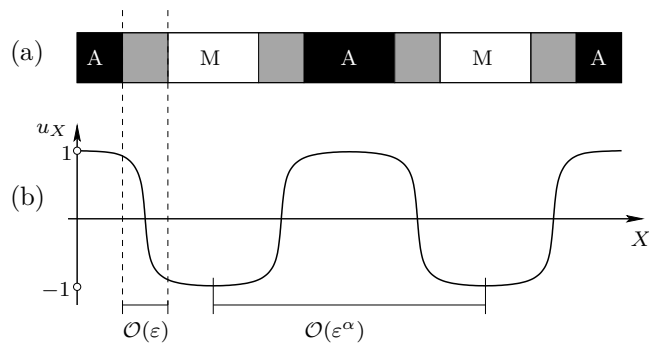


Figure 2.1: Schematic representation of simple laminates microstructures as periodic solutions. (a) Microstructures in one space dimension: austenite (A) and martensite (M) alternate, while the transition area is shown in gray. (b) Structure in space of the variable u_X , whose values ± 1 represent the two different phases of the material of width of order $\mathcal{O}(\varepsilon^\alpha)$, with $\alpha = 1/3$ for minimizers (as shown in [58]) and $\alpha = 0$ for other critical points. The width of the transition interval is of order $\mathcal{O}(\varepsilon)$.

In [58] minimizers are proven to exhibit a periodic multi-scale structure (Figure 2.1): a fast scale of order $\mathcal{O}(\varepsilon)$ describes the “jumps” between the two values of the derivative u_X , and a slow scale of order $\mathcal{O}(\varepsilon^{1/3})$ represents the distance between two points with equal value of u_X . From a physical viewpoint, the two values of the derivative $u_X = \pm 1$ model the two different phases of the material. The jumps describe the transition between the phases and the regions with almost constant values of u_X correspond to parts of the material

occupied by the same phase. One of the key results in [58] consists in an asymptotic formula for the period of minimizing solutions, when the solution space U is chosen as the set of all $u \in H^2(0, 1)$ subject to Dirichlet boundary conditions. For $\varepsilon \rightarrow 0$, the period P^ε behaves as

$$P^\varepsilon = 2(6A_0\varepsilon)^{1/3} + \mathcal{O}(\varepsilon^{2/3}), \quad (2.3)$$

where $A_0 = 2 \int_{-1}^1 W^{1/2}(w) dw$.

The approach based on fast-slow analysis of the Euler-Lagrange equation applied here allows us to identify geometrically certain classes of periodic orbits. These orbits are used as starting solutions for numerical continuation using the software package AUTO [18]. This powerful tool has been adopted for example by Grinfeld and Lord [26] in their numerical analysis of small amplitude periodic solutions of (2.1). We provide here a detailed study of periodic solutions based upon one-parameter continuation in the parameters ε and μ . It turns out that several fold bifurcations of periodic orbits structure the parameter space. A numerical comparison with the law (2.3) will be presented, by means of a minimization process of the functional \mathcal{I}^ε along certain families of periodic orbits. Our work also leads to new insights into the dependence of the period on the parameters ε and μ for non-minimizing sequences of periodic orbits.

The paper is structured as follows: Section 2.2 introduces the approach based on geometric singular perturbation theory using the intrinsic multi-scale structure of the problem. We describe the transformation of the Euler-Lagrange equation associated to the functional \mathcal{I}^ε into a multiscale ODE system, along with the decomposition of periodic orbits into slow and fast pieces using the Hamiltonian function. We identify a family of large amplitude singular periodic orbits and prove their persistence for ε small. A crucial point is the construction of an initial periodic orbit for $\varepsilon \neq 0$ in order to start numerical continuation: the strategy we use is illustrated in Section 2.3, where the continuation of the orbits with respect to the main parameters is also performed. This section includes also the comparison between the analytical expression of the period given by Müller and our numerical results as well as the general parameter study of periodic solutions. Section 2.4 is devoted to conclusions and an outline for future work.

2.2 The Euler-Lagrange equation as a fast-slow system

In this section, the critical points (not only the minimizers) of the functional \mathcal{I}^ε are analyzed. A necessary condition they have to satisfy is the Euler-Lagrange equation [14]. The Euler-Lagrange equation associated to \mathcal{I}^ε is the singularly perturbed, fourth order equation

$$\varepsilon^2 u_{XXXX} - \frac{1}{2} \sigma(u_X)_X + u = 0, \quad (2.4)$$

where $\sigma(u_X) = W'(u_X) = u_X^3 - u_X$. Equation (2.4) can be rewritten via

$$\begin{aligned} w &:= u_X, \\ v &:= -\varepsilon^2 w_{XX} + \frac{1}{2} \sigma(w), \\ z &:= \varepsilon w_X, \end{aligned}$$

as an equivalent system of first order ODEs

$$\begin{aligned} \dot{u} &= w, \\ \dot{v} &= u, \\ \varepsilon \dot{w} &= z, \\ \varepsilon \dot{z} &= \frac{1}{2} (w^3 - w) - v, \end{aligned} \quad (2.5)$$

where $\frac{d}{dX} = \cdot$. Equations (2.5) exhibit the structure of a (2,2)-fast-slow system, with u, v as slow variables and w, z as fast variables. We recall that a system is called (m,n) -fast-slow [22, 35, 46] when it has the form

$$\begin{aligned} \varepsilon \dot{x} &= f(x, y, \varepsilon), \\ \dot{y} &= g(x, y, \varepsilon), \end{aligned} \quad (2.6)$$

where $x \in \mathbb{R}^m$ are the *fast* variables and $y \in \mathbb{R}^n$ are the *slow* variables. The re-formulation of system (2.6) on the fast scale is obtained by using the change of variable $\xi = \frac{X}{\varepsilon}$, i.e.

$$\begin{aligned} \frac{dx}{d\xi} &= x' = f(x, y, \varepsilon), \\ \frac{dy}{d\xi} &= y' = \varepsilon g(x, y, \varepsilon). \end{aligned} \quad (2.7)$$

On the fast scale, system (2.5) has the form

$$\begin{aligned}
 u' &= \varepsilon w, \\
 v' &= \varepsilon u, \\
 w' &= z, \\
 z' &= \frac{1}{2}(w^3 - w) - v,
 \end{aligned} \tag{2.8}$$

which for $\varepsilon > 0$ is equivalent to (2.5).

The system possesses the unique equilibrium

$$p_0 = (0, 0, 0, 0), \tag{2.9}$$

which is a center, since the eigenvalues of the Jacobian are all purely imaginary. An important property of system (2.5) is stated in the following result:

Lemma 2.2.1. *Equations (2.5) and (2.8) are singularly perturbed Hamiltonian systems*

$$\begin{aligned}
 \dot{u} &= -\frac{\partial H}{\partial v} & u' &= -\varepsilon \frac{\partial H}{\partial v} \\
 \dot{v} &= \frac{\partial H}{\partial u} & \xi &= \frac{X}{\varepsilon} & v' &= \varepsilon \frac{\partial H}{\partial u} \\
 \varepsilon \dot{w} &= -\frac{\partial H}{\partial z} & & & w' &= -\frac{\partial H}{\partial z} \\
 \varepsilon \dot{z} &= \frac{\partial H}{\partial w}, & & & z' &= \frac{\partial H}{\partial w},
 \end{aligned} \tag{2.10}$$

i.e., they are Hamiltonian systems with respect to the symplectic form $dz \wedge dw + \frac{1}{\varepsilon}dv \wedge du$ and with Hamiltonian function

$$H(u, v, w, z) = \frac{1}{8}(4u^2 - 8vw - 2w^2 + w^4 - 4z^2). \tag{2.11}$$

Proof. The result follows by differentiating (2.11) with respect to the four variables. For more background on fast-slow Hamiltonian systems of this form see [24]. \square

Since the Hamiltonian (2.11) is a first integral of the system, the dynamics take place on level sets, defined by fixing $H(u, v, w, z)$ to a constant value $\mu \in \mathbb{R}$. This allows us to reduce the dimension of the system by one, which we use both in analytical and numerical considerations.

One main advantage in the use of geometric singular perturbation theory is that the original problem can be split into two subsystems by analyzing the singular limit $\varepsilon \rightarrow 0$ on the slow scale (2.6) and on the fast scale (2.7). The subsystems are usually easier to handle. Under suitable conditions the combination of both subsystems allows us to obtain information for the full system when $0 < \varepsilon \ll 1$. In particular, if one can construct a singular periodic orbit by combining pieces of slow and fast orbits, then the existence of a periodic orbit $\mathcal{O}(\varepsilon)$ -close to the singular one for small $\varepsilon \neq 0$ can frequently be proven under suitable technical conditions by tools from geometric singular perturbation theory [22, 35, 46, 73].

The slow singular parts of an orbit are derived from the *reduced problem* (or *slow subsystem*), obtained by letting $\varepsilon \rightarrow 0$ in (2.6)

$$\begin{aligned} 0 &= f(x, y, 0), \\ \dot{y} &= g(x, y, 0), \end{aligned} \tag{2.12}$$

which describes the slow dynamics on the *critical manifold*

$$\mathcal{C}_0 := \{(x, y) \in \mathbb{R}^m \times \mathbb{R}^n : f(x, y, 0) = 0.\} \tag{2.13}$$

Considering $\varepsilon \rightarrow 0$ on the fast scale (2.7) yields the *layer problem* (or *fast subsystem*)

$$\begin{aligned} x' &= f(x, y, 0), \\ y' &= 0, \end{aligned} \tag{2.14}$$

where the fast dynamics is studied on “layers” with constant values of the slow variables. Note that \mathcal{C}_0 can also be viewed as consisting of equilibrium points for the layer problem. \mathcal{C}_0 is called *normally hyperbolic* if the eigenvalues of the matrix $Df_x(p, 0) \in \mathbb{R}^{m \times m}$ do not have zero real parts for $p \in \mathcal{C}_0$. For normally hyperbolic invariant manifolds, Fenichel’s Theorem applies and yields the existence of a *slow manifold* \mathcal{C}_ε . The slow manifold lies at a distance $\mathcal{O}(\varepsilon)$ from \mathcal{C}_0 and the dynamics on \mathcal{C}_ε is well-approximated by the reduced problem; for the detailed technical statements of Fenichel’s Theorem we refer to [22, 35, 46].

In our Hamiltonian fast-slow context, we focus on the analysis of families of periodic orbits for system (2.5) which are parametrized by the level set parameter μ . The first

goal is to geometrically construct periodic orbits in the singular limit $\varepsilon = 0$. The reduced problem is given by

$$\begin{aligned} \dot{u} &= w, \\ \dot{v} &= u, \end{aligned} \tag{2.15}$$

on the critical manifold (see Fig. 2.2)

$$\mathcal{C}_0 = \left\{ (u, v, w, z) \in \mathbb{R}^4 : z = 0, v = \frac{1}{2}(w^3 - w) \right\}. \tag{2.16}$$

The equations of the layer problem are

$$\begin{aligned} w' &= z \\ z' &= \frac{1}{2}(w^3 - w) - \bar{v}, \end{aligned} \tag{2.17}$$

on “layers” where the slow variables are constant ($u = \bar{u}$, $v = \bar{v}$). Note that for Hamiltonian fast-slow systems such as (2.10), both reduced and layer problems are Hamiltonian systems with one degree of freedom.

2.2.1 The Reduced Problem

Equations (2.15) describe the reduced problem on \mathcal{C}_0 , if w is considered as a function of (u, v) on \mathcal{C}_0 .

Lemma 2.2.2. \mathcal{C}_0 is normally hyperbolic except for two fold lines

$$\begin{aligned} \mathcal{L}_- &= \left\{ (u, (w_-^3 - w_-)/2, w_-, 0) \in \mathbb{R}^4 \right\}, \\ \mathcal{L}_+ &= \left\{ (u, (w_+^3 - w_+)/2, w_+, 0) \in \mathbb{R}^4 \right\}, \end{aligned} \tag{2.18}$$

where w_{\pm} are defined by $\sigma'(w_{\pm}) = 0$, i.e., $w_{\pm} = \pm 1/\sqrt{3}$. For $p \in \mathcal{L}_{\pm}$, the matrix $D_x f(p, 0)$ has a double zero eigenvalue.

The lines \mathcal{L}_{\pm} naturally divide \mathcal{C}_0 into three parts

$$\mathcal{C}_{0,l} = \mathcal{C}_0 \cap \{w < w_-\}, \quad \mathcal{C}_{0,m} = \mathcal{C}_0 \cap \{w_- \leq w \leq w_+\}, \quad \mathcal{C}_{0,r} = \mathcal{C}_0 \cap \{w > w_+\},$$

as shown in Figure 2.2. The submanifolds involved in our analysis are only $\mathcal{C}_{0,l}$ and $\mathcal{C}_{0,r}$, which are normally hyperbolic. More precisely, $\mathcal{C}_{0,l}$ and $\mathcal{C}_{0,r}$ are of *saddle-type*, since the

matrix $D_x f(p, 0)$ along them always has two real eigenvalues of opposite sign. We remark that saddle-type critical manifolds have played an important role in the history of fast-slow systems in the context of the travelling wave problem for the FitzHugh-Nagumo equation, see for example [37, 43, 28].

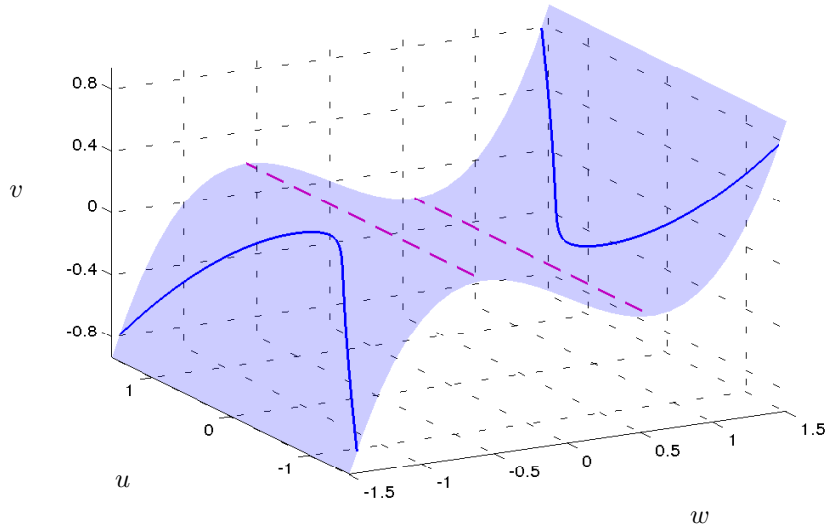


Figure 2.2: Critical manifold \mathcal{C}_0 in (w, u, v) -space. The magenta dashed lines are the fold lines \mathcal{L}_\pm . The blue solid curves correspond to $\mathcal{C}_{0,l}^\mu$ and $\mathcal{C}_{0,r}^\mu$, i.e., the intersection of $\mathcal{C}_{0,l}$ and $\mathcal{C}_{0,r}$ and the hypersurface $H(u, v, w, z) = \mu$ for $\mu = 0$.

Lemma 2.2.3. *On $\mathcal{C}_0 - \mathcal{L}_\pm$, the flow of the reduced system is, up to a time rescaling, given by*

$$\begin{aligned} \dot{u} &= (3w^2 - 1)w, \\ \dot{w} &= 2u. \end{aligned} \tag{2.19}$$

Proof. We differentiate $v = \frac{1}{2}(w^3 - w)$ with respect to X , re-write the equation in (u, w) -variables and apply the time rescaling corresponding to the multiplication of the vector field by the factor $(3w^2 - 1)$ (cf. [46, Sec.7.7]). On $\mathcal{C}_{0,m}$ this procedure changes the direction of the flow, but it does not affect the parts of the critical manifold involved in our analysis. \square

The Hamiltonian function allows us to restrict our attention to two subsets of $\mathcal{C}_{0,l}^\mu$ and

$\mathcal{C}_{0,r}^\mu$ by fixing the value of μ . Analyzing the slow flow on these two normally hyperbolic branches, we see that u decreases along $\mathcal{C}_{0,l}$ and increases along $\mathcal{C}_{0,r}$ as shown in Figure 2.3.

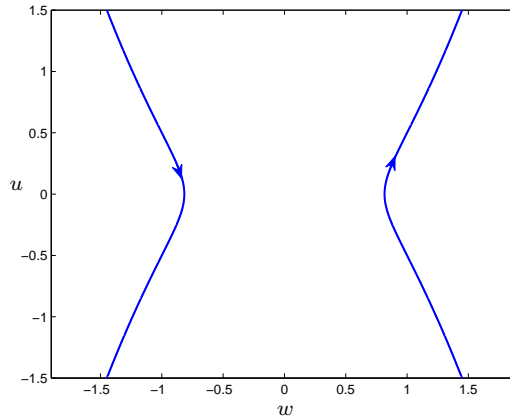


Figure 2.3: $\mathcal{C}_{0,l}^\mu$ and $\mathcal{C}_{0,r}^\mu$ in (w, u) -space with $\mu = 0$; cf. Figure 2.2.

2.2.2 The Layer Problem

The layer problem is obtained by setting $\varepsilon = 0$ in (2.8). We obtain a two-dimensional Hamiltonian vector field on “layers” where the slow variables are constant ($u = \bar{u}, v = \bar{v}$)

$$\begin{aligned} w' &= z, \\ z' &= \frac{1}{2}(w^3 - w) - \bar{v}. \end{aligned} \tag{2.20}$$

The two branches $\mathcal{C}_{0,l}^\mu$ and $\mathcal{C}_{0,r}^\mu$ are hyperbolic saddle equilibria for the system (2.20) for every value of \bar{u}, \bar{v} . To construct a singular limit periodic orbit we are particularly interested in connecting orbits between equilibria of the layer problem.

Lemma 2.2.4. *The layer problem (2.20) has a double heteroclinic connection if and only if $\bar{v} = 0$. These are the only possible heteroclinic connections of the layer problem (2.20).*

Proof. System (2.20) is Hamiltonian, with \bar{v} as a parameter and Hamiltonian function

$$H_f(w, z) = -\frac{z^2}{2} + \frac{w^4}{8} - \frac{w^2}{4} - \bar{v}w.$$

The lemma follows easily by discussing the level curves of the Hamiltonian; for the convenience of the reader we outline the argument.

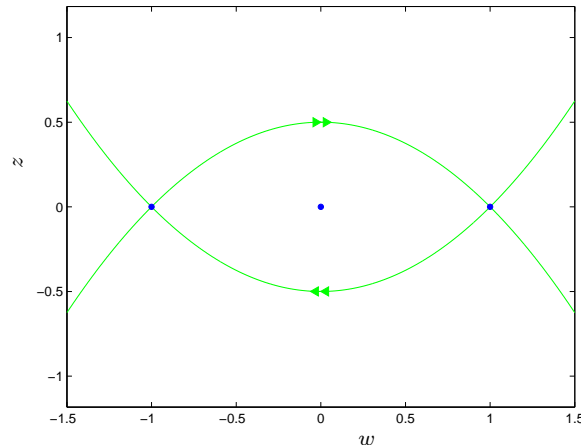


Figure 2.4: Fast flow in the (w, z) -space for (2.20). Equilibria are marked with blue dots and the stable and unstable manifold trajectories in green. The heteroclinic fast connections are indicated with double arrows.

Indexing the level set value of H_f as θ , the solutions of (2.20) are level curves $\{H_f(w, z) = \theta\}$. The equilibria of (2.20) are $\{z = 0, w = w_-, w_m, w_+\}$; here w_-, w_m, w_+ are the three solutions of

$$2\bar{v} - w^3 + w = 0 \quad (2.21)$$

which depend upon \bar{v} . We only have to consider the case where there are at least two real equilibria w_- and w_+ which occurs for $\bar{v} \in [-1/(3\sqrt{3}), 1/(3\sqrt{3})]$. Let

$$H_f(w_-, 0) =: \theta_l, \quad H_f(w_+, 0) =: \theta_r$$

and note that since (2.21) is cubic we can calculate $\theta_{l,r}$ explicitly. To get a heteroclinic connection we must have $\theta_l = \theta_r$ and by an explicit calculation this yields the condition $\bar{v} = 0$. Hence, heteroclinic connections of (2.20) can occur only if $\bar{v} = 0$. For $\bar{v} = 0$ one easily finds that the relevant equilibria are located at $w_- = -1$ and $w_+ = 1$ so that $\theta_l = -1/8 = \theta_r$. The double heteroclinic connection is then explicitly given by the curves $\{z = \pm \frac{1}{2}(1 - w^2)\}$ (see also Figure 2.4). \square

The next step is to check where the relevant equilibria of the layer problem are located on the critical manifold \mathcal{C}_0^μ for a fixed value of the parameter μ since we have a level set

constraint for the full system. Using Lemma 2.2.4 one must require $w = \pm 1, v = 0$ while $z = 0$ is the critical manifold constraint, hence

$$H(u, 0, \pm 1, 0) = \frac{1}{2}u^2 - \frac{1}{8} \stackrel{!}{=} \mu.$$

Therefore, the transition points where fast jumps from $\mathcal{C}_{0,l}$ to $\mathcal{C}_{0,r}$ and from $\mathcal{C}_{0,r}$ to $\mathcal{C}_{0,l}$ are possible are given by

$$\mathcal{C}_0^\mu \cap \{v = 0, w = \pm 1\} = \left\{ u = \pm \sqrt{2\mu + \frac{1}{4}}, v = 0, w = \pm 1, z = 0 \right\}. \quad (2.22)$$

Observe that fast orbits corresponding to positive values of u connect $\mathcal{C}_{0,r}^\mu$ to $\mathcal{C}_{0,l}^\mu$, while the symmetric orbits with respect to the $u = 0$ plane connect $\mathcal{C}_{0,l}^\mu$ to $\mathcal{C}_{0,r}^\mu$.

Recall that $w = \pm 1$ represent the two phases of the material. Hence, the heteroclinic orbits of the layer problem can be interpreted as instantaneous transitions between these phases.

2.2.3 Singular Fast-Slow Periodic Orbits

The next step is to define singular periodic orbits by combining pieces of orbits of the reduced and layer problem. Figure 2.5 illustrates the situation. The entire singular orbit γ_0^μ is obtained connecting two pieces of orbits of the reduced problem with heteroclinic orbits of the fast subsystem for a fixed value of μ , see Figure 2.5(a). The configuration of the two-dimensional critical manifold and the singular periodic orbit is indicated in Figure 2.5(b).

Here we are only interested in singular periodic orbits which have nontrivial slow *and* fast segments. Therefore, we do need transition points from the fast subsystem to the slow subsystem. This requirement implies, by using the result (2.22), the lower bound $\mu > -\frac{1}{8}$. A second requirement we impose is that the slow subsystem orbits lie inside the normally hyperbolic parts $\mathcal{C}_{0,l}^\mu$ and $\mathcal{C}_{0,r}^\mu$. The u -coordinate of the slow segment closest to the lines \mathcal{L}_\pm is located at $u = 0$. Hence, we calculate the value of the Hamiltonian under the condition that the slow trajectory is tangent to \mathcal{L}_\pm which yields

$$H\left(0, \frac{1}{2}(w_\pm^3 - w_\pm), w_\pm, 0\right) = \frac{1}{24}. \quad (2.23)$$

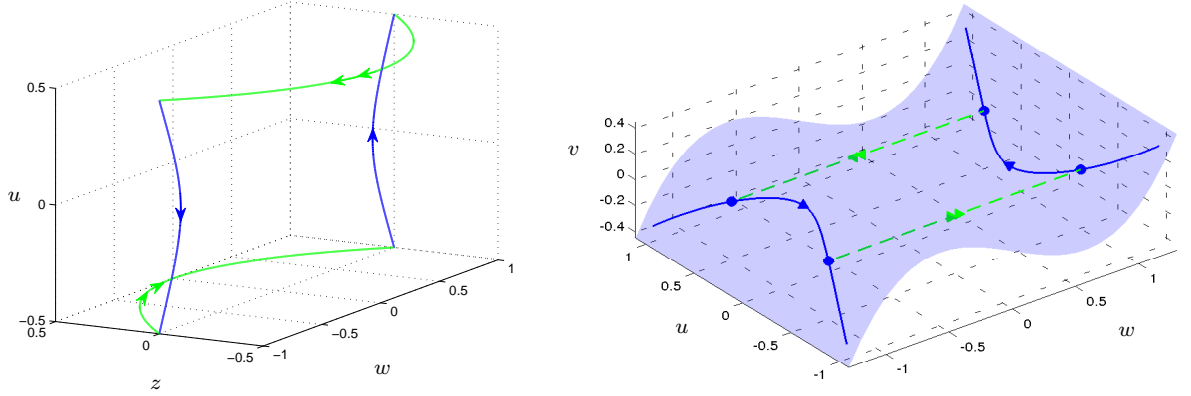


Figure 2.5: Singular periodic orbit γ_0^μ for a fixed value of μ ($\mu = 0$), obtained by composition of slow (blue) and fast (green) pieces. (a) Orbit in (w, z, u) -space. (b) Orbit in the (w, u, v) -space. The fast pieces are indicated via dashed lines to illustrate the fact we are here considering their projection in (w, u, v) , while they actually occur in the (w, z) -plane. Consequently, they do not intersect $\mathcal{C}_{0,m}$.

Combining these considerations with the results from Sections 2.2.1-2.2.2 gives the following result on the existence of singular periodic orbits ($\varepsilon = 0$):

Proposition 2.2.5. For $\varepsilon = 0$, the fast-slow system (2.5),(2.8) has a family of periodic orbits $\{\gamma_0^\mu\}_\mu$ consisting of precisely two fast and two slow subsystem trajectories with slow parts lying entirely in $\mathcal{C}_{0,l}$ and $\mathcal{C}_{0,r}$ if and only if

$$\mu \in I_\mu, \quad I_\mu := \left(-\frac{1}{8}, \frac{1}{24}\right). \quad (2.24)$$

The persistence of these periodic orbits for $0 < \varepsilon \ll 1$ on each individual surface level of the Hamiltonian can be proven by using an argument based on the theorem introduced by Soto-Treviño in [73].

Theorem 2.2.6. For every $\mu \in I_\mu$ and for $\varepsilon > 0$ sufficiently small, there exists a locally unique periodic orbit of the fast-slow system (2.5),(2.8) that is $\mathcal{O}(\varepsilon)$ close to the corresponding singular orbit γ_0^μ .

Proof. The Hamiltonian structure of the system suggests to study the individual levels as parametrized families by directly applying the Hamiltonian function as a first integral to reduce the dimension of the system. At first sight, a convenient choice is to express v as a function of the variables (u, w, z) and μ

$$v = \frac{4u^2 - 8\mu - 2w^2 + w^4 - 4z^2}{8w}. \quad (2.25)$$

Consequently, equations (2.5) transform into a (2, 1)-fast-slow system

$$\begin{aligned} \dot{u} &= w, \\ \varepsilon \dot{w} &= z, \\ \varepsilon \dot{z} &= \frac{1}{2}(w^3 - w) - \frac{4u^2 - 8\mu - 2w^2 + w^4 - 4z^2}{8w}. \end{aligned} \quad (2.26)$$

Theorem 1 in [73] for a C^r ($r \geq 1$) (2, 1)-fast-slow system guarantees the persistence of periodic orbits consisting of two slow pieces connected by heteroclinic orbits for $0 < \varepsilon \ll 1$ when the following conditions hold:

- The critical manifolds are one-dimensional and normally hyperbolic (given by Lemma 2.2.2).
- The intersection between $W^u(\mathcal{C}_{0,l})$ (resp. $W^u(\mathcal{C}_{0,r})$) and $W^s(\mathcal{C}_{0,r})$ (resp. $W^s(\mathcal{C}_{0,l})$) is transversal (confirmed by Lemma 2.2.4, see Fig. 3.12).
- The full system possesses a singular periodic orbit and the slow flow on the critical manifolds is transverse to touch-down and take-off sets, which reduce to 0-dimensional objects in this case as we explicitly obtained in (2.22).

However, system (2.26) appears to be nonsmooth at $w = 0$ and the fast orbits necessarily cross $w = 0$. To overcome this (apparent) difficulty we use other charts for the manifold $H(u, v, w, z) = \mu$ for parts of the singular orbit close to $w = 0$. Instead of (2.25) we now express u as a function of the other variables, i.e.

$$u = \pm \frac{1}{2} \sqrt{8vw + 2w^2 - w^4 + 4z^2 + 8\mu}. \quad (2.27)$$

This leads to the following description of the dynamics:

- System (2.26) describes the dynamics on the slow pieces away from $w = 0$;

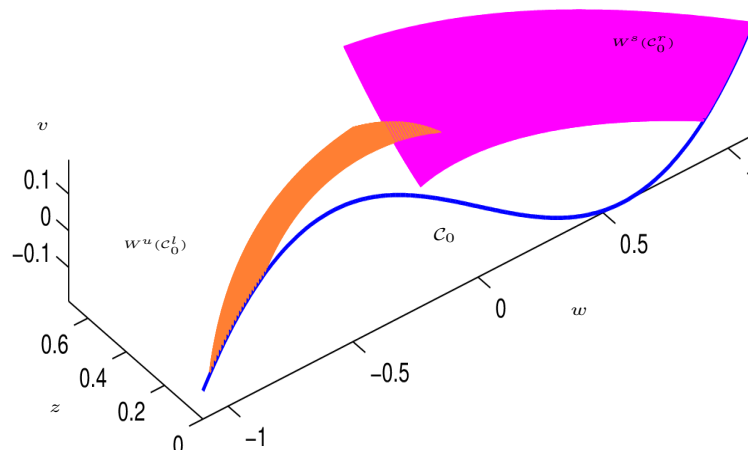


Figure 2.6: Transversal intersection in the (w, z, v) space between $W_u(\mathcal{C}_{0,l})$ (in orange) and $W_s(\mathcal{C}_{0,r})$ (in magenta). The blue line represents the critical manifold \mathcal{C}_0 .

- The heteroclinic connection corresponding to $u > 0$ is expressed by

$$\begin{aligned} v' &= +\frac{\varepsilon}{2}\sqrt{8vw + 2w^2 - w^4 + 4z^2 + 8\mu}, \\ w' &= z, \\ z' &= \frac{1}{2}(w^3 - w) - v. \end{aligned} \tag{2.28}$$

- The heteroclinic connection corresponding to $u < 0$ is expressed by

$$\begin{aligned} v' &= -\frac{\varepsilon}{2}\sqrt{8vw + 2w^2 - w^4 + 4z^2 + 8\mu}, \\ w' &= z, \\ z' &= \frac{1}{2}(w^3 - w) - v. \end{aligned} \tag{2.29}$$

If we consider system (2.5) as a smooth dynamical system on the manifold defined by $H = \mu$, the proof given in [73] (based on proving the transversal intersection of two manifolds obtained by flowing suitably chosen initial conditions forward and backward in time) goes through without being affected by the fact that we have to work with several coordinate systems, as described above. \square

System (2.26) has two parameters μ, ε , which naturally leads to the question how periodic orbits deform and bifurcate when the two parameters are varied. Furthermore, the fast-slow structure with orbits consisting of two fast jumps and two slow segments as shown

in Figure 2.5 and the three-dimensional form (2.26) provide analogies to the travelling wave frame system obtained from the partial differential equation version of the FitzHugh-Nagumo [23, 60] (FHN) equation. The three-dimensional fast-slow FHN system has been studied in great detail using various fast-slow systems techniques (see e.g. [12, 28, 37, 43]). One particular approach to investigate the FHN parameter space efficiently is to employ numerical continuation methods [29, 13]. In fact, numerical approaches to FHN have frequently provided interesting conjectures and thereby paved the way for further analytical studies. Adopting this approach, we are going to investigate the problem (2.26) considered here using numerical continuation to gain better insight into the structure of periodic orbits.

2.3 Numerical Continuation

This section is devoted to the numerical investigation of the the critical points of the functional \mathcal{I}^ε via the Euler-Lagrange formulation (2.26). A powerful tool for such computations is AUTO [18]. AUTO is able to numerically track periodic orbits depending upon parameters using a combination of a boundary value problem (BVP) solver with a numerical continuation algorithm. Using such a framework for fast-slow systems often yields a wide variety of interesting numerical and visualization results; for a few recent examples we refer to [15, 16, 27, 30, 31, 78].

The first task one has to deal with is the construction of a starting orbit for fixed $\varepsilon \neq 0$. For (2.26) this is actually a less trivial task than for the FHN equation as we are going to explain in Section 2.3.1. In Section 2.3.1, we are also going to construct a starting periodic orbit based upon the geometric insights of Section 2.2.

Once the starting periodic orbit is constructed, we use AUTO to perform numerical continuation in both parameters μ and ε . This yields bifurcation diagrams and the solutions corresponding to some interesting points on the bifurcation branches. Then, the connection between the parameters in the minimization process is investigated, in order to numerically determine the correspondence that leads to the functional minimum. Finally, a comparison with the period law (2.3) predicted by Müller [58] is performed.

2.3.1 Construction of the starting orbit

As indicated already, the construction of a starting periodic orbit is not trivial:

- The singular orbit itself, obtained by matching slow and fast subsystem orbits for a fixed value of μ and for $\varepsilon = 0$, cannot be used owing to re-scaling problems (the fast pieces would all correspond to $x = 0$).
- The computation of a full periodic orbit using a direct initial value solver approach for $0 < \varepsilon \ll 1$ is hard to perform since the slow manifolds are of saddle type and an orbit computed numerically would diverge from them exponentially fast [27].
- Matching slow segments obtained with a saddle-type algorithm [27, 42] and fast parts computed with an initial value solver may cause problems at the points where the four pieces should match.
- In contrast to the FitzHugh-Nagumo case [29, 13], the periodic orbits we are looking for cannot be detected as Hopf bifurcations from the zero equilibrium. In that case, we could use AUTO to locate such bifurcations and then find a periodic orbit for $0 < \varepsilon \ll 1$ fixed by branch-switching at the Hopf bifurcation point. In our case, however, the origin p_0 is a center equilibrium, and an infinite number of periodic orbits exist around it in the formulation (2.5).
- Starting continuation close to the equilibrium p_0 is difficult due to its degenerate nature ($w = 0$).

Our strategy is to use the geometric insight from Section 2.2 in combination with a slow manifolds of saddle-type (SMST) algorithm and a homotopy approach. We construct an approximate starting periodic orbit using a value of μ which leads to a short “time” spent on the slow parts of the orbits, so that the saddle-type branches do not lead to numerical complications. Then we use an SMST algorithm to find a suitable pair of starting points lying extremely close to the left and right parts of the slow manifolds $\mathcal{C}_{\varepsilon,l}^\mu$ and $\mathcal{C}_{\varepsilon,r}^\mu$. In the last step we employ numerical continuation to study the values of μ we are actually interested in; this is the homotopy step.

The value $\mu = -\frac{1}{8}$ is peculiar, since in this case the singular slow segments for (2.26) reduce to two points

$$\mathcal{C}_{0,l}^{-1/8} = \{(0, -1, 0)\}, \quad \text{and} \quad \mathcal{C}_{0,r}^{-1/8} = \{(0, 1, 0)\}, \quad (2.30)$$

i.e., touch-down and take-off sets for the fast dynamics coincide in this case. The range (2.24) we are considering does not include $\mu = -\frac{1}{8}$; however, this property makes it an excellent candidate for the first step of our strategy. Indeed, we know already from the geometric analysis in Section 2.2 that the time spent near slow manifolds is expected to be very short in this case.

Although it is still not possible to compute the full orbit using forward/backward integration, we can compute two halves, provided we choose the correct initial condition. We aim to find a point on the slow manifolds $\mathcal{C}_{\varepsilon,l}^{\mu}$ and $\mathcal{C}_{\varepsilon,r}^{\mu}$ as an initial value. The SMST algorithm [27] helps to solve this problem. The procedure is based on a BVP method to compute slow manifolds of saddle-type in fast-slow systems. Fixing ε and μ , we select manifolds B_l and B_r , which are transverse to the stable and unstable eigenspaces of $\mathcal{C}_{0,l}^{\mu}$ and $\mathcal{C}_{0,r}^{\mu}$, respectively (Figure 2.7). The plane B_l and the line B_r provide the boundary conditions for the SMST algorithm.

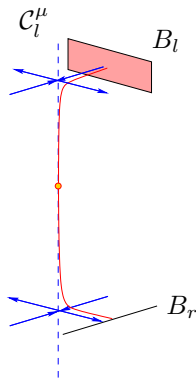


Figure 2.7: Schematic representation of the SMST algorithm applied to $\mathcal{C}_{0,l}^{\mu}$ (an analogous situation occurs for $\mathcal{C}_{0,r}^{\mu}$). The critical manifold is indicated by a dotted blue line, while the red line represents the slow manifold for $\varepsilon = 0.001$. The orange point corresponds to $(0, w_L, 0)$, which actually belongs to both manifolds.

Implementing the algorithm for $\mu = -\frac{1}{8}$ and $\varepsilon = 0.001$ for (2.26) shows that there are actually two points $(0, w_L, 0)$ and $(0, w_R, 0)$ which are contained in the slow manifold even for $\varepsilon \neq 0$ as well as in the critical manifold \mathcal{C}_0 . From the geometric analysis in Section 2.2 we know that at $\mu = -\frac{1}{8}$ the take-off and touch-down points coincide and a singular double-heteroclinic loop exists for $v = 0$. This motivates the choice of $(u, v, w, z) = (0, 0, w_L, 0)$ and $(u, v, w, z) = (0, 0, w_R, 0)$ in the following algorithm: a numerical integration of the full four-dimensional problem (2.5) forward and backward in x is performed, imposing the Hamiltonian constraint using a projective algorithm. The computation is stopped once the hyperplane $\{w = 0\}$ is reached. The full periodic orbit is then constructed by matching two symmetric pieces together.

In principle, there are different ways how one may arrive at a useful construction of a highly accurate starting periodic orbit. In our context, the geometric analysis guided the way to identify the simplest numerical procedure, which is an approach that is likely to be successful for many other non-trivial fast-slow numerical continuation problems.

2.3.2 Continuation in μ

A detailed analysis of the critical points' dependence on the Hamiltonian is performed. The value of μ can be arbitrarily chosen only in the interval I_μ , while ε is fixed to 0.001. Continuation is performed on system (2.26) using the initial orbit obtained numerically in Section 2.3.1. Starting at $\mu = -\frac{1}{8}$, AUTO is able to compute the variation of the orbits up to $\mu = \frac{1}{24}$. The bifurcation diagram of the period P with respect to the parameter μ is shown in Figure 2.8(a).

The first/upper branch of the continuation displays fast-slow orbits corresponding perturbations of the singular ones $\{\gamma_0^\mu\}_{\mu \in I_\mu}$ for fixed $\varepsilon \neq 0$. As predicted by the geometric analysis we observe that decreasing μ reduces the length of the slow parts, so that the orbits almost correspond to the double heteroclinic one analytically constructed at $\mu = -\frac{1}{8}$; see Figure 2.8. Near $\mu = -\frac{1}{8}$ the bifurcation branch has a fold in (μ, P) -space leading to the second/lower bifurcation branch. The difference between the orbits on the two branches for a fixed value of μ is shown in Figure 2.8(b). Along the second branch, periodic solu-

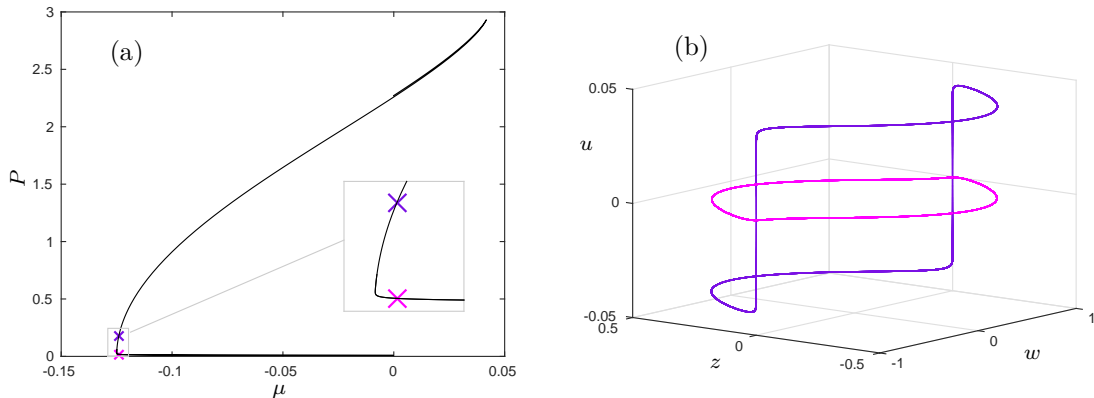


Figure 2.8: Continuation in μ : (a) bifurcation diagram in (μ, P) -space, where two periodic solutions corresponding to $\mu = -0.124$ are marked by crosses; (b) corresponding solutions in (w, z, u) -space: the one on the lower branch (magenta) is almost purely fast, while the one on the upper branch (purple) contains long non-vanishing slow pieces.

tions around the center equilibrium appear, which collapse into it with increasing μ (Figure 2.9(b)).

Furthermore, numerical continuation robustly indicates that the upper branch has another fold when continued from $\mu = 0$ to higher values of μ as shown in Figure 2.9(a). The orbits obtained by fixing a value of μ on the upper branch and its continuation after the fold differ only because of the appearance of two new fast parts near the plane $\{u = 0\}$ as shown in Figure 2.9(a). We conjecture that these parts arise due to the loss of normal hyperbolicity at \mathcal{L}_{\pm} ; see also Section 2.4.

2.3.3 Continuation in ε

We perform numerical continuation in ε by fixing three values of μ in order to capture the behavior of the solutions for the range I_{μ} from Proposition 2.2.5. We consider $\mu_l \approx -\frac{1}{8}$ with $\mu_l > -\frac{1}{8}$, $\mu_c \approx 0$, and $\mu_r \approx \frac{1}{24}$ with $\mu_r < \frac{1}{24}$; or more precisely $\mu_l = -0.12489619925$, $\mu_c = 1.5378905702 \cdot 10^{-5}$, and $\mu_r = 0.04100005066$. For each of these values, we find two bifurcation branches connected via a fold in (μ, P) -space; see Figure 2.10.

The bifurcation diagrams and the associated solutions shown in Figure 2.10 nicely illus-

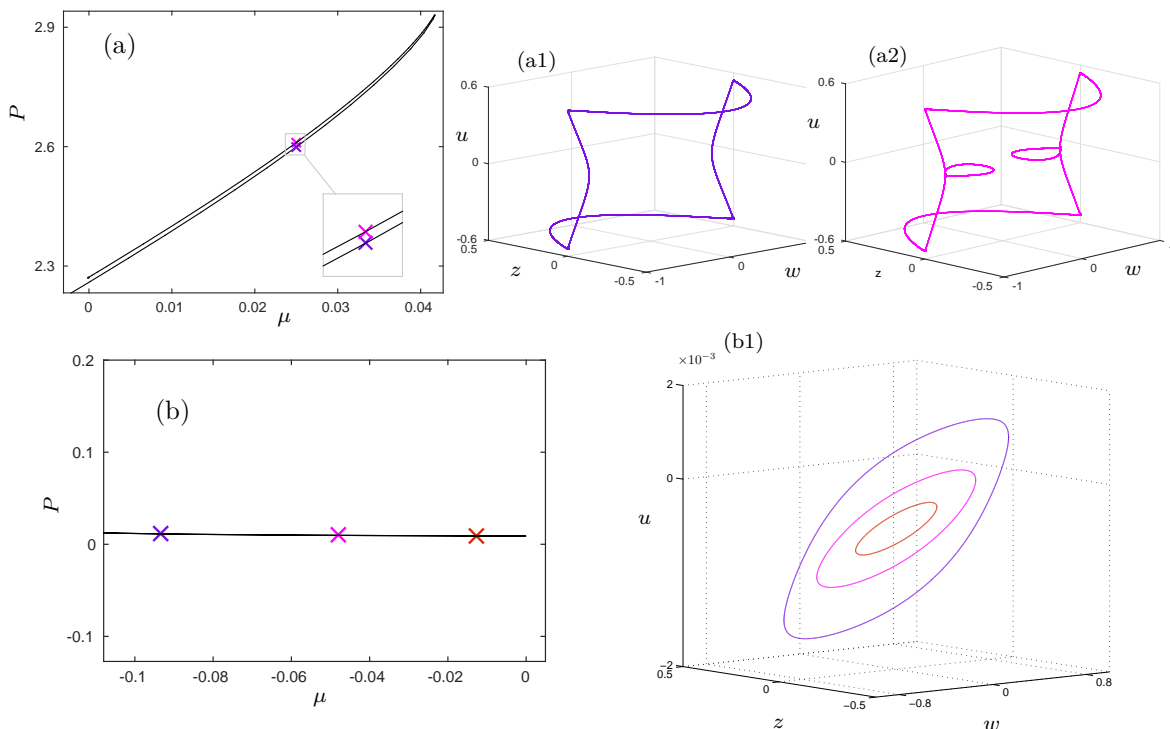


Figure 2.9: Continuation in μ . (a) Zoom on the upper part of the bifurcation diagram in (μ, P) space, where two periodic orbits corresponding to $\mu = 0.0025$ are marked by crosses. (a1)-(a2) The orbits are shown in (w, z, u) -space. The periodic orbit on the bottom part of the upper branch (purple) corresponds to analytical expectations with two fast and two slow segments. The periodic orbit on the top part of the upper branch (magenta) includes two new fast “homoclinic excursions”. (b) Zoom on the lower part of the bifurcation diagram in (μ, P) -space, where three solutions are marked. (b1) The solutions in phase space all correspond to periodic orbits around the center equilibrium p_0 ; note that the scale in the u -coordinate is extremely small so the three periodic orbits almost lie in the hyperplane $\{u = 0\}$.

trate the dependence of the period on the singular perturbation parameter ε . When $\varepsilon \rightarrow 0$ there are two very distinct limits for the period $P = P(\varepsilon)$ (Figure 2.10(a)-(b)) depending whether we are on the upper and lower parts of the main branch of solutions. In the case with $\mu_r \approx \frac{1}{24}$ when orbits come close to non-hyperbolic singularities on \mathcal{C}_0 , we actually

seem to observe that $P(0)$ seems to be independent on whether we consider the upper or lower part of the branch (see Figure 2.10(c)). Furthermore, functional forms of $P(\varepsilon)$ are clearly different for small ε so the natural conjecture is that there is no universal periodic scaling law if we drop the functional minimization constraint.

The deformation under variation of ε of the periodic orbits in (w, z, u) -space is also interesting. For $\mu = \mu_l$ (Figure 2.10(a)), we observe that the upper branch corresponds to the solutions that we expect analytically from Proposition 2.2.5 consisting of two fast and two slow segments when approaching $\varepsilon = 0$. A similar scenario occurs also for the other values of μ (Figure 2.10(b) and Figure 2.10(c)). When the ε value is too large, or when we are on a different part of the branch of solutions, the orbits closed to the equilibrium of the full system or additional pieces resembling new fast contributions appear.

2.3.4 Period scaling

So far, no boundary conditions have been imposed; moreover, all the computed solutions are not necessarily minimizers of the functional, but only critical points. Our conjecture is that the interaction between the two main parameters of the system μ and ε should allow us to obtain the true minimizers via a double-limit. In other words, for every value of ε there is a corresponding orbit which minimizes the functional \mathcal{I}^ε , and since along this orbit the Hamiltonian has to constantly assume a certain value $\bar{\mu}$, the minimization process should imply a direct connection between the parameters. Consequently, it is interesting to investigate this ansatz from the numerical viewpoint.

A first possibility is to establish a connection between the two parameters ε and μ via a direct continuation in both parameters, starting from certain special points, such as the fold points detected in Sections 2.3.2-2.3.3. However, it turns out that this process does not lead to the correct scaling law for minimizers of \mathcal{I}_ε as shown in Figure 2.11.

Another option is instead to check if among the critical points of the Euler-Lagrange equation (2.4) we have numerically obtained there are also the minimizers of the functional \mathcal{I}^ε respecting the power law (2.3). In [58], boundary conditions on the interval $[0, 1]$ are also included in the variational formulation, and from the results obtained from the continuation

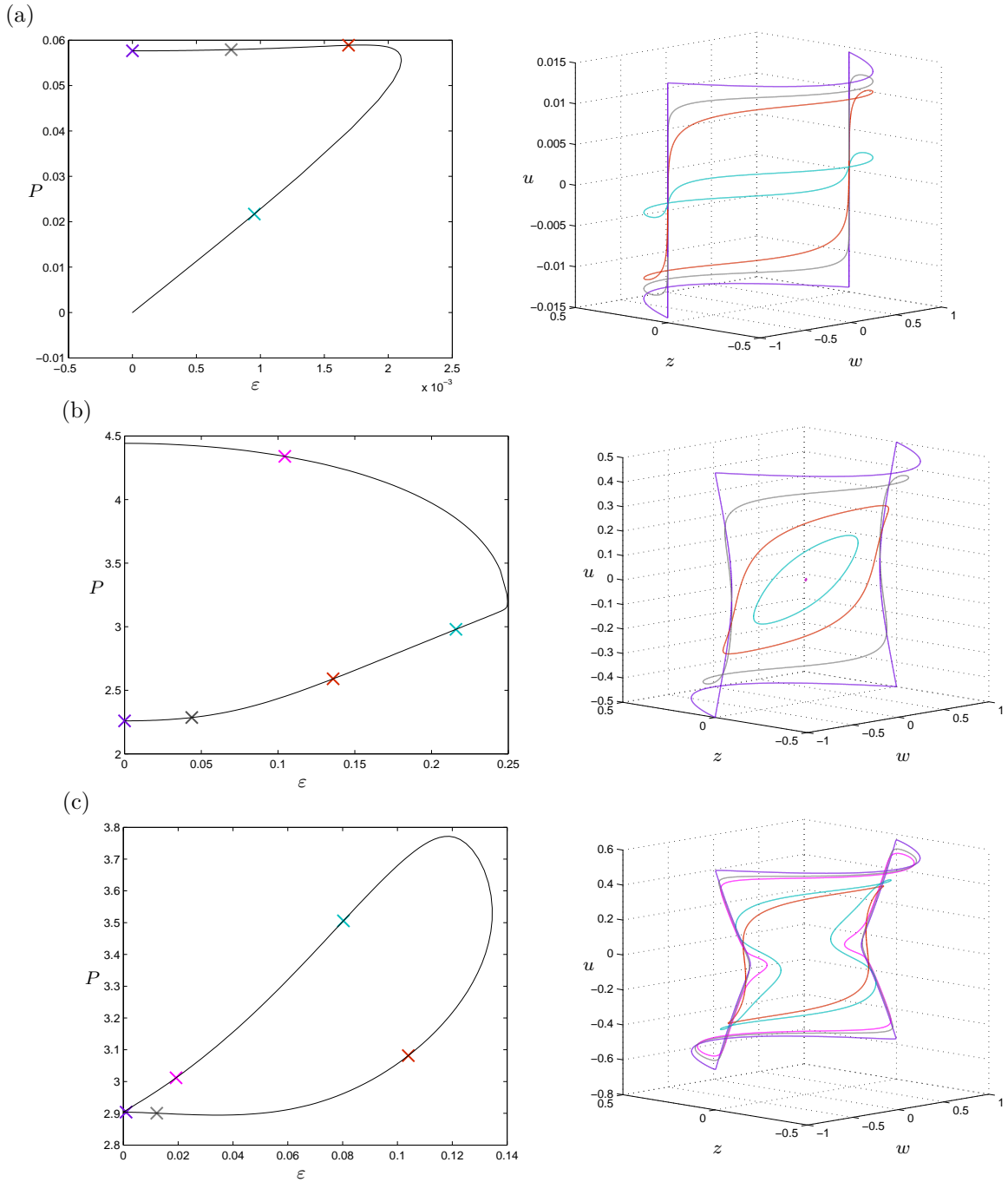


Figure 2.10: Continuation in ε : on the left side bifurcation diagrams in (ε, P) are shown, on the right the corresponding solutions in (w, z, u) -space are displayed. (a) $\mu = \mu_l$, (b) $\mu = \mu_c$, (c) $\mu = \mu_r$.

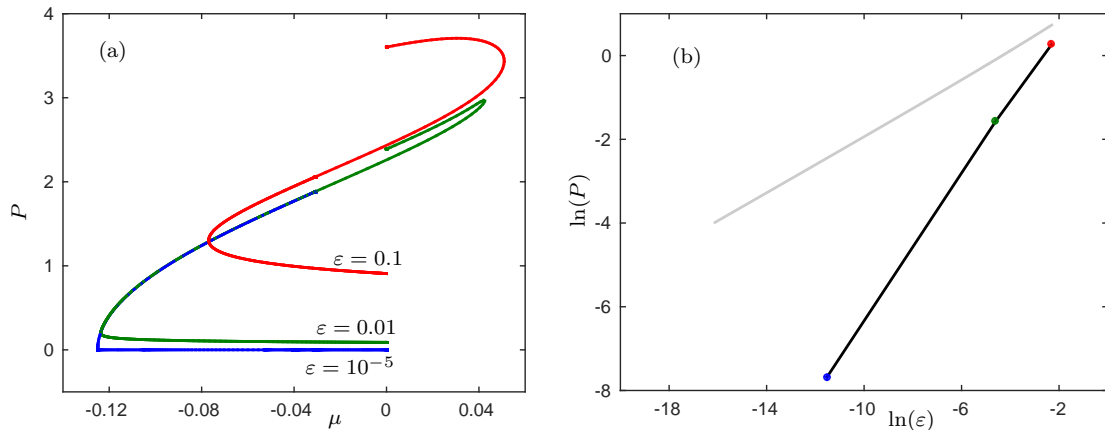


Figure 2.11: Illustration of two-parameter continuation. (a) Three different bifurcation diagrams have been computed, each starting from a solution at $\mu = 0$ for three different values of $\varepsilon = 0.1, 0.01, 10^{-5}$ (red, green, blue). It is already visible and confirmed by the computation that the sequence of leftmost fold points on each branch converges to $\mu = -1/8$ as $\varepsilon \rightarrow 0$. However, the period scaling law of the orbits precisely at these fold points, which is shown in (b) as three dots corresponding to the three folds in (a) and a suitable interpolation (black line), does not converge as $\mathcal{O}(\varepsilon^{1/3})$ (grey reference line with slope $\frac{1}{3}$).

in ε , one may expect that high values of μ would not be able to fit them, since the period is always too high. Lower values of μ , instead, seem to have sufficiently small period. Hence, one could fix one of those (for example, μ_l) and look at what happens as $\varepsilon \rightarrow 0$. The hope is that the $\mathcal{O}(\varepsilon^{1/3})$ leading-order scaling for the period naturally emerges. Unfortunately, this does not happen, as we can see in Figure 2.12; the lower branch seems to give a linear dependence on ε , while the upper branch gives a quadratic one.

The reason why from this naive approach the $\mathcal{O}(\varepsilon^{1/3})$ leading-order scaling does not emerge lies in the lack of connection with the minimization process. However, Figure 2.12 demonstrates that there are several nontrivial scalings of natural families of periodic orbits as $\varepsilon \rightarrow 0$.

So far, we have just assumed that the Hamiltonian value of the minimizers should be “low”, but indeed there is a strict connection between the values of ε one is considering

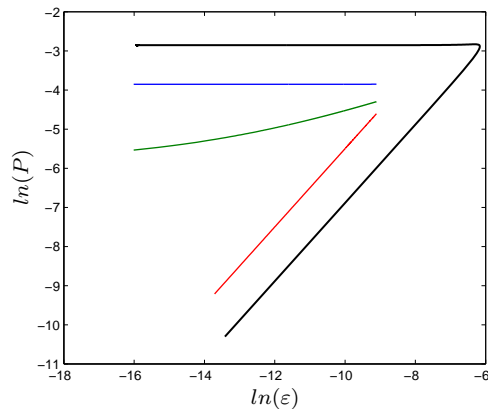


Figure 2.12: Possible fits of the form $P \simeq \varepsilon^\alpha$ for the numerical data computed with $\mu = \mu_l$ (black line): $\alpha = 2$, blue; $\alpha = 1/3$, green; $\alpha = 1$, red.

and the value of μ of the minimizers. In other words, there is not a unique value of μ given by the minimizers for every ε small but minimizers move over different Hamiltonian energy levels as $\varepsilon \rightarrow 0$. Starting from this consideration, another option, which turns out to be the correct one to recover the scaling (2.3), is to use the periodic orbits from numerical continuation to compute the numerical value of the functional \mathcal{I}^ε as a function of the period P fixing different values of ε in a suitable range, such as:

$$I_\varepsilon = [10^{-7}, 10^{-1}]. \quad (2.31)$$

Then, we obtain different parabola-shaped diagrams where we can extract the value of the period minimizing the functional (Figure 2.13). When plotting these values related to the value of ε for which they have been computed, one obtains the results shown in Figure 2.14. The values numerically extracted from our solutions match the analytical results on the period proven by Müller (2.3) when the value of ε is sufficiently small. As ε increases, the period law is less accurate, as one would expect.

2.4 Conclusion & Outlook

In summary, we have shown that geometric singular perturbation theory and numerical continuation methods can be very effective tools to understand nonconvex multiscale variational problems via the Euler-Lagrange formulation. We have proven the existence of a

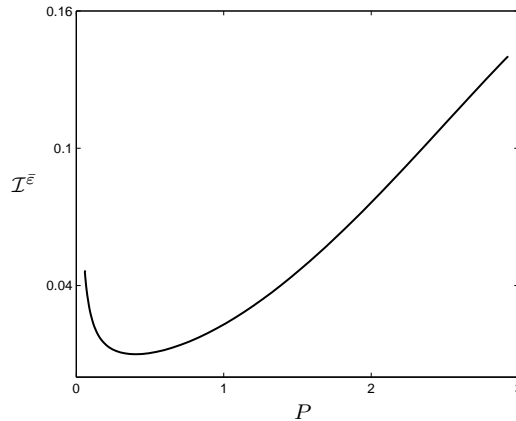


Figure 2.13: Parabola-shaped diagram obtained by fixing $\varepsilon = 0.001$ and numerically computing the value of the functional \mathcal{I}^ε along the solutions computed via continuation in AUTO. The plot presents a minimum, and the value of P corresponding to ε where this minimum is realized is recorded in order to check the period law (2.3).

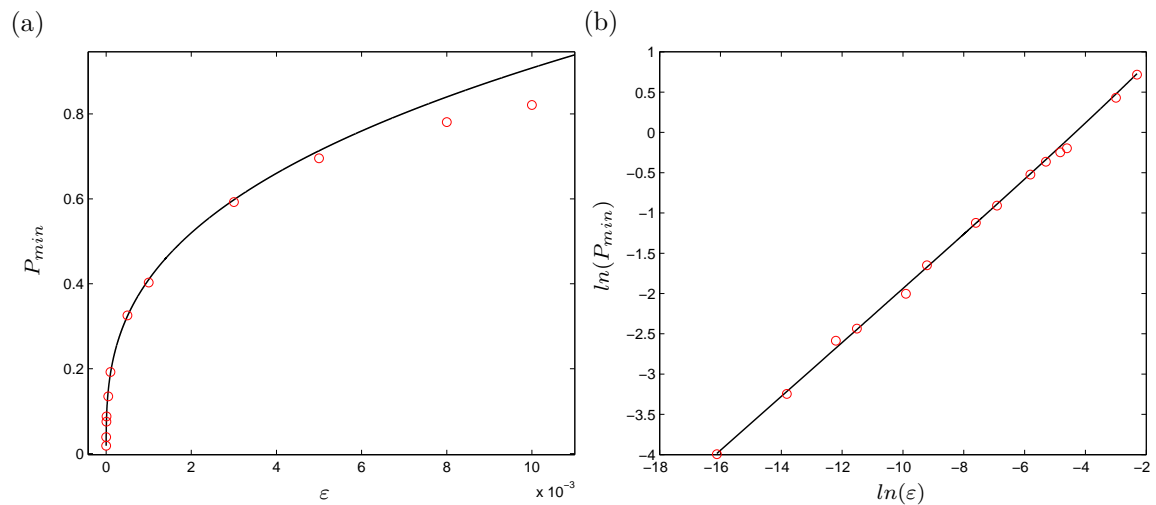


Figure 2.14: Comparison between the values of P minimizing \mathcal{I}^ε for several discrete values in the range I_ε (red circles) and the period law (2.3) (black line). (a) Zoom on the range $[10^{-7}, 10^{-2}]$, where it is expected that large values of ε tend to deviate from the $\mathcal{O}(\varepsilon^{1/3})$ leading-order scaling, while for low values the scaling agrees. (b) The same plot as in (a) on a log-log scale.

class of singular periodic orbits based upon a fast-slow decomposition approach and we have shown that these orbits persist for ε small.

The geometric insight was used to determine a starting solution for numerical continuation in the context of a reduced three-dimensional fast-slow system. Then we studied the dependence of periodic orbits on the singular perturbation parameter as well as the Hamiltonian energy level set parameter arising in the reduction from a four- to a three-dimensional system. The parameter space is structured by several fold points. Furthermore, we were able to study the shape of non-minimizing periodic orbits for very broad classes of parameters. Finally, we showed that several natural scaling laws for non-minimizing sequences of periodic solutions exist and also confirmed numerically the leading-order scaling predicted by Müller for minimizing sequences.

Based upon this work, there are several open problems as well as generalizations one might consider. In particular, it would be desirable to extend the persistence result to the general class of singularly-perturbed Hamiltonian fast-slow systems (2.10); this is the subject of ongoing work.

Another important observation of our numerical study are the intricate orbits that seem to arise when parts of the slow segments start to interact with the singularities \mathcal{L}_\pm where the critical manifold is not normally hyperbolic. The natural conjecture is that the additional small fast loops that we observe numerically could correspond to homoclinic “excursions” in the fast subsystem anchored at points close to \mathcal{L}_\pm . The blow-up method [21] is likely to provide an excellent tool to resolve the non-normally hyperbolic singularities; see e.g. [41, 47] where the existence of complicated fast-slow periodic orbits involving loss of normal hyperbolicity is proven.

The construction of an initial orbit has been one of the hardest problems to tackle. It was solved using analytical and numerical tools, after discarding several other plausible approaches. The SMST algorithm [27] has been a helpful tool to determine good starting points on the slow manifolds and then use an initial value solver to obtain segments of a complete whole orbit. Although our approach works well in practical computations, there are interesting deep numerical analysis questions still to be answered regarding the

interplay between certain classes of fast-slow “initial guess” starting orbits and the success or failure of Newton-type methods for the associated BVPs. In particular, can one prove certain geometric conditions or restrictions on ε to guarantee the convergence for the first solution?

Another highly relevant direction would be to extend our approach to more general classes of functionals. There are many different singularly-perturbed variational problems, arising e.g. in materials science, to which one may apply the techniques presented here. In this context, it is important to emphasize that we expect that particularly other non-convex functionals could be excellent candidates for future work.

From the viewpoint of applications, it would be interesting to study the practical relevance of non-minimizing sequences of periodic solutions. Although we expect the long-term behavior to be governed by minimizers, it is evident that non-minimizing periodic orbits can have a high impact on time-dependent dynamics, e.g., either via transient behavior, via noise-induced phase transitions, or as dynamical boundaries between different regimes.

3 Singular perturbation analysis of a regularized MEMS model

3.1 Introduction

Micro-Electro Mechanical Systems (MEMS) are very small structures that combine electrical and mechanical components on a common substrate to perform various tasks. In particular, electrostatic-elastic devices find important applications in drug-delivery [77], micro pumps [34], optics [17] and micro-scale actuators [81]. Such devices are structured as follows: an elastic membrane is allowed to deflect above a ground plate under the action of an electric potential V , where the diameter of both objects is assumed to be much smaller than their distance. When a critical threshold V^* (“*pull-in voltage*”) is reached, a phenomenon called *touchdown* or *snap-through* can occur, i.e., the membrane enters into contact with the ground plate and the system undergoes a short circuit. The physical forces acting between the elastic components of the device – which can, *e.g.*, be of Casimir or Van der Waals type – lead to *stiction*, which causes complications in reverting the process in order to return to the original state. In the canonical mathematical models proposed in the literature [32, 50, 63, 64], this situation is described by a parabolic partial differential equation (PDE) with a singular source term. The touchdown phenomenon leads to non-existence of steady states and/or blow-up of solutions in finite time. Hence, no information on post-touchdown configurations can be captured.

Recently, an extension of the model has been proposed, where the introduction of a potential mimicking the effect of a thin insulating layer above the ground plate prevents physical contacts between the elastic membrane and the substrate [54]. Mathematically,

this corresponds to the addition of a nonlinear source term to the PDE that depends on a small “regularization” parameter ε . For devices whose deflecting surface is represented by either a membrane or a beam, the resulting regularized models have been studied in relevant works by Lindsay *et al.*. The first case is modeled by a second-order PDE [54, 55], while the case of a beam [54, 51, 57, 55, 53] is described by a fourth-order PDE. In one space dimension, these correspond to:

Membrane: (3.1)

$$u_t = u_{xx} - \frac{\lambda}{(1+u)^2} + \frac{\lambda\varepsilon^{m-2}}{(1+u)^m} \quad \text{for } x \in [-1, 1], \text{ with } u = 0 \text{ when } x = \pm 1; \quad (3.2)$$

Beam: (3.3)

$$u_t = -u_{xxxx} - \frac{\lambda}{(1+u)^2} + \frac{\lambda\varepsilon^{m-2}}{(1+u)^m} \quad \text{for } x \in [-1, 1], \text{ with } u = \partial_n u = 0 \text{ when } x = \pm 1. \quad (3.4)$$

Physically speaking, the variable u denotes the (dimensionless) deflection of the surface, while the parameter λ is proportional to the square of the applied voltage V . The regularizing term $\lambda\varepsilon^{m-2}(1+u)^{-m}$ with $m > 2$ accounts for several physical effects of particular relevance in proximity of $u = -1$. In the following we will consider $m = 4$, corresponding to a Casimir effect; alternative choices describe other physical phenomena and can be studied in a similar fashion. This term induces a potential which simulates the effect of an insulating layer above the ground plate, whose nondimensional width is proportional to ε .

In this work, we focus our attention on the steady states solutions of the Laplacian case corresponding to Equation (3.2):

$$u_{xx} = \frac{\lambda}{(1+u)^2} \left[1 - \frac{\varepsilon^2}{(1+u)^2} \right], \quad \text{for } x \in [-1, 1], \text{ with } u = 0 \text{ when } x = \pm 1. \quad (3.5)$$

For the literature concerning the bi-Laplacian case (3.4) we refer to [54, 55, 52].

Due to the symmetry of the boundary value problem (3.5) under the transformation $x \rightarrow -x$, all solutions of (3.5) are even. We could not find a coincide reference for this result and therefore include a proof for completeness.

Lemma 3.1.1. *Let us consider generic equations of the type*

$$u'' = f(u), \quad x \in [-a, a], \quad a > 0, \quad (3.6a)$$

$$u(\pm a) = u_0, \quad u_0 \in \mathbb{R}, \quad (3.6b)$$

where $f \in C^1$. Then, all functions u which solve (3.6) are even and satisfy $u'(0) = 0$.

Proof. Equation (3.6) can be rewritten as the system

$$u' = w, \quad (3.7a)$$

$$w' = f(u), \quad (3.7b)$$

$$u(\pm a) = u_0. \quad (3.7c)$$

System (3.7) is Hamiltonian, with the energy function given by

$$H(u, w) = \frac{w^2}{2} - F(u), \quad (3.8)$$

where F is the primitive of f , i.e., $F' = f$. This implies that the energy $H(u, u')$ associated to a solution (u, u') of (3.7) stays constant on the interval $[-a, a]$.

Let us consider (u, u') solution of (3.7). Then, there exists $\mu \in \mathbb{R}$ such that $H(u, u') = \mu \quad \forall x \in [-a, a]$, i.e.,

$$\frac{(u'(x))^2}{2} - F(u(x)) = \mu \quad \forall x \in [-a, a]. \quad (3.9)$$

In particular $H(u(-a), u'(-a)) = H(u(a), u'(a))$, i.e.,

$$\frac{(u'(-a))^2}{2} - F(u(-a)) = \frac{(u'(a))^2}{2} - F(u(a)). \quad (3.10)$$

Thanks to the boundary conditions (3.7c) we have $F(u(-a)) = F(u(a))$. Hence, Equation (3.10) implies

$$(u'(-a))^2 = (u'(a))^2. \quad (3.11)$$

Let us now consider $v(x) := u(-x)$. If u is a solution, so is v , thanks to the invariance of System (3.7) under the transformation $(u, w, x) \mapsto (u, -w, -x)$. Hence, there exists $\nu \in \mathbb{R}$ such that $H(v, v') = \nu \quad \forall x \in [-a, a]$, i.e.,

$$\frac{(v'(x))^2}{2} - F(v(x)) = \nu \quad \forall x \in [-a, a]. \quad (3.12)$$

Our goal is to prove that $\mu = \nu$. On every level curve of H there can in fact be only one solution of (3.7), so if u and v lie in the same level curve, it must be $u(x) = v(x)$, *i.e.*, $u(x) = u(-x) \quad \forall x \in [-a, a]$.

From (3.12) it follows that at $x = a$:

$$\frac{(v'(a))^2}{2} - F(v(a)) = \nu. \quad (3.13)$$

Thanks to (3.11) and (3.7c) we have

$$\begin{aligned} (v'(a))^2 &= (-u'(-a))^2 = (u'(-a))^2 = (u'(a))^2, \\ F(v(a)) &= F(u(-a)) = F(u(a)). \end{aligned} \quad (3.14)$$

Combining (3.13) and (3.14) it hence follows

$$\nu = \frac{(v'(a))^2}{2} - F(v(a)) = \frac{(u'(a))^2}{2} - F(u(a)) = H(u(a), u'(a)) = \mu, \quad (3.15)$$

as we wanted to prove.

Finally, the result $u'(0) = 0$ straightly follows from even functions' properties. \square

In order to understand the novelties of the regularized model, we briefly summarize the main properties of the non-regularized case corresponding to $\varepsilon = 0$, which are well understood [63, 64]. The bifurcation diagram associated to (3.5) shown in Figure 3.1(a) contains two branches of equilibria, the lower one consisting of stable steady states and the upper one of unstable steady states, separated by a fold point located at $\lambda = \lambda^*$. For $\lambda > \lambda^*$, steady-state solutions of (3.2) cease to exist and the transient dynamics lead to a blow up of the solutions in finite time. Some solutions along these two branches are plotted in Figure 3.1(b). In addition, a piecewise linear singular solution existing for $\lambda = 0$ is also shown. For the singular solution, touchdown occurs at $x = 0$.

The inclusion of the ε -dependent regularizing term, where $0 < \varepsilon \ll 1$, considerably changes the structure of the bifurcation diagram. The main difference is the development of a third branch of stable equilibria which leads to the S -shaped curve shown in Figure 3.2(a). Additionally to the fact that the fold point λ^* is now depending on ε , there exists an additional fold point λ_* (also ε -dependent) such that for $\lambda_* < \lambda < \lambda^*$ three equilibria exist, while for $\lambda < \lambda_*$ and $\lambda > \lambda^*$ there is a unique stable equilibrium. In contrast to

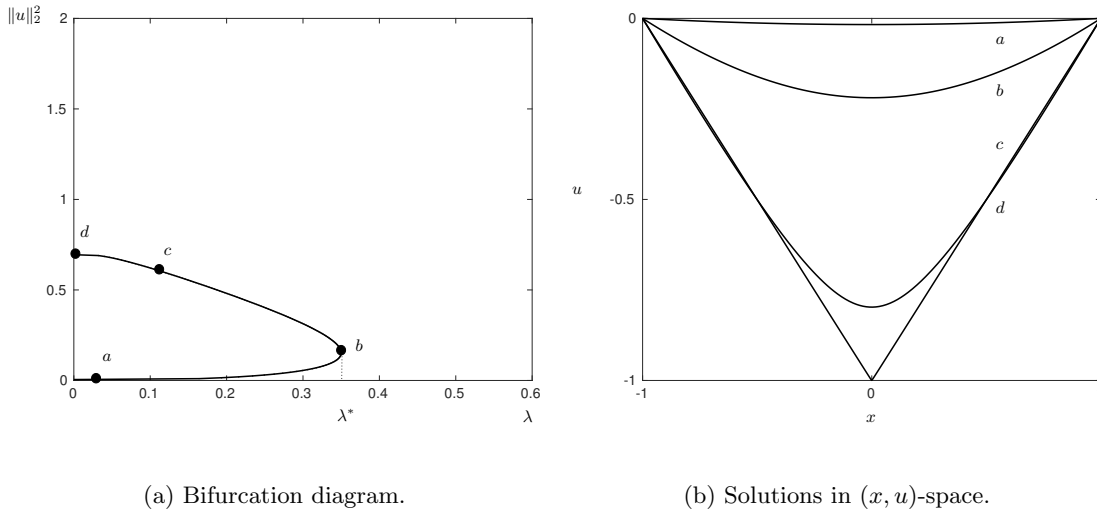


Figure 3.1: (a) Bifurcation diagram of the membrane model, Equation (3.5), for $\varepsilon = 0$. The lower and upper branch correspond to stable and unstable equilibrium solutions, respectively. The point d corresponds to $(0, \frac{2}{3})$ and represents the singular solution for $\lambda = 0$. (b) Corresponding solutions in (x, u) space.

the non-regularized case, numerical computations indicate that a stable equilibrium exists for every value of $\lambda > 0$ [54]. Solutions on the newly emerged branch in the bifurcation diagram are in fact bounded below by $u = -1 + \varepsilon$. For increasing λ , the solution has an increasing “flat” portion close to $u = -1 + \varepsilon$; cf. solution d in Figure 3.2(b).

Remark 1. Figures 3.1, 3.2 correspond to numerical computations performed with the algorithm developed by Lindsay in [54].

For very small values of ε , the diagram is difficult to resolve, even numerically, due to its highly singular character. The singular nature of the bifurcation diagram, as well as the influence of the regularization parameter ε on the structure thereof, are the principal features of interest. In this chapter, we focus on a detailed analysis of the singular dependence of the bifurcation diagram for Equation (3.5) on ε . To this aim, we first reformulate the problem in a dynamical systems framework and identify two main parameters in the equations, which leads to a 2-parameter singular perturbation problem. A detailed asymptotic resolution of the structure of the corresponding $(\lambda, \|u\|_2^2)$ -bifurcation diagram – both

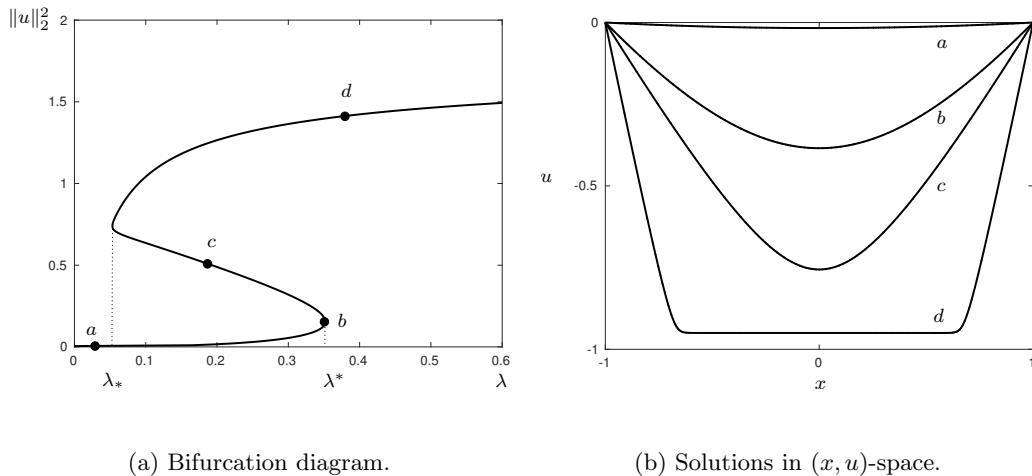


Figure 3.2: (a) Numerically computed bifurcation diagram of the one-dimensional membrane model, Equation (3.5), for $\varepsilon = 0.05$. (b) Corresponding solutions in (x, u) space.

in the singular limit of $\varepsilon = 0$ and for ε positive and sufficiently small – is accomplished through separate investigation of three distinguished (overlapping) regions. This will allow us to show how the third branch emerges from the singular limit $\varepsilon = 0$ and to identify the corresponding limiting solutions.

In all scenarios, we show existence and uniqueness of solutions close to the corresponding limiting solutions and prove the validity of the corresponding part of the bifurcation diagram. While the three regions share some common features, we argue that they need to be investigated separately for their dynamics to be fully resolved. Our analysis is based on a variety of dynamical systems techniques, principally, on geometric singular perturbation theory [22, 35, 46] and the blow-up technique [20, 21]. In particular, a combination of these methods allows us to perform a detailed study of the saddle-node bifurcation at λ_* and to calculate its asymptotic expansion in (3.5), which has been studied by Lindsay by the method of matched asymptotic expansions [54]; cf. Figure 12 therein, as well as Figure 3.2(a). The coefficients of the leading order terms of the expansion are explicitly computed. In the process, it is shown that the occurrence of logarithmic switchback terms in the steady-state asymptotics for Equation (3.5), which has also been observed via

matched asymptotic expansions in [54], is due to a resonance phenomenon in one of the coordinate charts after blow-up [66] (cf. Section 3.5).

In summary, our principal result can be expressed as

Theorem 3.1.1. *For $\varepsilon \in (0, \varepsilon_0)$, with ε_0 positive and sufficiently small, and $\lambda \in [0, \Lambda]$, with $\Lambda = \mathcal{O}(1)$ positive and fixed, the bifurcation diagram for Equation (3.2) is as illustrated in Figure 3.2(a).*

Without loss of generality we fix $\Lambda = 1$. The proof of Theorem 3.1.1 follows from a combination of Propositions 3.4.2, 3.4.5, and 3.4.6 below, each of which pertains to one of the three regions which have been mentioned above.

This chapter is structured as follows: in Section 3.2, we reformulate Equation (3.5) as a dynamical system, and we state our main result. In Section 3.3, we introduce the principal blow-up transformation on which our analysis of the dynamics of (3.5) close to the touchdown singularity is based. In Section 3.4, we describe in detail the structure of the corresponding bifurcation diagram by separately investigating three main regions, as illustrated in Figure 3.8. In Section 3.5, we derive the logarithmic switchback terms as a consequence of a resonance phenomenon. Finally, in Section 3.6, we discuss our findings, and present an outlook to future research.

3.2 Dynamical Systems Formulation

We consider the steady state equation for the regularized membrane model, Equation (3.5), as introduced by Lindsay *et al.* in [54] for $m = 4$.

To allow for an application of the various techniques from the theory of dynamical systems on which our analysis is based, we rewrite (3.5) as a first-order system of ordinary differential equations (ODEs) by introducing the new variable $w = u'$, and by including the trivial dynamics of both the regularizing parameter ε and the spatial variable x , which

we relabel as ξ :

$$u' = w, \tag{3.16a}$$

$$w' = \frac{\lambda}{(1+u)^2} \left[1 - \frac{\varepsilon^2}{(1+u)^2} \right], \tag{3.16b}$$

$$\xi' = 1, \tag{3.16c}$$

$$\varepsilon' = 0; \tag{3.16d}$$

here, the prime denotes differentiation with respect to x . Next, we multiply the right-hand sides in Equation (3.16) with a factor of $(1+u)^4$, which allows us to desingularize the corresponding flow near the touchdown singularity at $u = -1$ ¹. Finally, we define a shift in u via $\tilde{u} = 1 + u$, which translates that singularity to $\tilde{u} = 0$.

Omitting the tilde and still denoting differentiation with respect to the new independent variable by a prime, as before, we obtain the system

$$u' = u^4 w, \tag{3.17a}$$

$$w' = \lambda(u^2 - \varepsilon^2), \tag{3.17b}$$

$$\xi' = u^4, \tag{3.17c}$$

$$\varepsilon' = 0, \tag{3.17d}$$

in (u, w, ξ, ε) -space with parameter λ subject to the boundary conditions

$$u = 1 \quad \text{for } \xi = \mp 1. \tag{3.18}$$

Since $\varepsilon \ll 1$, it is a natural idea to use perturbation methods to construct solutions of (3.17), (3.18). Despite the apparent simplicity of the equations, this turns out to be a nontrivial task. For $\varepsilon = 0$, System (3.17) can be solved explicitly and admits degenerate equilibria at $u = 0$, which corresponds to the touchdown singularity $u = -1$ in the original model. We denote this manifold of equilibria as

$$\mathcal{S}^0 = \{(0, w, \xi, 0) \mid w \in \mathbb{R}, \xi \in \mathbb{R}\}. \tag{3.19}$$

¹The multiplication corresponds to a transformation of the independent variable which leaves the phase portrait of (3.16) unchanged for $u > -1$, since in that case the factor $(1+u)^4$ is positive throughout.

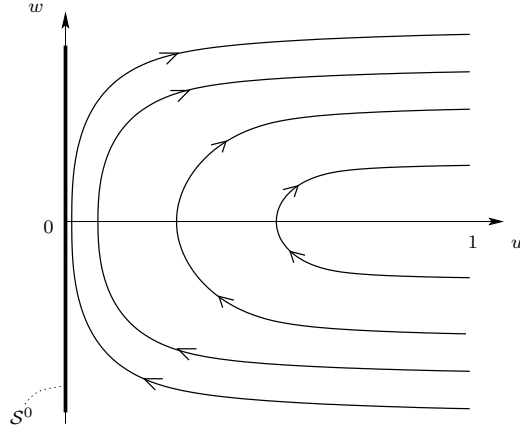


Figure 3.3: Projection of the $\varepsilon = 0$ flow for Equations (3.17) into the (u, w) -space for $\lambda \neq 0$. The solid black line corresponds to the invariant manifold \mathcal{S}^0 defined in (3.19). In view of the boundary conditions in (3.18), we consider solutions starting from $u = 1$. All solutions stay to the right of \mathcal{S}^0 ; those with initial large w -value get arbitrarily close to it, but still never reach it. Hence, singular orbits are not transverse to \mathcal{S}^0 .

One complication is introduced by the fact that, for $\lambda \neq 0$, the singular flow of (3.17) in the (u, w) -space that is obtained for $\varepsilon = 0$ is not transverse to \mathcal{S}^0 , cf. Figure 3.3. As outlined in Chapter 1, transversality is a necessary requirement to build solutions of (3.5) by means of geometric tools [22, 46]. Therefore, we need to find a way to remedy this lack of transversality.

For $\lambda = 0$ in (3.17), the singular flow changes and becomes even more degenerate (see Figure 3.4). Furthermore, the set

$$\mathcal{M}^0 := \{(u, 0, \xi, 0) \mid u \in \mathbb{R}^+, \xi \in \mathbb{R}\} \quad (3.20)$$

now also represents a set of equilibria for Equations (3.17a), (3.17b).

As it turns out, a good strategy is to first introduce the following rescaling of w :

$$w = \frac{\tilde{w}}{\delta}, \quad (3.21)$$

where

$$\delta = \sqrt{\frac{\varepsilon}{\lambda}} \quad (3.22)$$

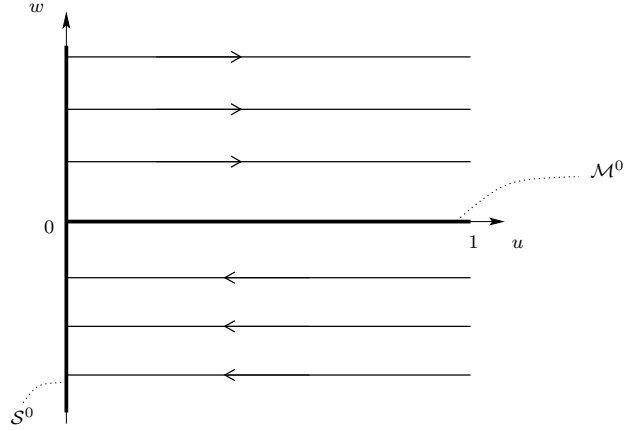


Figure 3.4: Singular flow for Equations (3.23) in (u, w) -space for $\lambda = 0$. The solid black lines corresponds to the invariant manifolds \mathcal{S}^0 and \mathcal{M}^0 defined in (3.19) and (3.20), respectively. Orbits with $w \neq 0$ in the (u, w) -space are now transverse to \mathcal{S}^0 . For $w < 0$, they tend to \mathcal{S}^0 , while for $w > 0$ they move away from it. All these equilibria are nonhyperbolic, the corresponding linearizations of the u, w equations (3.17a), (3.17b) have a double zero eigenvalue.

is a nonnegative parameter.

Remark 2. The scaling of w by $\sqrt{\lambda}$ in (3.21) moves λ from (3.17b) to the equation for ξ (3.17c) (after a rescaling of time). The scaling by $1/\sqrt{\varepsilon}$ in (3.21) reflects the fact that, for $\lambda = \mathcal{O}(1)$, $w = \mathcal{O}(\varepsilon^{-\frac{1}{2}})$ (in agreement with numerical computations and asymptotic analysis performed in [54]).

Remark 3. Some parts of our analysis are more conveniently carried out by using the parameters ε and λ , while others by using parameters ε and δ . Hence, we will often switch between these two descriptions.

Substituting (3.21) into (3.17), multiplying the right-hand sides in the resulting equations with a factor of δ , omitting the tilde and retaining the prime for differentiation with respect

to the new independent variable, as before, we find

$$u' = u^4 w, \tag{3.23a}$$

$$w' = \varepsilon(u^2 - \varepsilon^2), \tag{3.23b}$$

$$\xi' = \delta u^4, \tag{3.23c}$$

$$\varepsilon' = 0, \tag{3.23d}$$

still subject to the boundary conditions in (3.18).

Equations (3.23) with boundary conditions (3.18) will form the basis for the following analysis.

Solutions of the boundary value problem will be constructed by the following two strategies. The first one consists of considering two sets of boundary conditions corresponding to a suitable interval of w values for $x = -1$ and $x = 1$. Following the set of boundary conditions given at $x = -1$ by the flow forward and the set of boundary conditions given at $x = 1$ backwards, we obtain two sets at $x = 0$ and we check the transversality of their intersection. Each initial w -value w_0 for which these two manifolds intersect gives a solution of the boundary value problem (3.23), (3.18).

Since all solutions of the boundary value problem (3.23), (3.18) are even (cf. Lemma 3.1.1), another possible strategy consists of considering the boundary value problem (3.23) on the interval $[-1, 0]$ with boundary conditions $u(-1) = 1$ and $w(0) = 0$. The intrinsic symmetry of the problem is also clearly visible in Figure 3.2(b). We track the flow of a manifold of initial conditions with $\xi = -1$ and $u = 1$ but arbitrary initial w -value w_0 up to the hyperplane $\{w = 0\}$. We parametrize this manifold by $u(w, \varepsilon, \delta, w_0)$ and $\xi(w, \varepsilon, \delta, w_0)$. The unique “correct” value $w_0(\varepsilon, \delta)$ leading to a solution of the boundary value problem (3.23), (3.18) is then obtained by solving $\xi(w_0, \varepsilon, \delta) = 0$ when $w(w_0, \varepsilon, \delta) = 0$. More details will be presented in the individual proofs. Because of Lemma 3.1.1, all solutions of the boundary value problem (3.23), (3.18) can be obtained with this strategy.

Equation (3.23) constitutes a two-parameter fast-slow system in its fast formulation (for an overview on fast-slow systems, we refer to Chapter 1). The parameter $\varepsilon \ll 1$ is the main singular perturbation parameter, while the case $\delta \rightarrow 0$ is also singular. For $\delta = \mathcal{O}(1)$, the variables u and ξ are fast, while w is slow. For δ small, however, the variable ξ is also slow.

The manifold \mathcal{S}^0 defined in (3.19) is still invariant under the flow of (3.23). Furthermore, for $\delta = 0$ the manifold \mathcal{M}^0 defined in (3.20) now also represents a set of equilibria for (3.23). We remark that the same scenario occurs for $\lambda = 0$ in (3.17).

Setting $\varepsilon = 0$ in Equation (3.23), we obtain the so-called “layer problem”

$$u' = u^4 w, \tag{3.24a}$$

$$w' = 0, \tag{3.24b}$$

$$\xi' = \delta u^4, \tag{3.24c}$$

$$\varepsilon' = 0. \tag{3.24d}$$

See Figure 3.4 for an illustration of the corresponding phase portrait in (u, w) -space and, in particular, of transversality of orbits of the layer problem to \mathcal{S}^0 . Rescaling the independent variable in (3.23) by multiplying it by ε yields the slow formulation

$$\varepsilon \dot{u} = u^4 w, \tag{3.25a}$$

$$\dot{w} = u^2 - \varepsilon^2, \tag{3.25b}$$

$$\varepsilon \dot{\xi} = \delta u^4, \tag{3.25c}$$

$$\varepsilon' = 0. \tag{3.25d}$$

The “reduced” problem, which is found by taking $\varepsilon \rightarrow 0$ in (3.25), is

$$0 = u^4 w, \tag{3.26a}$$

$$\dot{w} = u^2, \tag{3.26b}$$

$$0 = \delta u^4, \tag{3.26c}$$

$$\varepsilon' = 0. \tag{3.26d}$$

The manifolds \mathcal{S}^0 in (3.19) and \mathcal{M}^0 in (3.20) for $\delta = 0$ now represent two branches of the “critical manifold” for Equation (3.23); however, neither branch is normally hyperbolic, as the Jacobian of the linearization of the layer flow about both \mathcal{S}^0 and \mathcal{M}^0 is nilpotent. Moreover, as is obvious from (3.26), the reduced flow on \mathcal{S}^0 vanishes, hence is very degenerate. Therefore, standard GSPT does not apply directly (cf. Chapter 1).

The underlying non-hyperbolicity can be remedied by means of the *blow-up method*, or “geometric desingularization” [20, 21, 44, 45]. A blow-up with respect to ε will allow us to

describe the dynamics of (3.17) in a neighbourhood of the manifold \mathcal{S}^0 (cf. Section 3.3). Additionally, a blow-up including δ is needed to desingularize the flow in the vicinity of \mathcal{M}^0 (cf. Section 3.4.3 below). Our analysis relies on a number of dynamical systems techniques, such as classical GSPT [22], normal form transformations [82], and the Exchange Lemma [72, 46], the combination of which will result in precise and rigorous asymptotics for Equation (3.23).

To find the appropriate blow-up transformation, we focus on Equations (3.23a), (3.23b), which for $\varepsilon > 0$ has two saddle equilibria $(\pm\varepsilon, 0)$. As we focus our attention on $u \geq 0$, we consider the positive equilibrium only. The scaling $u = \varepsilon\tilde{u}$ transforms Equations (3.23a), (3.23b) into

$$\begin{aligned}\tilde{u}' &= \varepsilon^3 \tilde{u}^4 w, \\ w' &= \varepsilon^3 (\tilde{u}^2 - 1),\end{aligned}$$

which turn into the integrable system

$$\tilde{u}' = \tilde{u}^4 w, \tag{3.27a}$$

$$w' = \tilde{u}^2 - 1, \tag{3.27b}$$

after dividing out the common factor ε^3 . The saddle equilibrium $(1, 0)$ together with its stable and unstable manifolds will play a crucial role in the following. The line $\tilde{u} = 0$ is invariant, with w decreasing on it. The corresponding phase portrait is shown in Figure 3.5.

3.3 Geometric Desingularization (“Blow-Up”)

In this section, we apply the blow-up method (described in more details in Chapter 1) to our problem. In particular, we define the blow-up transformation that will allow us to desingularize the flow of Equation (3.23) near the non-hyperbolic manifold \mathcal{S}^0 . The arguments at the end of Section 3.2 suggest the blow-up:

$$u = \bar{r}\bar{u}, \quad w = \bar{w}, \quad \xi = \bar{\xi}, \quad \varepsilon = \bar{r}\bar{\varepsilon}, \tag{3.28}$$

where $(\bar{w}, \bar{\xi}) \in \mathbb{R}^2$ and $(\bar{u}, \bar{\varepsilon}) \in S^1$, *i.e.*, $\bar{u}^2 + \bar{\varepsilon}^2 = 1$. Note that the singularity $(u, \varepsilon) = (0, 0)$ is blown up to the circle $\bar{r} = 0$. We emphasize that we do not blow up the variables w or ξ .

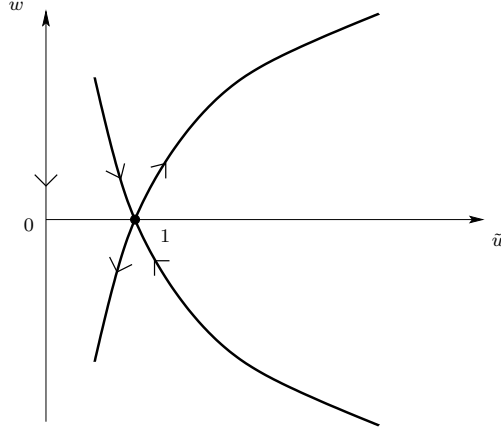


Figure 3.5: The saddle point $(1, 0)$ of System (3.27) and its stable and unstable manifolds.

The vector field that is induced by (3.23) on the cylindrical manifold in $(\bar{u}, \bar{w}, \bar{\xi}, \bar{\varepsilon}, \bar{r})$ -space is best described in coordinate charts. We require two charts here, K_1 and K_2 , which are defined by $\bar{u} = 1$ and $\bar{\varepsilon} = 1$, respectively:

$$K_1 : (u, w, \xi, \varepsilon) = (r_1, w_1, \xi_1, r_1 \varepsilon_1), \quad (3.29a)$$

$$K_2 : (u, w, \xi, \varepsilon) = (r_2 u_2, w_2, \xi_2, r_2). \quad (3.29b)$$

Remark 4. The phase-directional chart K_1 describes the “outer” region, *i.e.*, the part of the orbits approaching \mathcal{S}^0 – which corresponds to the transient from $u = 1$ to $u = 0$ – while the rescaling chart K_2 (also known as *scaling chart*) covers the “inner” region $u \approx 0$ in the context of Equation (3.23). In particular, in chart K_2 we recover Equation (3.27).

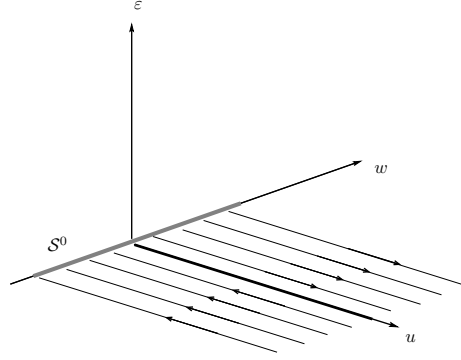
The transition map κ_{12} between charts K_1 and K_2 , *i.e.*, the change of coordinates between them can be written as

$$\kappa_{12} : (u_2, w_2, \xi_2, r_2) = (\varepsilon_1^{-1}, w_1, \xi_1, r_1 \varepsilon_1), \quad (3.30)$$

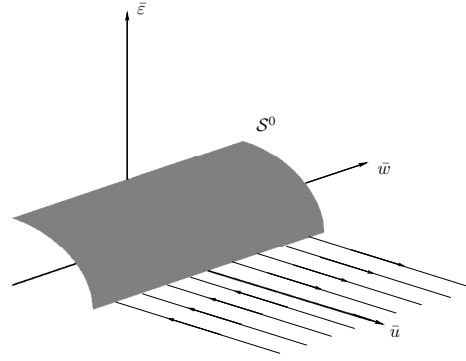
while its inverse κ_{21} is given by

$$\kappa_{21} : (r_1, w_1, \xi_1, \varepsilon_1) = (r_2 u_2, w_2, \xi_2, u_2^{-1}). \quad (3.31)$$

Finally, we define various sections for the blown-up vector field, which will be used through-



(a) Flow in (u, w, ε) -space; the thick gray line represents the critical manifold \mathcal{S}^0 .



(b) Geometry in blown-up $(\bar{u}, \bar{w}, \bar{\varepsilon})$ -space; \mathcal{S}^0 is now represented by the cylinder corresponding to $\bar{u}^2 + \bar{\varepsilon}^2 = 1$.

Figure 3.6: Flow of Equation (3.23) for $\varepsilon = 0$ before and after the blow-up in (3.28).

out the following analysis: in K_1 , we will require the entry and exit sections

$$\Sigma_1^{\text{in}} := \{(\rho, w_1, \xi_1, \varepsilon_1) \mid w_1 \in [w_-, w_+], \xi_1 \in [\xi_-, \xi_+], \text{ and } \varepsilon_1 \in [0, \sigma]\}, \quad (3.32a)$$

$$\Sigma_1^{\text{out}} := \{(r_1, w_1, \xi_1, \sigma) \mid r_1 \in [0, \rho], w_1 \in [w_-, w_+], \text{ and } \xi_1 \in [\xi_-, \xi_+]\}, \quad (3.32b)$$

where $0 < \rho < 1$ and $0 < \sigma < 1$ are appropriately defined constants, while $w_{l,r}$ and $\xi_{l,r}$ are real constants. Similarly, in chart K_2 , we will employ the section

$$\Sigma_2^{\text{in}} := \{(\sigma^{-1}, w_2, \xi_2, r_2) \mid w_2 \in [w_-, w_+], \xi_2 \in [\xi_-, \xi_+], \text{ and } r_2 \in [0, \rho\sigma]\}; \quad (3.33)$$

here, we note that $\Sigma_2^{\text{in}} = \kappa_{21}(\Sigma_1^{\text{out}})$.

Remark 5. In the following, we will index a general variable z in blown-up space with \bar{z} . In charts K_i , $i = 1, 2$ it will instead be labeled with the corresponding subscript z_i .

3.3.1 Dynamics in chart K_1

To obtain the equations in K_1 , we substitute the transformation from (3.29a) into Equation (3.23). A short computation gives

$$r_1' = r_1^4 w_1, \quad (3.34a)$$

$$w_1' = r_1^3 \varepsilon_1 (1 - \varepsilon_1^2), \quad (3.34b)$$

$$\xi_1' = \delta r_1^4, \quad (3.34c)$$

$$\varepsilon_1' = -r_1^3 \varepsilon_1 w_1. \quad (3.34d)$$

Since $\varepsilon = r_1 \varepsilon_1$, the singular limit $\varepsilon = 0$ corresponds to the restriction of the flow of (3.34) to one of the invariant planes $\{r_1 = 0\}$ or $\{\varepsilon_1 = 0\}$. In order to obtain a non-vanishing vector field for $r_1 = 0$, we desingularize Equation (3.34) by dividing out a factor of r_1^3 from the right-hand sides, which again represents a rescaling of the independent variable:

$$r_1' = r_1 w_1, \quad (3.35a)$$

$$w_1' = \varepsilon_1 (1 - \varepsilon_1^2), \quad (3.35b)$$

$$\xi_1' = \delta r_1, \quad (3.35c)$$

$$\varepsilon_1' = -\varepsilon_1 w_1. \quad (3.35d)$$

3.3.2 Dynamics in chart K_2

The equations in K_2 are obtained by substituting the transformation in (3.29b) into (3.23), which yields

$$u'_2 = r_2^3 u_2^4 w_2, \quad (3.36a)$$

$$w'_2 = r_2^3 (u_2^2 - 1), \quad (3.36b)$$

$$\xi'_2 = \delta r_2^4 u_2^4. \quad (3.36c)$$

$$r'_2 = 0. \quad (3.36d)$$

Desingularizing as before, by dividing out a factor of r_2^3 from the right-hand sides in (3.36), we find

$$u'_2 = u_2^4 w_2, \quad (3.37a)$$

$$w'_2 = u_2^2 - 1, \quad (3.37b)$$

$$\xi'_2 = \delta r_2 u_2^4, \quad (3.37c)$$

$$r'_2 = 0. \quad (3.37d)$$

Note that Equations (3.37a),(3.37b) correspond to System (3.27).

3.4 Analysis of the Bifurcation Diagram

In this section, we establish the bifurcation diagram in Figure 3.2(a) by analyzing existence and uniqueness of solutions to Equation (3.23) subject to the boundary conditions (3.18) for ε positive and sufficiently small. All solutions of the boundary value problem arise as perturbations of certain limiting solutions obtained from various limiting $\varepsilon = 0$ problems. We denote these limiting solutions as singular solutions, as usual in GSPT (see Chapters 1, 2). The approach adopted thereby is the following: first, singular solutions are constructed by analyzing the dynamics in charts K_1 and K_2 separately in the limit $\varepsilon \rightarrow 0$. Then, the persistence of singular solutions for non-zero ε is shown via the shooting argument outlined in Section 3.2 that relies on the transversality of the geometric objects involved. This translates to the existence of solutions of the boundary value problem along the curve shown in the bifurcation diagram (cf. Figure 3.2(a)).

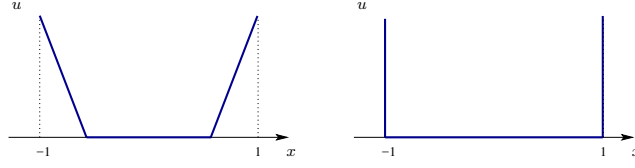
Definition 3.4.1. We distinguish three types of singular solutions of Equation (3.23) (See Figure 3.7):

Type I. Solutions of type I satisfy $u = 0$ for $x \in I$, where I is an interval centered at $x = 0$. Consequently, the slope must initially satisfy $|w| > 1$ (in terms of the original w -variable). Type I-solutions will henceforth be depicted in blue. Type I-solutions occur in two forms. The ones corresponding to $\lambda = \mathcal{O}(\varepsilon)$ have constant finite slope w outside of I . The others corresponding to $\lambda = \mathcal{O}(1)$ vanish on $I = (-1, 1)$ and hence the original w is infinite at the boundary.

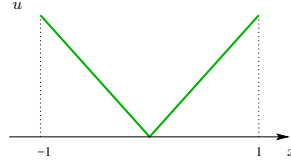
Type II. Solutions of type II are those of slope $w \equiv \mp 1$ (in terms of the original w - variable) that exhibit “touchdown” $u = 0$ at one point only, namely at $\xi = 0$. Type II-solutions will be indicated in green in all subsequent figures.

Type III. Solutions of type III never reach $\{u = 0\}$; hence, no touchdown phenomena occur. These solutions correspond to solutions of the non-regularized problem.

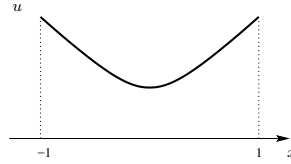
Remark 6. The use of plural in the definition of type II-solutions needs some additional comment. For System (3.17) there exists just one singular solution of type II for $\lambda = 0$ with slope $w = \mp 1$ (see Solution d in Figure 3.1). However, in our blow-up analysis this singular solution corresponds to a one-parameter family of type II-solutions.



(a) Illustration of type I-solutions for $\lambda = \mathcal{O}(\varepsilon)$ (left panel) and $\lambda = \mathcal{O}(1)$ (right panel).



(b) Type II-solutions.



(c) Type III-solutions.

Figure 3.7: Singular solutions corresponding to Definition 3.4.1.

For $\varepsilon > 0$, we divide the bifurcation diagram in $\lambda, \|u\|_2^2$ into three overlapping regions, as shown in Figure 3.8.

Remark 7. From now on, in the context of the bifurcation diagram we refer to the norm $\|u\|_2^2$ in terms of the original variable u in order to be able to compare our analysis with Lindsay's (see Figures 3.1, 3.2).

Region \mathcal{R}_1 is defined as

$$\mathcal{R}_1 := [0, 1] \times \left[\frac{2}{3} + \nu_1, 2 \right], \quad \nu_1 > 0. \quad (3.38)$$

This region covers the upper part of the bifurcation diagram where we find the newly emerged bifurcation branch by perturbing from singular solutions of type I. Region \mathcal{R}_2 ,

defined as

$$\mathcal{R}_2 := [0, \varepsilon\lambda_2] \times \left[\frac{2}{3} - \nu_2, \frac{2}{3} + \nu_2 \right], \quad \lambda_2, \nu_2 > 0, \quad (3.39)$$

(with $\nu_2 > \nu_1$ and λ_2 large but fixed) is a small neighbourhood of the point $(0, \frac{2}{3})$ shown as a rectangle in Figure 3.8. This region shrinks as ε decreases and collapses to the line $\{0\} \times [\frac{2}{3} - \nu_2, \frac{2}{3} + \nu_2]$ as $\varepsilon \rightarrow 0$. The bifurcation curve contained in this transition region is constructed by perturbing from singular solutions of type I and II. Finally, region \mathcal{R}_3 is defined as

$$\mathcal{R}_3 := [0, 1] \times \left[0, \frac{2}{3} + \nu_2 \right] \setminus [0, \varepsilon\lambda_3] \times \left[\frac{2}{3} - \nu_3, \frac{2}{3} + \nu_2 \right], \quad \lambda_3, \nu_3 > 0, \quad (3.40)$$

where $\nu_3 < \nu_2$ and λ_3 again large but fixed, $\lambda_3 < \lambda_2$. This region covers the lower part containing the bifurcation curve which is obtained by perturbing from type II and type III-solutions.

The true meaning of these regions is clearer when we blow-up the bifurcation diagram in parameter space, *i.e.*, with respect to λ and ε , as illustrated in Figure 3.9. (This procedure will also be needed in parts of the following proofs.) To this aim, we first embed the bifurcation diagram in $(\lambda, \|u\|_2^2)$ into \mathbb{R}^3 by including the third variable ε . Then, we blow-up the line $\{(0, 0)\} \times \mathbb{R}$ by introducing $r, \bar{\lambda}$ and $\bar{\varepsilon}$ such that

$$\lambda = r\bar{\lambda}, \quad \varepsilon = r\bar{\varepsilon}, \quad (3.41)$$

with $\bar{\lambda}^2 + \bar{\varepsilon}^2 = 1$, *i.e.*, $(\bar{\lambda}, \bar{\varepsilon}) \in S^1$. In the blown-up space $S^1 \times \mathbb{R} \times \mathbb{R}$, the line $\{(0, 0)\} \times \mathbb{R}$ is hence blown up to a cylinder $S^1 \times \{0\} \times \mathbb{R}$.

In the blown-up space, the singular ($\varepsilon = 0$) bifurcation curve consists of three parts corresponding to type I–III singular solutions (cf. Figure 3.7) shown in blue, green, and black. The black (type III) curve lies in $\bar{\varepsilon} = 0$, the green curve (type II) lies on the cylinder ($r = 0$) with constant value $\|u\|_2^2 = \frac{2}{3}$. The blue curve (type I) has a part on the cylinder (corresponding to $\lambda = \mathcal{O}(\varepsilon)$) and a part in the plane $\{\bar{\varepsilon} = 0\}$ (corresponding to $\lambda = \mathcal{O}(1)$). In the first case, the structure of type I-solutions resembles the one shown in the left panel of Figure 3.7(a). In the second case, type I-solutions are as in the right panel of Figure 3.7(a). These two parts of the bifurcation branch respectively correspond to \mathcal{B}_1 and \mathcal{B}_2 defined in Figure 3.8.

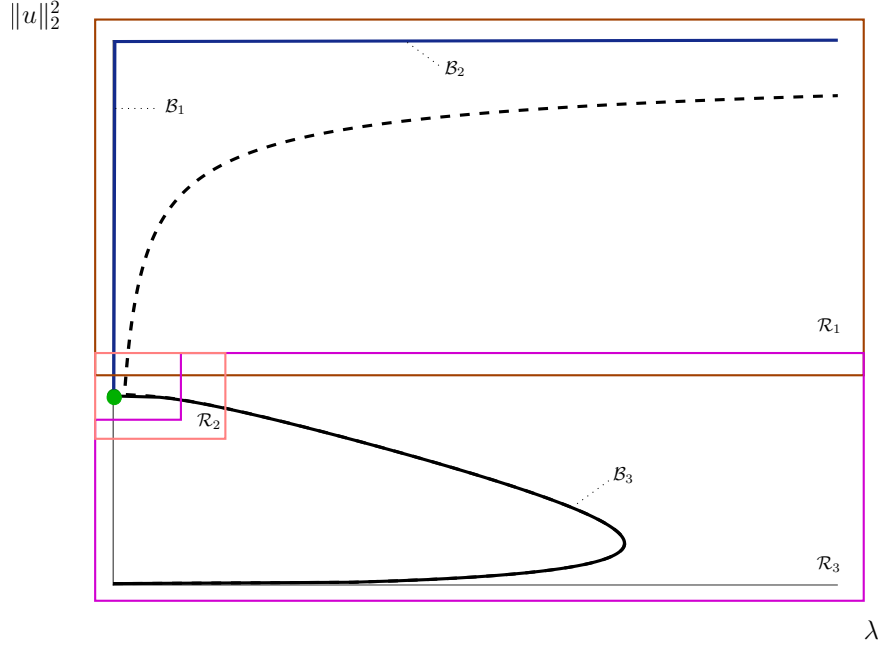


Figure 3.8: The bifurcation diagram is covered by three overlapping regions \mathcal{R}_1 (brown), \mathcal{R}_2 (pink) and \mathcal{R}_3 (magenta) for ε positive (for visibility purposes, the regions have been slightly extended below $\|u\|_2^2 = 0$, above $\|u\|_2^2 = 2$ and to negative λ). (Recall Remark 7 concerning the interpretation of $\|u\|_2^2$ in this context.) The bifurcation curves corresponding to Equations (3.23), (3.18) for $\varepsilon = 0.01$ (dotted curve) and $\varepsilon = 0$ (solid curve) are also displayed. In \mathcal{R}_3 these curves overlap almost completely. For $\varepsilon = 0$, the blue bifurcation branch is given by the union of a vertical part \mathcal{B}_1 corresponding to $\lambda = \mathcal{O}(\varepsilon)$ and a horizontal part \mathcal{B}_2 corresponding to $\lambda = \mathcal{O}(1)$. The green dot at $(0, \frac{2}{3})$ corresponds to the singular solution of type II for $\lambda = 0$ labeled by d in Figure 3.1(a). The black curve, corresponding to the bifurcation curve for the non-regularized model, is labeled with \mathcal{B}_3 . In the limit $\varepsilon \rightarrow 0$, \mathcal{R}_2 shrinks to a segment on the $\|u\|_2^2$ axis containing the point $(0, \frac{2}{3})$ (cf. (3.39)). In the limit $\varepsilon \rightarrow 0$ region \mathcal{R}_3 grows to a rectangle minus a slightly smaller segment again on the $\|u\|_2^2$ axis containing the point $(0, \frac{2}{3})$ (cf. (3.40)).

Loosely speaking, in the blown-up space a neighbourhood of the green curve is covered by region \mathcal{R}_2 and parts of \mathcal{R}_3 , more precisely by the preimage of $\mathcal{R}_2 \times [0, \varepsilon_0]$ and parts of the preimage of $\mathcal{R}_3 \times [0, \varepsilon_0]$ under the blow-up map. Similarly, we use the preimage of $\mathcal{R}_1 \times [0, \varepsilon_0]$ in the blown-up space. For sake of simplicity, we will just talk about \mathcal{R}_i , $i = 1, 2, 3$ in this context, always keeping in mind the above meaning. Hence, the green curve is covered by both \mathcal{R}_2 and \mathcal{R}_3 . The blue curve is mostly covered by \mathcal{R}_1 , with a small part (close to $\delta = \frac{2}{\sqrt{3}}$) covered by \mathcal{R}_2 . Region \mathcal{R}_3 covers the remainder of the green curve (close to $\delta = 0$) and the black curve. In the blown-up space, the bifurcation curve for $0 < \varepsilon \ll 1$ lifts off from the singular bifurcation curve (corresponding to the limit $\varepsilon = 0$).

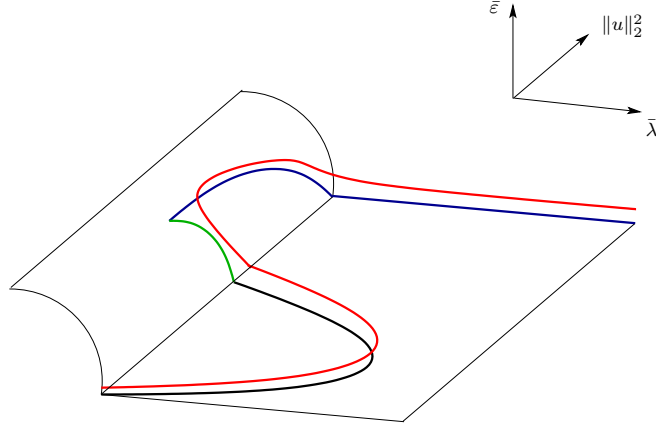


Figure 3.9: Bifurcation diagram corresponding to Equations (3.23), (3.18) in blown-up parameter space. The bifurcation curve in the singular limit $\varepsilon = 0$ is represented by the union of the blue, green and black solid curves, covered by \mathcal{R}_1 , \mathcal{R}_2 , and \mathcal{R}_3 , respectively. The part of the blue curve on the cylinder corresponds to the line \mathcal{B}_1 and the part contained in the plane $\{\bar{\varepsilon} = 0\}$ corresponds to the line \mathcal{B}_2 . The red curve which lifts off from the $\varepsilon = 0$ curve corresponds to solutions of the boundary value problem for the case $0 < \varepsilon \ll 1$.

As stated in Theorem 3.1.1, we consider $\lambda \in [0, \Lambda]$, with $\Lambda = 1$ for sake of simplicity. In region \mathcal{R}_3 , away from the point $(0, \frac{2}{\sqrt{3}})$ the perturbation by ε is regular. In regions \mathcal{R}_1 and \mathcal{R}_2 we will see that singular solutions exist only for $\lambda \geq \frac{3}{4}\varepsilon$ (i.e., $\delta \leq \frac{2}{\sqrt{3}}$; cf. Sections 3.4.1

and 3.4.2). Hence, in these regions we need to consider $\lambda \in [\frac{3}{4}\varepsilon, 1]$, *i.e.*,

$$\delta \in \left[\sqrt{\varepsilon}, \frac{2}{\sqrt{3}} \right], \quad (3.42)$$

which corresponds to the gray area in Figure 3.10.

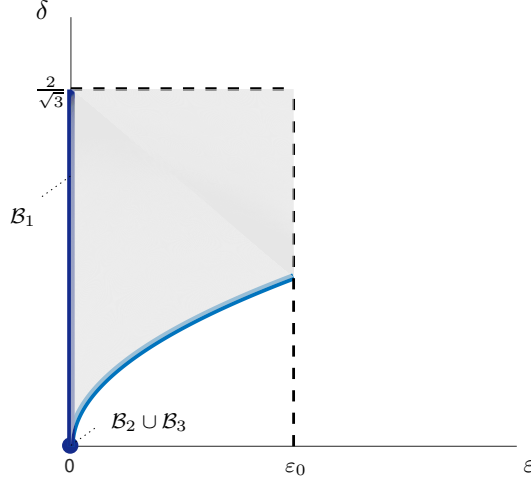


Figure 3.10: Region considered in our analysis in (ε, δ) -space. This region is shaded in gray. It is bounded from below by $\{\delta = \sqrt{\varepsilon}\}$ (light blue curve) and from above by $\{\delta = \frac{2}{\sqrt{3}}\}$ (dashed horizontal line; cf. (3.42)). The dark blue line for $\varepsilon = 0$ corresponds to the union of the two parts of the blue bifurcation branch in Figure 3.8, 3.9. The vertical line corresponds to the line \mathcal{B}_1 and the dot corresponds to the curves $\mathcal{B}_2 \cup \mathcal{B}_3$.

As evidenced in Figure 3.10, $\delta = 0$ occurs only when $\varepsilon = 0$ (this case is represented by the blue dot therein). This very degenerate situation gives the singular orbit of type I, right panel in Figure 3.7(a) with a very singular structure. Hence, the whole line \mathcal{B}_2 in the bifurcation diagram for $\varepsilon = 0$ shown in Figure 3.8 corresponds to this one singular solution.

3.4.1 Region \mathcal{R}_1

Region 1 of the bifurcation diagram deals with solutions whose singular limit are solutions of type I (cf. Definition 3.4.1). For ε positive and sufficiently small, solutions on that branch come very close to $\{u = \varepsilon\}$ and the length of the interval I where u is close to ε grows

with λ . In the singular limit $\varepsilon = 0$, the slope of the respective solutions is moderate for $\lambda = \mathcal{O}(\varepsilon)$ (corresponding to $0 < \delta < \frac{2}{\sqrt{3}}$) and tends to infinity for $\lambda = \mathcal{O}(1)$ (i.e., as $\delta \rightarrow 0$) along the two segments where u changes from $u = 0$ to $u = 1$. This is confirmed by the rescaling of w in (3.21): for $\lambda = \mathcal{O}(\varepsilon)$ that rescaling translates into $w = \mathcal{O}(1)$, while for $\lambda = \mathcal{O}(1)$ that rescaling gives $w \rightarrow \infty$ (cf. Figure 3.7(a)). Interestingly, the proof for these different λ regimes is very similar.

We have the following result:

Proposition 3.4.2. *For fixed δ_1 with $0 < \delta_1 < \frac{2}{\sqrt{3}}$, δ_1 close to $\frac{2}{\sqrt{3}}$, there exists $\varepsilon_0 > 0$ sufficiently small such that in region \mathcal{R}_1 the boundary value problem (3.23), (3.18) for $\varepsilon < \varepsilon_0$ has a unique branch of solutions for $\lambda \in \left[\frac{\varepsilon}{\delta_1^2}, 1\right]$ which limit on a singular solution Γ of type-I as $\varepsilon \rightarrow 0$.*

Remark 8. The singular solution Γ depends on λ (equivalently, on δ). If interpreted in terms of δ , the range for which these solutions exist corresponds to $\delta \in [\sqrt{\varepsilon}, \delta_1]$ (recall (3.22)).

To prove Proposition 3.4.2, we construct the solutions corresponding to the bifurcation branch contained in region \mathcal{R}_1 for fixed λ in the regime considered here.

For fixed δ , a unique suitable singular orbit Γ is constructed in the blown-up space by investigating the dynamics of Equations (3.23),(3.18) separately in charts K_1 and K_2 , and then combining them. This singular orbit is shown to persist for $0 < \varepsilon \ll 1$. The singular orbit is essentially determined by the dynamics in chart K_2 , which we consider now.

Dynamics in chart K_2

The flow of Equation (3.23) from the section Σ_2^{in} back to itself, whereby w changes its sign from negative to positive, is naturally described in chart K_2 (cf. Figure 3.11).

Recalling that $r_2 = \varepsilon$, we observe that Equation (3.37) constitutes a fast-slow system in the standard form of geometric singular perturbation theory [22, 35, 46], with (u_2, w_2) the fast variables and ξ_2 the slow variable. The fast system is (3.37), whence the corresponding

slow system is obtained by rescaling the independent variable by r_2 which gives

$$r_2 \dot{u}_2 = u_2^4 w_2, \quad (3.43a)$$

$$r_2 \dot{w}_2 = u_2^2 - 1, \quad (3.43b)$$

$$\dot{\xi}_2 = \delta u_2^4, \quad (3.43c)$$

$$\dot{r}_2 = 0. \quad (3.43d)$$

The associated layer and reduced problems (obtained by setting $r_2 = 0$ in (3.37) and (3.43)) are given by

$$u'_2 = u_2^4 w_2, \quad (3.44a)$$

$$w'_2 = u_2^2 - 1, \quad (3.44b)$$

$$\xi'_2 = 0, \quad (3.44c)$$

$$r'_2 = 0 \quad (3.44d)$$

and

$$0 = u_2^4 w_2, \quad (3.45a)$$

$$0 = u_2^2 - 1, \quad (3.45b)$$

$$\dot{\xi}_2 = \delta u_2^4, \quad (3.45c)$$

$$\dot{r}_2 = 0, \quad (3.45d)$$

respectively. Note that System (3.44a)-(3.44b) is precisely System (3.27). The critical manifold for Equation (3.45) is given by the line

$$\mathcal{S}_2^0 := \{(1, 0, \xi_2, 0) \mid \xi_2 \in [\xi_-, \xi_+]\}. \quad (3.46)$$

Remark 9. While steady states are also found for $u_2 = -1$ in (3.37), these states are irrelevant since u_2 and r_2 are both non-negative and $\{u_2 = 0\}$ is an invariant hyperplane for (3.37), which the flow cannot cross.

Linearization of (3.44) about the critical manifold \mathcal{S}_2^0 shows that any point $Q_2 = (1, 0, \xi_2, 0) \in \mathcal{S}_2^0$ is a saddle, with Jacobian

$$\left[\begin{array}{cc} 4u_2^3 w_2 & u_2^4 \\ 2u_2 & 0 \end{array} \right] \Big|_{(u_2, w_2) = (1, 0)} = \left[\begin{array}{cc} 0 & 1 \\ 2 & 0 \end{array} \right]$$

and eigenvalues $\pm\sqrt{2}$. Hence, the manifold \mathcal{S}_2^0 is normally hyperbolic. The reduced flow thereon is described by $\dot{\xi}_2 = \delta$, which corresponds to a constant drift in the positive u_2 -direction with speed δ .

To describe the integrable layer flow away from \mathcal{S}_2^0 , we introduce u_2 as the independent variable, dividing (3.44b) formally by (3.44a):

$$\frac{dw_2}{du_2} = \frac{u_2^2 - 1}{u_2^4 w_2(u_2)}.$$

Solving the above equation, with $w_2(1) = 0$, we find

$$w_2^\mp(u_2) = \mp \sqrt{\frac{4}{3} - \frac{2}{u_2} + \frac{2}{3u_2^3}}. \quad (3.47)$$

In particular, it follows from (3.47) that, for any fixed choice of ξ_2 , the stable and unstable manifolds of Q_2 can be written as graphs over u_2 :

$$\mathcal{W}_2^s(Q_2) = \{(u_2, w_2^-(u_2), \xi_2, 0) \mid u_2 \in [1, \infty)\}, \quad (3.48a)$$

$$\mathcal{W}_2^u(Q_2) = \{(u_2, w_2^+(u_2), \xi_2, 0) \mid u_2 \in [1, \infty)\}. \quad (3.48b)$$

We have the following result.

Lemma 3.4.3. *Let $r_2 \in (0, r_0)$, with r_0 positive and sufficiently small. Then, the following statements hold for System (3.37):*

1. *The normally hyperbolic critical manifold \mathcal{S}_2^0 becomes a slow manifold*

$$\mathcal{S}_2^{r_2} = \{(1, 0, \xi_2, r_2) \mid \xi_2 \in [\xi_-, \xi_+]\},$$

where ξ_- and ξ_+ are appropriately chosen constants. In particular, we emphasize that $(u_2, w_2) = (1, 0)$ on $\mathcal{S}_2^{r_2}$.

2. *The corresponding stable and unstable foliations $\mathcal{F}_2^s(\mathcal{S}_2^{r_2})$ and $\mathcal{F}_2^u(\mathcal{S}_2^{r_2})$ are identical to $\mathcal{F}_2^s(\mathcal{S}_2^0)$ and $\mathcal{F}_2^u(\mathcal{S}_2^0)$ except for their constant r_2 -component. For $r_2 \in [0, r_0)$ fixed, these foliations may be written as*

$$\mathcal{F}_2^s(\mathcal{S}_2^{r_2}) = \{(u_2, w_2^-(u_2), \xi_2, r_2) \mid u_2 \in [1, \infty], \xi_2 \in [\xi_-, \xi_+]\}, \quad (3.49a)$$

$$\mathcal{F}_2^u(\mathcal{S}_2^{r_2}) = \{(u_2, w_2^+(u_2), \xi_2, r_2) \mid u_2 \in [1, \infty], \xi_2 \in [\xi_-, \xi_+]\}. \quad (3.49b)$$

Proof. Both statements follow immediately from standard GSPT [22], in combination with the preceding analysis; in particular, the fact that the plane $\{(u_2, w_2) = (1, 0)\}$ is invariant for Equation (3.37) irrespective of the choice of r_2 implies that the restrictions of $\mathcal{S}_2^{r_2}$ and \mathcal{S}_2^0 to (u_2, w_2, ξ_2) -space do not depend on r_2 . \square

Remark 10. The fast-slow structure of System (3.37) is very simple, since Equations (3.37a) and (3.37b) decouple from Equation (3.37c). Even for $\varepsilon > 0$, the fast dynamics is just the integrable planar system (3.37a)–(3.37b), controlled by the saddle point and its stable and unstable manifolds. The slow flow on the slow manifold is just the drift $\dot{\xi} = \delta$.

In the limit $u_2 \rightarrow \infty$, $w_2^\mp(u_2)$ converges to $w_2^\mp(\infty) = \mp \frac{2}{\sqrt{3}}$. If we transform the stable manifold $\mathcal{W}_2^s(Q_2)$ and the unstable manifold $\mathcal{W}_2^u(Q_2)$ to chart K_1 by the coordinate change κ_{21} in (3.31) these manifolds limit on the points $(0, \mp \frac{2}{\sqrt{3}}, \xi_1, 0)$ (see Figure 3.11).

Dynamics in chart K_1

The parts Γ_1^\mp of the singular orbit, corresponding to the flow between two sets of boundary conditions at $\xi = \mp 1$ and the section Σ_1^{out} , are here determined based on Equation (3.35) in connection with the results obtained in chart K_2 . These parts in chart K_1 must in fact match with the manifolds $\mathcal{W}_2^{s,u}(Q_2)$ in chart K_2 (see Figure 3.11).

To this aim, we analyze the flow induced by Equation (3.23) in the singular limit as $\varepsilon \rightarrow 0$. The dynamics in K_2 will define the boundary values of w for the singular orbit we aim to describe.

A simple calculation reveals that Equation (3.35) admits a line of steady states at

$$\mathcal{S}_1^0 := \{(0, 0, \xi_1, 1) \mid \xi_1 \in [\xi_-, \xi_+]\}, \quad (3.50)$$

as well as a plane of steady states

$$\pi_1 := \{(0, w_1, \xi_1, 0) \mid w_1 \in [w_-, w_+] \text{ and } \xi_1 \in [\xi_-, \xi_+]\}; \quad (3.51)$$

here, w_\mp and ξ_\mp are defined as in (3.32). Another set of equilibria, with $\varepsilon_1 = -1$, is irrelevant to us due to our assumption that r_1 and ε_1 are both non-negative. The line \mathcal{S}_1^0 corresponds to the saddle $(\tilde{u}, w) = (1, 0)$ of System (3.27) and coincides with the critical manifold \mathcal{S}_2^0 introduced in chart K_2 (cf. Equation (3.46)).

In chart K_1 the singular limit $\varepsilon = 0$ corresponds to either $r_1 = 0$ or $\varepsilon_1 = 0$ in Equation (3.35), which yields the following two limiting systems in the corresponding invariant hyperplanes

$$r_1' = 0, \tag{3.52a}$$

$$w_1' = \varepsilon_1(1 - \varepsilon_1^2), \tag{3.52b}$$

$$\xi_1' = 0, \tag{3.52c}$$

$$\varepsilon_1' = -\varepsilon_1 w_1 \tag{3.52d}$$

and

$$r_1' = r_1 w_1, \tag{3.53a}$$

$$w_1' = 0, \tag{3.53b}$$

$$\xi_1' = \delta r_1, \tag{3.53c}$$

$$\varepsilon_1' = 0, \tag{3.53d}$$

respectively. System (3.52) on the hyperplane $r_1 = 0$ is precisely System (3.44) from K_2 after the transformation κ_{21} in (3.31). These equations describes the portion of Γ_1^- between Σ_1^{out} and $\varepsilon_1 = 0$. On the other hand, System (3.53) (corresponding to the dynamics on the hyperplane $\varepsilon_1 = 0$) determines the part of the singular orbit which connects with the boundary conditions. Hence, we first focus our attention on this case.

The value of w_1 in Equations (3.53) is constant: $w_1 \equiv w_0$, for some constant w_0 . Since it must match with the w_2 -value obtained in the limit $u_2 \rightarrow \infty$ in (3.47), it must be $w_1 \equiv \mp \frac{2}{\sqrt{3}}$ on the hyperplane $\{\varepsilon_1 = 0\}$. The orbits of (3.53) are then easily computed by dividing (3.53c) formally by (3.53a) and using the above result on w_1 : $\frac{d\xi_1}{dr_1} = \frac{\delta}{w_0}$. For any initial condition $\xi_1(1) = \xi_0$, the solution to that equation reads

$$\xi_1(r_1) = \frac{\delta}{w_0}(r_1 - 1) + \xi_0. \tag{3.54}$$

The boundary conditions (3.18) imply $\xi_0 = \mp 1$. Hence we obtain

$$\xi_1^\mp(r_1) = \mp \frac{\sqrt{3}}{2} \delta (r_1 - 1) \mp 1. \tag{3.55}$$

Any orbit of (3.53) can hence be written as

$$\left\{ \left(r_1, \mp \frac{2}{\sqrt{3}}, \xi_1^\mp(r_1), 0 \right) \mid r_1 \in [0, 1] \right\}. \quad (3.56)$$

For the integrable Equation (3.52), a representation of all orbits can be found by introducing ε_1 as the independent variable: dividing formally (3.52b) by (3.52d), we obtain $\frac{dw_1}{d\varepsilon_1} = -\frac{1-\varepsilon_1^2}{w_1(\varepsilon_1)}$, which can be solved explicitly with $w_1(0) = \mp \frac{2}{\sqrt{3}}$ to yield

$$w_1^\mp(\varepsilon_1) = \mp \sqrt{\frac{4}{3} - 2\varepsilon_1 + \frac{2}{3}\varepsilon_1^3}, \quad (3.57)$$

where the sign in (3.57) equals that of the initial w_1 -value. (This corresponds to Equation (3.47) in K_1 -coordinates.) The value of ξ_1 on each Γ_1^\mp is constant and corresponds to the respective value of $\xi_1^\mp(r_1)$ in (3.55) at $r_1 = 0$, *i.e.*,

$$\xi_1^\mp(0) = \pm \frac{\sqrt{3}}{2} \delta \mp 1. \quad (3.58)$$

Remark 11. For $\delta = \frac{2}{\sqrt{3}}$ this implies $\xi_1^\mp(0) = 0$, *i.e.*, we obtain a singular orbit of type II, see Figure 3.7(b) and Figure 3.14. This explains why we need the assumption $\delta < \frac{2}{\sqrt{3}}$ in Proposition 3.4.2.

Any orbit of (3.52) can be hence represented as

$$\{(0, w_1^\mp(\varepsilon_1), \xi_1^\mp(0), \varepsilon_1) \mid \varepsilon_1 \in [0, \sigma]\}, \quad (3.59)$$

where σ is as in the definition of the section Σ_1^{out} ; recall (3.32).

Concatenation of the two orbit segments defined in Equations (3.56) and (3.59) with the respective signs will yield the singular orbits Γ_1^- and Γ_1^+ , which are shown in Figure 3.11 in blue between the sections \mathcal{V}_{10}^- and Σ_1^{out} and between the sections Σ_1^{out} and \mathcal{V}_{10}^+ , respectively.

Singular orbit Γ

A singular orbit Γ for Equation (3.23) can now be constructed based on the dynamics in charts K_1 and K_2 by taking into account the corresponding boundary conditions in Equation (3.18).

The manifolds $\mathcal{W}_2^{s,u}(Q_2)$ transformed to K_1 and the parts of Γ_1^\mp in $\varepsilon_1 = 0$ given by (3.59) meet in the points

$$P_1^\mp = \left(0, \mp \frac{2}{\sqrt{3}}, \pm \frac{\sqrt{3}}{2} \delta \mp 1, 0 \right). \quad (3.60)$$

These points belong to the two lines

$$\ell_1^- = \left\{ \left(0, -\frac{2}{\sqrt{3}}, \xi_1, 0 \right) \mid \xi_1 \in [\xi_-, \xi_+] \right\}, \quad (3.61a)$$

$$\ell_1^+ = \left\{ \left(0, \frac{2}{\sqrt{3}}, \xi_1, 0 \right) \mid \xi_1 \in [\xi_-, \xi_+] \right\}, \quad (3.61b)$$

both located in the plane of steady states π_1 (cf. (3.51)). The part Γ_1 of the singular orbit can hence be finally written as

$$\begin{aligned} \Gamma_1^- &= \left\{ \left(r_1, -\frac{2}{\sqrt{3}}, -\frac{\sqrt{3}}{2}\delta(r_1 - 1) - 1, 0 \right) \mid r_1 \in (0, 1] \right\} \cup P_1^- \\ &\cup \left\{ \left(0, -\sqrt{\frac{4}{3} - 2\varepsilon_1 + \frac{2}{3}\varepsilon_1^3}, \frac{\sqrt{3}}{2}\delta - 1, \varepsilon_1 \right) \mid \varepsilon_1 \in (0, \sigma] \right\}, \end{aligned} \quad (3.62a)$$

$$\begin{aligned} \Gamma_1^+ &= \left\{ \left(r_1, \frac{2}{\sqrt{3}}, \frac{\sqrt{3}}{2}\delta(r_1 - 1) + 1, 0 \right) \mid r_1 \in (0, 1] \right\} \cup P_1^+ \\ &\cup \left\{ \left(0, \sqrt{\frac{4}{3} - 2\varepsilon_1 + \frac{2}{3}\varepsilon_1^3}, -\frac{\sqrt{3}}{2}\delta + 1, \varepsilon_1 \right) \mid \varepsilon_1 \in (0, \sigma] \right\}. \end{aligned} \quad (3.62b)$$

It remains to identify the portion of Γ that is located in chart K_2 ; we denote the corresponding singular orbit by Γ_2 . We note that for $r_2 = 0$, Equation (3.44) implies $\xi_2 \equiv \text{constant}$ on Γ_2 . Given the definition of Γ_1 and the fact that $\xi_2 = \xi_1$, we hence define the points

$$Q_2^\mp = \left(1, 0, \pm \frac{\sqrt{3}}{2}\delta \mp 1, 0 \right) \in \mathcal{S}_2^0. \quad (3.63)$$

Therefore, we may write

$$\Gamma_2 = \mathcal{W}_2^s(Q_2^-) \cup Q_2^- \cup \left\{ (1, 0, \xi_2, 0) \mid \xi_2 \in \left(\frac{\sqrt{3}}{2}\delta - 1, -\frac{\sqrt{3}}{2}\delta + 1 \right) \right\} \cup Q_2^+ \cup \mathcal{W}_2^u(Q_2^+), \quad (3.64)$$

recall Equation (3.48), with u_2 now varying in the range $[1, \sigma^{-1}]$. This corresponds to the union of three pieces: the first one is the stable manifold of Q_2^- , the second piece corresponds to the slow drift in ξ_2 from Q_2^- to Q_2^+ (shown in the inset of Figure 3.11) and finally the third piece is the unstable manifold of Q_2^+ . The sought-after singular orbit Γ corresponding to the singular ($\varepsilon = 0$) solution of the boundary value problem (3.23), (3.18) is hence given by the union of Γ_1^- , Γ_2 , and Γ_1^+ in the blow-up space, *i.e.*

$$\Gamma := \Gamma_1^- \cup \Gamma_2 \cup \Gamma_1^+. \quad (3.65)$$

A visualization of the singular orbit Γ is given in Figure 3.11.

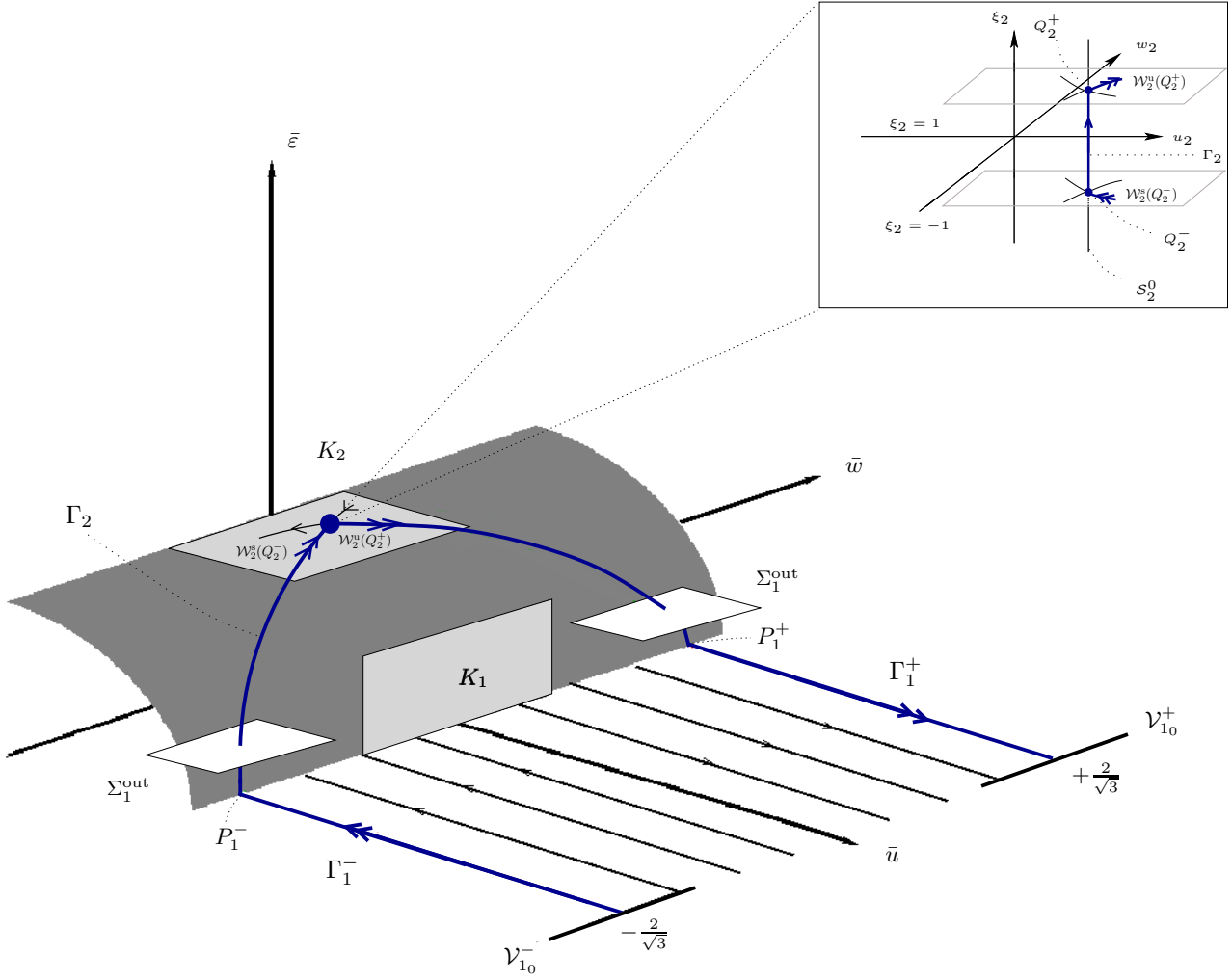


Figure 3.11: Geometry of the singular orbit $\Gamma = \Gamma_1^- \cup \Gamma_2 \cup \Gamma_1^+$ (in blue) for Equation (3.23) in blown-up space, corresponding to a singular solution of type I. The inset shows more details of the fast-slow structure in (u_2, w_2, ξ_2) -space in chart K_2 , e.g., the critical manifold \mathcal{S}_2^0 and the resulting singular connection between Q_2^- and Q_2^+ .

Persistence of the singular orbit – Proof of Proposition 3.4.2

The proof of Proposition 3.4.2 is based on the shooting argument outlined in Section 3.2. This method is implemented by approximating the dynamics of (3.23) for ϵ small in the

two coordinate charts K_1 and K_2 . We begin by defining the two manifolds

$$\mathcal{V}_{1_\varepsilon}^\mp := \{(1, w, \mp 1, \varepsilon) \mid w \in I^\mp\} \quad \text{for } \varepsilon \in [0, \varepsilon_0), \quad (3.66)$$

which represent the boundary conditions in (3.18) in chart K_1 , with $r_1 = 1$ for $\xi_1 = \mp 1$; hence, it also follows that $\varepsilon_1 = \frac{\varepsilon}{r_1} = \varepsilon$ there. The intervals I^-, I^+ represent neighbourhoods of the points $w_0^- = -\frac{2}{\sqrt{3}}$ and $w_0^+ = \frac{2}{\sqrt{3}}$, respectively.

We note that the manifolds $\mathcal{V}_{1_\varepsilon}^\mp$ are mapped onto each other by the transformation $(r_1, w_1, \xi_1, \varepsilon_1) \mapsto (r_1, -w_1, -\xi_1, \varepsilon_1)$, in accordance with the symmetry properties of Equation (3.23). It is thus sufficient to consider the transition from $\mathcal{V}_{1_\varepsilon}^-$ to Σ_1^{out} under the flow of (3.35), as its counterpart, the transition between Σ_1^{out} and $\mathcal{V}_{1_\varepsilon}^+$, can be obtained in a symmetric fashion.

We now introduce ε_1 as the independent variable in Equation (3.35), whence

$$\frac{dr_1}{d\varepsilon_1} = -\frac{r_1}{\varepsilon_1}, \quad (3.67a)$$

$$\frac{dw_1}{d\varepsilon_1} = -\frac{1 - \varepsilon_1^2}{w_1(\varepsilon_1)}, \quad (3.67b)$$

$$\frac{d\xi_1}{d\varepsilon_1} = -\delta \frac{r_1(\varepsilon_1)}{\varepsilon_1 w_1(\varepsilon_1)}. \quad (3.67c)$$

Here, we remark that $w_1(\varepsilon_1)$ remains non-zero for ε sufficiently small, as we know that $w_1 = \mp \frac{2}{\sqrt{3}} + \mathcal{O}(\varepsilon_1) \neq 0$ in the singular limit, *i.e.*, when $\varepsilon = 0$. Solving Equations (3.67a) and (3.67b), with initial condition $(1, w, -1, \varepsilon)$ in $\mathcal{V}_{1_\varepsilon}^-$, we find

$$r_1(\varepsilon_1) = \frac{\varepsilon}{\varepsilon_1} \quad \text{and} \quad w_1^-(\varepsilon_1) = -\sqrt{w^2 + 2(\varepsilon - \varepsilon_1) - \frac{2}{3}(\varepsilon^3 - \varepsilon_1^3)}. \quad (3.68)$$

Substituting the expressions in (3.68) into (3.67c) and expanding the result for ε_1 small, we find

$$\begin{aligned} \frac{d\xi_1^-}{d\varepsilon_1} &= \delta \frac{\varepsilon}{\varepsilon_1^2} \frac{1}{\sqrt{w^2 + 2(\varepsilon - \varepsilon_1) - \frac{2}{3}(\varepsilon^3 - \varepsilon_1^3)}} \\ &= \delta \frac{\varepsilon}{\varepsilon_1} \frac{1}{\sqrt{w^2 + 2\varepsilon - \frac{2}{3}\varepsilon^3}} \left[\frac{1}{\varepsilon_1} + \frac{1}{w^2 + 2\varepsilon - \frac{2}{3}\varepsilon^3} \right] + \mathcal{O}(1), \end{aligned}$$

which can be solved to the order considered here and evaluated in Σ_1^{out} – *i.e.*, for $\varepsilon_1 = \sigma$ – to yield

$$\xi_1^{\text{out}-} = -1 - \frac{\delta}{w} + \frac{\delta}{w^3} \varepsilon \ln \varepsilon + \mathcal{O}(\varepsilon). \quad (3.69)$$

Similarly, evaluating (3.68) in Σ_1^{out} , we find

$$(r_1^{\text{out-}}, w_1^{\text{out-}}, \xi_1^{\text{out-}}, \varepsilon_1^{\text{out-}}) = \left(\frac{\varepsilon}{\sigma}, -\sqrt{w^2 + 2(\varepsilon - \sigma) - \frac{2}{3}(\varepsilon^3 - \sigma^3)}, -1 - \frac{\delta}{w} + \mathcal{O}(\varepsilon \ln \varepsilon), \sigma \right),$$

which defines a curve $(w_1^{\text{out-}}, \xi_1^{\text{out-}})(w)$ that is parametrized by the initial w_1 -value w in $\mathcal{V}_{1\varepsilon}^-$. That curve, which we denote by $\mathcal{V}_{1\varepsilon}^{\text{out-}}$, is located in a two-dimensional subset of Σ_1^{out} – specifically, the (w_1, ξ_1) -plane, with (r_1, ε_1) fixed:

$$\mathcal{V}_{1\varepsilon}^{\text{out-}} := \left\{ \left(-\sqrt{w^2 + 2(\varepsilon - \sigma) - \frac{2}{3}(\varepsilon^3 - \sigma^3)}, -1 - \frac{\delta}{w} + \mathcal{O}(\varepsilon \ln \varepsilon) \right) \mid w \in I^- \right\}. \quad (3.70)$$

It remains to study the stable foliation $\mathcal{F}_2^s(\mathcal{S}_2^{r_2})$ in coordinate chart K_2 , and to show that the intersection thereof with $\mathcal{V}_{1\varepsilon}^{\text{out-}}$ is transverse for ε sufficiently small. To that end, we recall the definition $\mathcal{F}_2^s(\mathcal{S}_2^{r_2})$ in (3.49a), which we evaluate in the section $\Sigma_2^{\text{in}} = \kappa_{12}(\Sigma_1^{\text{out}})$. Taking $r_2 (= \varepsilon)$ fixed, as before, and evaluating $\mathcal{F}_2^s(\mathcal{S}_2^{r_2})$ at $u_2 = \sigma^{-1}$ defines a curve $\mathcal{F}_2^{\text{in-}}$ in Σ_2^{in} which is parametrized by $\xi_2 \in [\xi_-, \xi_+]$ via

$$(u_2^{\text{in}}, w_2^{\text{in}}, \xi_2^{\text{in}}, r_2^{\text{in}}) = \left(\sigma^{-1}, -\sqrt{\frac{4}{3} - 2\sigma + \frac{2}{3}\sigma^3}, \xi_2, r_2 \right),$$

for any $r_2 \in [0, \rho\sigma]$ (cf. (3.33)). Transforming $\mathcal{F}_2^{\text{in-}}$ into chart K_1 , we obtain the corresponding curve $\mathcal{F}_1^{\text{in-}}$ given by

$$\mathcal{F}_1^{\text{in-}} := (w_1^{\text{out}}, \xi_1^{\text{out}}) = \left\{ \left(-\sqrt{\frac{4}{3} - 2\sigma + \frac{2}{3}\sigma^3}, \xi_1 \right) \mid \xi_1 \in [\xi_-, \xi_+] \right\}. \quad (3.71)$$

Comparing Equations (3.70) and (3.71) and expanding

$$-\sqrt{w^2 + 2(\varepsilon - \sigma) - \frac{2}{3}(\varepsilon^3 - \sigma^3)} = w + \frac{\varepsilon - \sigma}{w} + \mathcal{O}[(\varepsilon - \sigma)^2],$$

and

$$-\sqrt{\frac{4}{3} - 2\sigma + \frac{2}{3}\sigma^3} = -\frac{2}{\sqrt{3}} + \frac{\sqrt{3}}{2}\sigma + \mathcal{O}(\sigma^2),$$

we see that $\mathcal{V}_{1\varepsilon}^{\text{out-}}$ and $\mathcal{F}_1^{\text{in-}}$ intersect in some point

$$P_1^{\text{out-}} = \left(-\frac{2}{\sqrt{3}} + \mathcal{O}(\varepsilon), -1 - \frac{\delta}{w} + \mathcal{O}(\varepsilon \ln \varepsilon) \right),$$

as the corresponding tangent vectors in the (w_1, ξ_1) -plane are given by $(1, \frac{\delta}{w^2})$ and $(0, 1)$ to leading order.

This intersection is transversal for any ε small. The transversality between $\mathcal{V}_{1_\varepsilon}^{\text{out}-}$ and $\mathcal{F}_1^{\text{in}-}$ occurs already for $\varepsilon = 0$ (*i.e.*, $r_1 = 0$), which is sufficient for the Exchange Lemma to apply in chart K_2 (cf. Figure 3.12). As these sets smoothly perturb, the transversality of their intersection persists for $\varepsilon \neq 0$ as well.

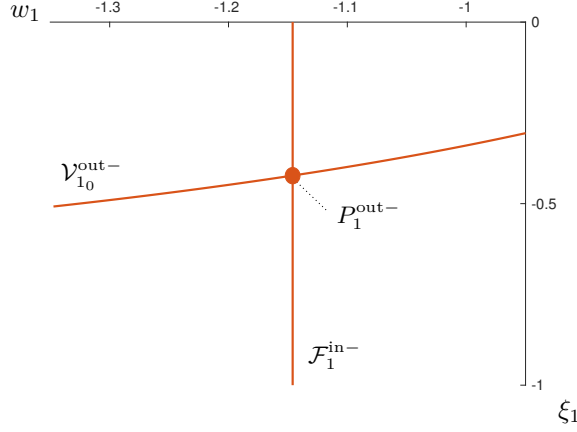


Figure 3.12: Transversal intersection of the sets $\mathcal{V}_{1_0}^{\text{out}-}$ and $\mathcal{F}_1^{\text{in}-}$ in the (w_1, ξ_1) -space.

As stated above, the symmetry of Equation (3.35) implies the existence of a point $P_1^{\text{out}+} = \left(\frac{2}{\sqrt{3}} + \mathcal{O}(\varepsilon), 1 - \frac{\delta}{w} + \mathcal{O}(\varepsilon \ln \varepsilon)\right)$ in Σ_1^{out} in which the curves

$$\mathcal{V}_{1_\varepsilon}^{\text{out}+} = \left\{ \left(\sqrt{w^2 + 2(\varepsilon - \sigma) - \frac{2}{3}(\varepsilon^3 - \sigma^3)}, 1 - \frac{\delta}{w} + \mathcal{O}(\varepsilon \ln \varepsilon) \right) \mid w \in I^+ \right\}$$

and

$$\mathcal{F}_1^{\text{out}+} = \left\{ \left(\sqrt{\frac{4}{3} - 2\sigma + \frac{2}{3}\sigma^3}, \xi_1 \right) \mid \xi_1 \in [\xi_-, \xi_+] \right\}$$

intersect transversely.

So far, we constructed a connection between the two manifolds of boundary conditions $\mathcal{V}_{1_\varepsilon}^-$ and $\mathcal{V}_{1_\varepsilon}^+$ in the singular limit $\varepsilon = 0$ as follows: in Σ_1^{out} , the forward flow of $\mathcal{V}_{1_0}^-$ (corresponding to $\mathcal{V}_{1_0}^{\text{out}-}$) transversely intersects the transformation of the stable manifold $\mathcal{W}_2^s(Q_2)$ under the change of coordinates in chart K_1 (namely $\mathcal{F}_1^{\text{out}-}$). Then, the slow drift occurs along the critical manifold \mathcal{S}_2^0 until the flow leaves along the unstable manifold $\mathcal{W}_2^u(Q_2)$. In Σ_1^{out} , this manifold (corresponding to $\mathcal{F}_1^{\text{out}+}$ after the transformation in K_1 -coordinates) again

intersects the backward flow of the boundary value manifold $\mathcal{V}_{1_0}^+$ (i.e., $\mathcal{V}_{1_0}^{\text{out}+}$) transversely. This construction persists for small $\varepsilon \neq 0$ small. The above argument guarantees in fact that the transversality between $\mathcal{V}_{1_\varepsilon}^{\text{out}\mp}$ and $\mathcal{F}_1^{\text{out}\mp}$ persists for $0 < \varepsilon \ll 1$. The fact that the perturbed orbit approaching the stable foliation of the slow manifold $\mathcal{S}_2^{r_2}$ will leave along its unstable foliation is finally guaranteed by the Exchange Lemma (cf. Section 1.1.3).

The above argument allows us to obtain the part of the bifurcation curve which perturbs from \mathcal{B}_1 for $\delta > 0$ (see Figure 3.9). The part of the bifurcation curve perturbing from the remainder of \mathcal{B}_1 and from \mathcal{B}_2 can be obtained analogously. However, as this regime involves the limiting case $\delta = 0$, it needs further consideration. The limit $\delta = 0$ does not affect our construction in chart K_1 but destroys the slow drift on \mathcal{S}_2^0 in chart K_2 for $\varepsilon = 0$ (cf. Equation (3.45)).

The branch \mathcal{B}_2 is associated to the regime $\lambda = \mathcal{O}(1)$. Singular solutions in this regime are of type I with infinitely steep boundary layers; see Figure 3.7(a), right panel. To deal with this scenario, we recall that $\delta = 0$ occurs only for $\varepsilon = 0$ (cf. Figure 3.10) and is bounded below by $\sqrt{\varepsilon}$. Hence, it is convenient to introduce the rescaling

$$\delta = \sqrt{\varepsilon} \tilde{\delta}, \tag{3.72}$$

with $\tilde{\delta} \geq 1$, and plug it into Equations (3.35) and (3.37) for chart K_1 and K_2 , respectively. In chart K_1 , this rescaling yields the same dynamics we would have obtained by setting $\delta = 0$ into (3.35): the singular limit $\varepsilon = 0$ leads to $\xi_1 \equiv \mp 1$ in the invariant hyperplane $\{\varepsilon_1 = 0\}$ (cf. Equation (3.53)). This implies that the value of x in the transition from $u = 1$ to $u = 0$ does not change, exactly as we see in the corresponding type I-solution (Figure 3.7(a), right panel). In chart K_2 , introducing the scaling in (3.72) yields again a fast-slow system

$$u_2' = u_2^4 w_2, \tag{3.73a}$$

$$w_2' = u_2^2 - 1, \tag{3.73b}$$

$$\xi_2' = \tilde{\delta} r_2^{3/2} u_2^4, \tag{3.73c}$$

$$r_2' = 0. \tag{3.73d}$$

The only difference with the previous case $\delta \neq 0$ is that the slow dynamics are now slower, as the small perturbation parameter in (3.37) is now $r_2^{3/2}$ rather than just r_2 . This, however,

does not affect the global construction we illustrated in this section, as the methods we have relied on (such as, *e.g.*, the Exchange Lemma) still apply. As $\tilde{\delta}$ grows up to $\mathcal{O}(\frac{1}{\sqrt{r_2}})$, the transition between the two regimes occurs.

Remark 12. The presence of an $\varepsilon \ln \varepsilon$ -term in the expansion for ξ_1^{out} in (3.69) is due to resonance between the eigenvalues $-1, 0$ (double), and 1 of the linearization of Equation (3.35) about the steady states $P_1^* = (0, -\frac{2}{\sqrt{3}}, \xi_1^*, 0) \in \pi_1$. The proof is based on a sequence of near-identity normal form transformations about that state which reduces (3.35) to the system of equations

$$\begin{aligned} r_1' &= -r_1, \\ \hat{w}_1' &= \mathcal{O}(3), \\ \hat{\xi}_1' &= \frac{3\sqrt{3}}{8}\delta\varepsilon + \mathcal{O}(3), \\ \varepsilon_1' &= \varepsilon_1, \end{aligned}$$

where $\mathcal{O}(3)$ denotes here terms of order 3 and higher in $(\hat{w}_1, \hat{\xi}_1)$. One easily sees that the resonant $\frac{3\sqrt{3}}{8}\delta\varepsilon$ -term cannot be removed from the $\hat{\xi}_1$ -equation, resulting in logarithmic switchback after integration. Details can be found in Section 3.5.

Remark 13. We emphasize that the restriction on δ in the statement of Proposition 3.4.2 is due to the fact that we require $Q_2^- \neq Q_2^+$ (cf. also Remark 11). Specifically, for the Exchange Lemma to apply, we need that $\frac{\sqrt{3}}{2}\delta - 1 < -\frac{\sqrt{3}}{2}\delta + 1$ holds, which is equivalent to $\delta < \frac{2}{\sqrt{3}}$. The case where that condition is violated is studied in Section 3.4.2, which covers region \mathcal{R}_2 . In particular, it is shown there that Equation (3.23) then locally admits a pair of solutions which limit on a type I and a type II-solution, respectively.

3.4.2 Region \mathcal{R}_2

For $\varepsilon > 0$, this region covers a small neighbourhood of the point $(0, \frac{2}{3})$ in $(\lambda, \|u\|_2^2)$ -space (see Figure 3.8). According to its definition in (3.39), the size of this region depends on ε and in particular collapses onto a line as $\varepsilon \rightarrow 0$. This region contains the part of the bifurcation curve which corresponds to solutions limiting on type I and type II-solutions and it connects with the bifurcation curves obtained in regions \mathcal{R}_1 and \mathcal{R}_3 .

We will show that for $0 < \varepsilon \ll 1$ a saddle-node bifurcation occurs in region \mathcal{R}_2 at $\lambda = \lambda_*$ as defined in [54] (see Fig. 3.13).

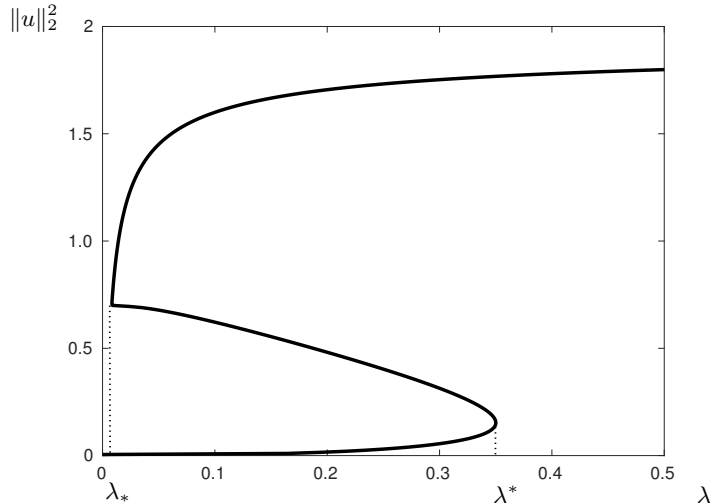


Figure 3.13: Numerical bifurcation diagram showing solutions of (3.5) for $\varepsilon = 0.01$. Saddle-node bifurcations occur at λ_* and λ^* .

Due to the singular nature of λ_* , an accurate numerical approximation is tricky to obtain for small values of the regularization parameter ε . Using matched asymptotics, it was shown in [54] that $\lambda_* = \mathcal{O}(\varepsilon)$, with an expansion of the form

$$\lambda_*(\varepsilon) = \lambda_{*0}\varepsilon + \lambda_{*1}\varepsilon^2 \ln \varepsilon + \lambda_{*2}\varepsilon^2 + \mathcal{O}(\varepsilon^3).$$

However, the coefficients λ_{*i} remained undetermined there. Here, we confirm rigorously the structure of the above expansion, and we determine explicitly the values of the coefficients λ_{*i} therein for $i = 0, 1$. Moreover, we indicate how higher-order coefficients may be found systematically, and we identify the source of the logarithmic (‘switchback’) terms (in ε) in the expansion for λ_* (cf. Proposition 3.4.5 below).

Remark 14. While a saddle-node bifurcation is equally observed in the fourth-order Equation (3.4), Lindsay’s work [52] shows that the asymptotics of the associated λ -value λ_* is far less singular in that case, allowing for a straightforward and explicit determination of the corresponding coefficients.

At leading order, λ_* is equal to the above mentioned critical value $\frac{3}{4}\varepsilon$, which corresponds

to $\delta_* = \frac{2}{\sqrt{3}}$ in terms of δ . This critical value for δ was not covered in the analysis of \mathcal{R}_1 in the previous section, as the argument applied in that region failed there (cf. Remark 13). Hence, a further argument needs to be used in order to analyze the local dynamics around this saddle-node bifurcation point.

Before dealing in more details with the local dynamics around the saddle-node bifurcation point located at δ_* , we deal with the existence of singular solutions as δ varies. In particular, the existence of type II-solutions in region \mathcal{R}_2 is guaranteed by the following

Lemma 3.4.4. *Let $\frac{1}{\sqrt{\lambda_2}} \leq \delta \leq \delta_1$, with $\delta_1 < \frac{2}{\sqrt{3}}$. Then, a singular solution of type II exists if and only if $w_1 = \mp\delta$ at $\xi_1 = \mp 1$.*

Proof. In the original model, the type II (“touchdown”) solution satisfies $w = \mp 1$ at $x = \mp 1$ (cf. Definition 3.4.1). Recalling the w -rescaling in (3.21), this is equivalent to $\tilde{w} = \pm\delta$ at $\xi = \mp 1$. The dynamics close to the boundary sets are studied in our analysis in chart K_1 . Consequently, this constraint becomes $w_1 = \mp\delta$ at $\xi_1 = \mp 1$ (cf. (3.29a)). For $\frac{1}{\sqrt{\lambda_2}} \leq \delta \leq \delta_1$ these orbits can be fully studied in chart K_1 , as they stay away from the slow manifold \mathcal{S}_2^0 (cf. Equation (3.46)) previously studied in K_2 (unlike type I-solutions; cf. Section 3.4.1). The connection between the two pieces $w_1 = -\delta$ and $w_1 = \delta$ on the blow-up cylinder is automatically satisfied (see Figure 3.14, upper panel). \square

Remark 15. For $\delta = 0$, the type II-solution collapses onto the line $\{w_1 = 0\}$. This case, which needs further consideration, is studied in region \mathcal{R}_3 (cf. Section 3.4.3). As previously mentioned, in fact, it takes both \mathcal{R}_2 and \mathcal{R}_3 to cover the green curve in Figure 3.9.

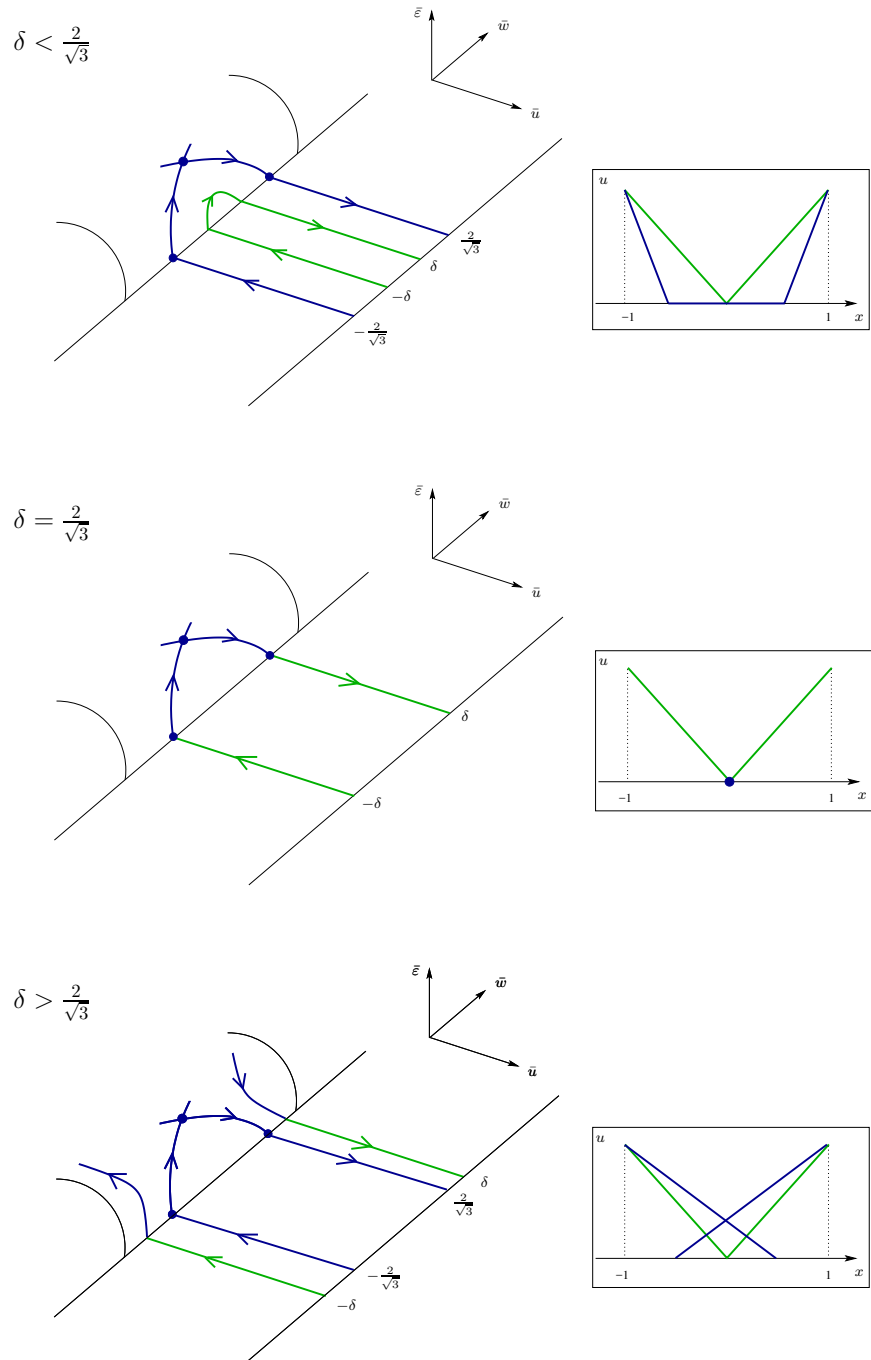


Figure 3.14: Saddle-node bifurcation at the singular level $\varepsilon = 0$ in Equation (3.23) upon variation of δ . In the respective insets, the corresponding singular solutions of type I (blue) and II (green) are shown. In particular, for $\delta > \frac{2}{\sqrt{3}}$ solutions of type I and type II do not exist.

Lemma 3.4.4 guarantees the existence of a type II-solution for every $\delta \in \left[\frac{1}{\sqrt{\lambda_2}}, \delta_1\right]$, with $\delta_1 < \delta_*$. For the same range of δ (i.e., where regions \mathcal{R}_1 and \mathcal{R}_2 overlap), Proposition 3.4.2 implies the local existence of type I-solutions. Hence, we can conclude that Equation (3.23) admits a pair of singular solutions for $\delta < \delta_*$; one of these is of type I, while the other is of type II. At $\delta = \delta_*$, the two singular solutions coalesce in a type II-solution. Finally, for $\delta > \delta_*$, no singular solution exists. The resulting three scenarios are illustrated in Figure 3.14. In particular, we note that solutions of type I satisfy $w_1 = \mp \frac{2}{\sqrt{3}}$ – or, equivalently, $w = \mp \frac{2}{\sqrt{3}\delta}$ in the original formulation – for $\xi_1 = \mp 1$, while those of type II are characterised by $w_1 = \mp \delta$ at $\xi_1 = \mp 1$, as proved in Lemma 3.4.4 (see Figure 3.14).

The main result of this section is the following:

Proposition 3.4.5. *There exists $\varepsilon_0 > 0$ sufficiently small such that in region \mathcal{R}_2 the boundary value problem (3.23), (3.18) has a unique curve of solutions for $\varepsilon < \varepsilon_0$. The curve consists of two branches of solutions which limit on singular solutions of type I and type II, respectively, as $\varepsilon \rightarrow 0$.*

These two branches are connected at a point $\lambda_(\varepsilon)$ in a saddle-node bifurcation. The saddle-node point has the expansion*

$$\lambda_*(\varepsilon) = \frac{3}{4}\varepsilon - \left(\sqrt{\frac{3}{2}} + \frac{9}{8}\right)\varepsilon^2 \ln \varepsilon + \mathcal{O}(\varepsilon^2). \quad (3.74)$$

Proof. The proof of the Proposition consists of two parts: in the first part, we have to consider a small neighborhood of $\delta_* = \frac{2}{\sqrt{3}}$, i.e., $\lambda = \frac{3}{4}\varepsilon$, where the saddle-node bifurcation occurs. We define a suitable bifurcation equation, which describes the transition from solutions which limit on type I-solutions to solutions which limit on type II-solutions. Based on this bifurcation equation, we conclude the occurrence of the saddle-node bifurcation and we compute the expansion of the saddle-node bifurcation. The branch of solutions limiting on solutions of type I connects to the branch already constructed in Proposition 3.4.2. In a second easier step we continue the branch of solutions limiting on type II-solutions for the remaining values of λ in \mathcal{R}_2 . Later, this branch will be shown to connect to solutions treated in \mathcal{R}_3 .

We start by constructing the bifurcation equation. Since $w \approx -\frac{2}{\sqrt{3}}$ and $\delta \approx \frac{2}{\sqrt{3}}$, we also

write

$$w_0 = -\frac{2}{\sqrt{3}} + \Delta w \quad \text{and} \quad \delta = \frac{2}{\sqrt{3}} + \Delta\delta. \quad (3.75)$$

in chart K_1 .

Using the shooting argument outlined in Section 3.2, we first track the corresponding orbit from the initial manifold $\mathcal{V}_{1\varepsilon}^-$ defined in (3.66) through K_1 and into the section Σ_1^{out} . We denote that orbit by γ_1^- . In chart K_2 , the point of intersection of the equivalent orbit γ_2^- with the section Σ_2^{in} is then given by $(\sigma^{-1}, w_2^{\text{in}}, \xi_2^{\text{in}}, \varepsilon)$, for appropriately defined w_2^{in} and ξ_2^{in} .

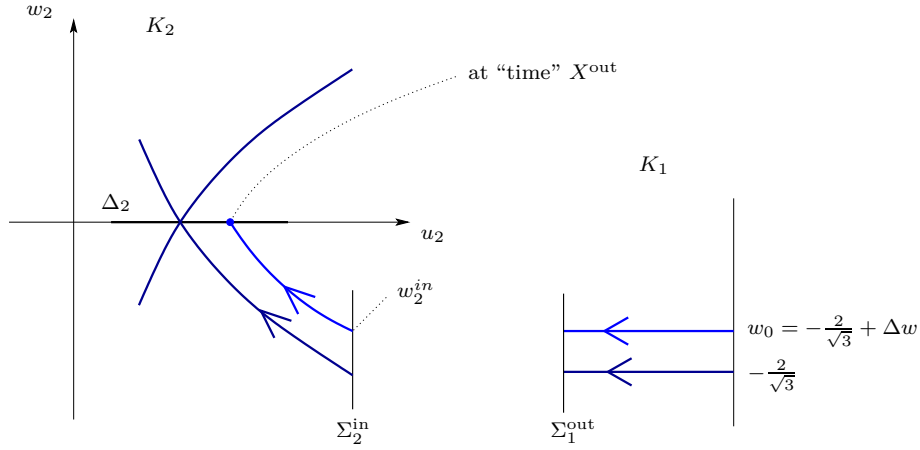


Figure 3.15: Sketch of the shooting argument underlying the proof of Proposition 3.4.5.

Next, we consider the evolution of the orbit γ_2^- through K_2 . Let X^{out} denote the “time” at which γ_2^- reaches the hyperplane $\Delta_2 = \{w_2 = 0\}$, viz. $w_2(X^{\text{out}}) = 0$. (By symmetry, it then follows that the reflection γ_2^+ of γ_2^- under the map $(u_2, w_2, \xi_2, r_2) \mapsto (u_2, -w_2, -\xi_2, r_2)$ will satisfy the boundary condition at $\mathcal{V}_{1\varepsilon}^+$, with $w_0 = \frac{2}{\sqrt{3}} - \Delta w$, after transformation to K_1 .) Clearly, X^{out} depends on w_2^{in} and, in particular, on Δw , *i.e.*, on the initial deviation of the orbit from its singular limit Γ_1^- in chart K_1 .

Our usual shooting argument gives the constraint $\xi_2(X^{\text{out}}) = 0$. Dividing Equation (3.37c) by Equation (3.37a) and recalling that $r_2 = \varepsilon$ in chart K_2 we find $\frac{d\xi_2}{du_2} = \frac{\delta\varepsilon}{w_2}$ and, therefore,

$$\xi_2(u_2) = \xi_2^{\text{in}} + \delta\varepsilon \int_{u_2^{\text{in}}}^{u_2^{\text{out}}} \frac{1}{w_2(u_2)} du_2. \quad (3.76)$$

Here, $u_2^{\text{in}} = \sigma^{-1}$ as in the definition of Σ_2^{in} in (3.33), while u_2^{out} denotes the value of u_2 such that $w_2(u_2^{\text{out}}) = 0$ (cf. again Figure 3.15).

The sought-after bifurcation equation now corresponds to a relation between Δw , ε , and δ that is satisfied for any solution of the boundary value problem (3.23), (3.18) close to the saddle-node bifurcation in (3.23). To derive such a relation, we must first approximate u_2^{out} : recalling the explicit expression for $w_1(\varepsilon_1)$ on γ_1^- , as given in Equation (3.68), substituting the Ansatz in (3.75), and rewriting the result in the coordinates of chart K_2 , we find

$$w_2(u_2) = -\sqrt{\left(-\frac{2}{\sqrt{3}} + \Delta w\right)^2 + 2\left(\varepsilon - \frac{1}{u_2}\right) - \frac{2}{3}\left(\varepsilon^3 - \frac{1}{u_2^3}\right)} \quad (3.77)$$

on γ_2^- . Next, we write $u_2^{\text{out}} = 1 + \Delta u$ in (3.77), where Δu is assumed to be sufficiently small due to the fact that we stay close to the saddle-node equilibrium at $(u_2, w_2) = (1, 0)$ in K_2 . Then, we solve the resulting expression for Δu to find three roots; two of these are complex conjugates and are hence irrelevant due to the real character of our problem. Expanding the third root, which is real independent of the value of Δw , in a series with respect to Δw and ε , we find

$$u_2^{\text{out}} = 1 + \frac{13\sqrt{3}}{9}\Delta w - \frac{13}{6}\varepsilon + \mathcal{O}(2) \quad (3.78)$$

to first order.

It remains to determine the leading-order asymptotics of the integral in (3.76). To that end, we expand the integrand therein as

$$\frac{1}{w_2(u_2)} = -\sqrt{\frac{3u_2^3}{2(u_2 - 1)^2(2u_2 + 1)}} + \mathcal{O}(\Delta w, \varepsilon), \quad (3.79)$$

which can be shown to be sufficient to the order of accuracy considered here. (The inclusion of higher-order terms in (3.76) would yield a refined bifurcation equation, and would hence allow us to take the expansion for $\lambda_*(\varepsilon)$ in (3.74) to higher order in ε .)

Combining (3.79) and (3.78) and noting that u_2^{in} only enters through higher-order terms in Δw , which are hence neglected, we finally obtain the expansion

$$\int_{u_2^{\text{in}}}^{u_2^{\text{out}}} \frac{1}{w_2(u_2)} du_2 = -\frac{\sqrt{2}}{2} \ln \Delta w + C + \mathcal{O}(\Delta w) \quad (3.80)$$

where C is a computable constant. (The above expansion reflects the fact that, as $\Delta w \rightarrow 0$, *i.e.*, as the point $(\sigma^{-1}, w_2^{\text{in}}, \xi_2^{\text{in}}, \varepsilon)$ tends to the stable manifold $\mathcal{W}_2^s(Q_2)$, the “time” required for reaching Δ_2 tends to infinity. Moreover, it agrees with the observation that expansions of solutions passing close to equilibria or slow manifolds of saddle type frequently involve logarithmic terms.)

Next, we substitute $\xi_2^{\text{in}} (= \xi_1^{\text{out}}) = -1 - \frac{\delta}{w_0} + \frac{\delta}{w_0^3} \varepsilon \ln \varepsilon + \mathcal{O}(\varepsilon)$ from (3.69) into (3.80) to obtain

$$\xi_2(u_2^{\text{out}}) = -1 - \frac{\delta}{w_0} - \frac{\sqrt{2}}{2} \delta \varepsilon \ln \Delta w + \frac{\delta}{w_0^3} \varepsilon \ln \varepsilon + \mathcal{O}(\varepsilon) \stackrel{!}{=} 0. \quad (3.81)$$

Shifting w_0 and δ to Δw and $\Delta \delta$ (cf. (3.75)) and solving (3.81) for $\Delta \delta$, we obtain the following bifurcation equation in $(\Delta w, \Delta \delta, \varepsilon)$

$$\Delta \delta = -\Delta w + \frac{2\sqrt{2}}{3} \varepsilon \ln \Delta w + \frac{\sqrt{3}}{2} \varepsilon \ln \varepsilon + \mathcal{O}(\varepsilon). \quad (3.82)$$

The last step consists in finding the Δw -value Δw_* at which the bifurcation equation in (3.82) attains its minimum, corresponding to the approximate location of the saddle-node bifurcation in (3.23), and in reverting to the original scalings. To that aim, we differentiate (3.82) and solve $\frac{d\Delta \delta}{d\Delta w} = 0$ to leading order, which yields $\Delta w_* = \frac{2\sqrt{2}}{3} \varepsilon$ (see Figure 3.16).

Substituting into (3.82), we hence obtain the corresponding value of $\Delta \delta_*$, which implies $\lambda_* = \frac{\varepsilon}{\delta_*^2} = \frac{\varepsilon}{\left(\frac{2}{\sqrt{3}} + \Delta \delta_*\right)^2}$, by Equation (3.75). Hence, we obtain the desired asymptotic expansion for λ_* , *viz.*

$$\lambda_*(\varepsilon) = \frac{3}{4} \varepsilon - \left(\sqrt{\frac{3}{2}} + \frac{9}{8} \right) \varepsilon^2 \ln \varepsilon + \mathcal{O}(\varepsilon^2), \quad (3.83)$$

as claimed. Finally, since

$$\left. \frac{d^2 \Delta \delta}{d(\Delta w)^2} \right|_{\Delta w = \Delta w_*} = -\frac{2\sqrt{2}}{3} \frac{\varepsilon}{(\Delta w_*)^2}$$

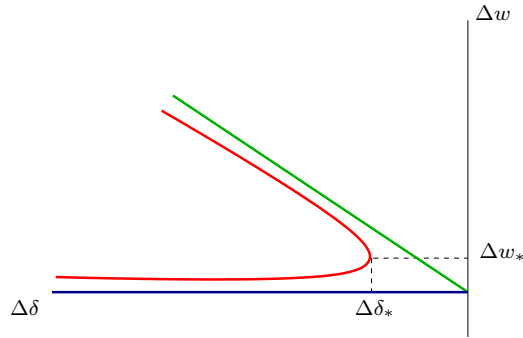
is negative, the function $\Delta \delta(\Delta w)$ is locally concave, which implies that the unfolding of solutions to Equation (3.23) for $|\lambda - \lambda_*|$ small is as claimed in the statement of the proposition (see Figure 3.16(a)).

The last part of the proof deals with the existence of solutions of the boundary value problem (3.23), (3.18) which limit on type II-solutions as $\varepsilon \rightarrow 0$ for the remaining values of λ

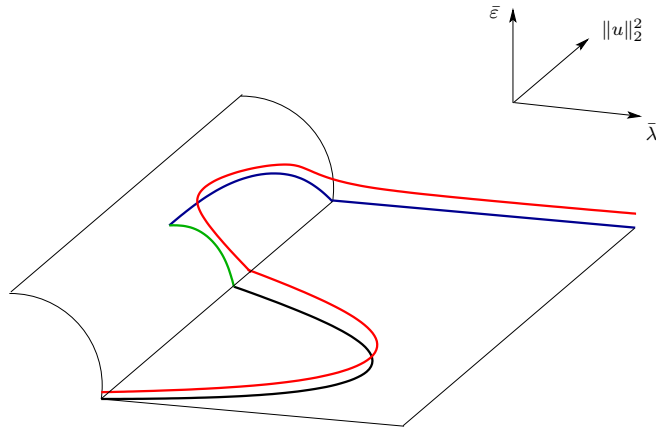
in \mathcal{R}_2 , *i.e.*, for $\delta \in \left(\frac{1}{\sqrt{\lambda_2}}, \delta_1\right)$. For this range, the existence of singular solutions of type II is ensured by Lemma 3.4.4. For singular solutions (*i.e.*, for $\varepsilon = 0$) we have transversality at $\xi_1 = 0$ with respect to the variation of the boundary values of w_1 at $\xi_1 = \mp 1$ around $\mp\delta$. Hence, these singular solutions perturb to solutions of the boundary value problem for $0 < \varepsilon \ll 1$. \square

Remark 16. The branch of solutions derived in the last part of the proof is described by the bifurcation equation (3.82) without the $\ln \Delta w$ term. These solutions in fact stay away from the saddle-node, which is responsible for the logarithmic term in Δw .

Remark 17. The above proof also implies that $\Delta\delta$ must be larger than $\mathcal{O}(\varepsilon)$. In fact, Lindsay's work shows that $\Delta\delta = \mathcal{O}(\varepsilon \ln \varepsilon)$.



(a) Local view.



(b) Global view.

Figure 3.16: Illustration of the saddle-node bifurcation in (3.23). The red curve corresponds to the case of $\varepsilon \neq 0$, while the singular limit of $\varepsilon = 0$ is represented in blue (type I), green (type II) and black (type III). The point of intersection of the two singular segments corresponds to the critical δ -value δ_* . A small neighbourhood of the point where the transition between the green and the blue curve occurs is treated in the first part of Proposition 3.4.5. The rest of the green curve up to an arbitrary small fixed distance from the intersection with the black curve is studied in the second part of Proposition 3.4.5. The transition between the green and the black segment is finally described in Section 3.4.3.

The asymptotic expansion for λ_* in (3.74) shows excellent agreement with the numerical values obtained using the continuation software package AUTO [18] (see Figure 3.17). In particular, the distance between the two curves is of higher order in ε , *i.e.*, $\mathcal{O}(\varepsilon^2)$, as postulated.

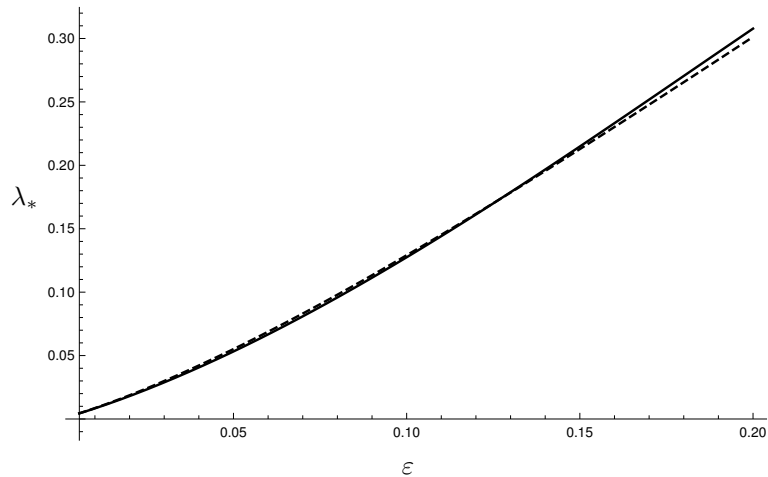


Figure 3.17: Comparison between the asymptotic expansion for $\lambda_*(\varepsilon)$ in (3.74) (continuous line) and numerical values obtained with AUTO (dashed line).

3.4.3 Region \mathcal{R}_3

It remains to analyze region \mathcal{R}_3 , which contains the bifurcation branch of solutions perturbing from type III-solutions corresponding to the non-regularized problem:

$$\begin{aligned} u'' &= \frac{\lambda}{u^2}, & x \in [-1, 1] \\ u(\pm 1) &= 1 \end{aligned} \tag{3.84}$$

Type III-solutions (cf. Definition 3.4.1) differ from type I-II solutions as they do not exhibit touchdown phenomena. Regularization affects them only weakly (regularly), the effect becoming slightly more pronounced as $\lambda \rightarrow 0$ (cf. Figure 3.18). Thus, most of the bifurcation curve contained in region \mathcal{R}_3 perturbs from \mathcal{B}_3 in a regular way and is hence easy to obtain. The limit $\lambda \rightarrow 0$, *i.e.*, the transition from \mathcal{R}_3 to \mathcal{R}_2 , needs to be treated more carefully.

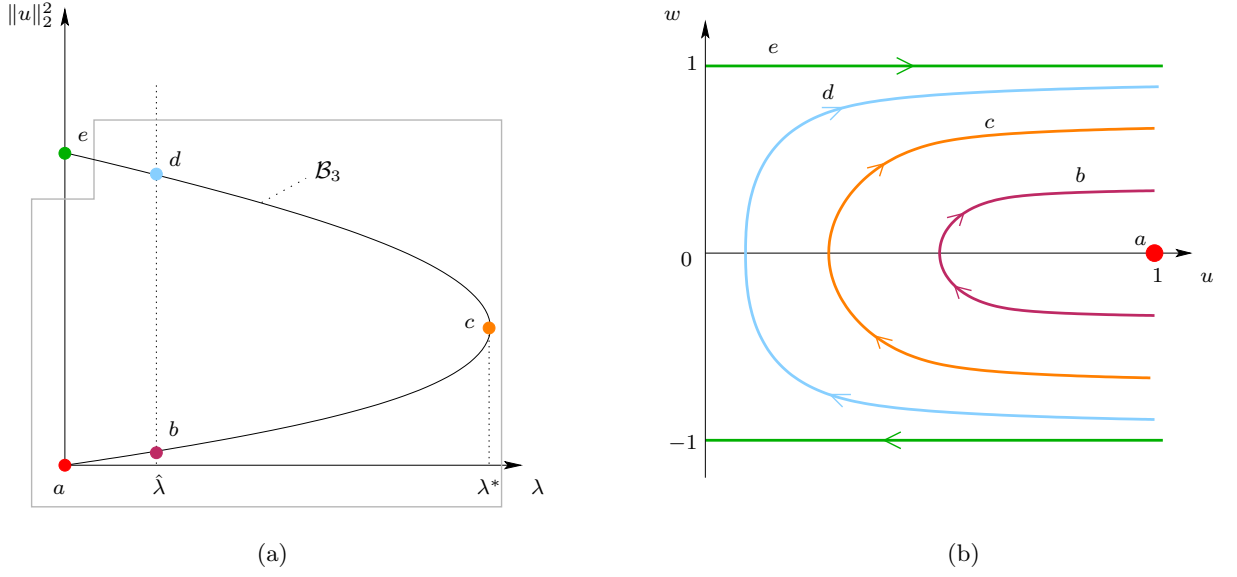


Figure 3.18: (a) Bifurcation branch \mathcal{B}_3 covered by region \mathcal{R}_3 for $\varepsilon > 0$ and (b) corresponding singular solutions in the original (u, w) -space. The green solution is of type II and corresponds to the limit $\lambda \rightarrow 0$. Recall that for $\varepsilon \rightarrow 0$ \mathcal{R}_3 approaches the line $\lambda = 0$ near the point labeled $e = (0, \frac{2}{3})$. Singular solutions corresponding to $\lambda > 0$ are of type III and do not exhibit touchdown phenomena. The orange solution at the fold point $\lambda = \lambda^*$ is the one where the two parts of the bifurcation branch \mathcal{B}_3 meet.

Type III-solutions are contained in the branch \mathcal{B}_3 in the limit $\delta = 0$ (see Figure 3.10). This case was not covered in region \mathcal{R}_2 , as the approach used there needed the assumption $\delta \geq \frac{1}{\sqrt{\lambda_2}}$. The limit $\delta \rightarrow 0$ leads to singular dynamics in chart K_1 , as the type II-solution (green) – corresponding to $w_1 = \mp\delta$ at $\xi_1 = \mp 1$ – collapses onto the line

$$\mathcal{M}_1^0 := \{(r_1, 0, \xi_1, 0) \mid r_1 \in \mathbb{R}^+, \xi_1 \in \mathbb{R}\} \quad (3.85)$$

(see Figure 3.4 and the upper panel of Figure 3.14). Clearly, \mathcal{M}_1^0 constitutes a line of non-hyperbolic equilibria for Equation (3.35) which corresponds to the manifold \mathcal{M}^0 in (3.20), after blow-down. This issue is related to the rescaling of w introduced in (3.21). That rescaling (which corresponded to “zooming out”) turned out to be particularly useful to carry out the analysis in regions \mathcal{R}_1 and \mathcal{R}_2 . However, it cannot provide a good description

of region \mathcal{R}_3 . To study \mathcal{R}_3 , we would have to perform another blow up involving δ , w_1 , and ε_1 in chart K_1 in order to basically undo this rescaling. It is much simpler to deal with the range of δ covered by \mathcal{R}_3 by returning to the original system without the w -rescaling (cf. (3.17)).

The main result of this section is the following:

Proposition 3.4.6. *There exists $\varepsilon_0 > 0$ sufficiently small such that in region \mathcal{R}_3 the boundary value problem (3.23), (3.18) has a unique curve of solutions for $\varepsilon < \varepsilon_0$. Outside of a fixed neighbourhood of the point $(0, \frac{2}{3})$ the curve smoothly converges for $\varepsilon \rightarrow 0$ to the curve \mathcal{B}_3 , along which solutions of the non-regularized boundary value problem exist. In the ε -dependent region overlapping with \mathcal{R}_2 the transition from solutions limiting on type III singular solutions to solutions limiting on type II singular solution occurs.*

Proof. The original system is

$$\begin{aligned} u' &= u^4 w, \\ w' &= \lambda(u^2 - \varepsilon^2), \\ \xi' &= u^4, \\ \varepsilon' &= 0. \end{aligned}$$

Because of Equation (3.22), we express $\varepsilon = \delta^2 \lambda$ and obtain the equivalent system

$$u' = u^4 w, \tag{3.86a}$$

$$w' = \lambda(u^2 - \delta^4 \lambda^2), \tag{3.86b}$$

$$\xi' = u^4, \tag{3.86c}$$

$$\delta' = 0. \tag{3.86d}$$

Here, the parameter δ plays the role of the small perturbation parameter. The range of δ corresponding to \mathcal{R}_3 is

$$\delta \in \left[0, \frac{1}{\sqrt{\lambda_3}}\right]$$

(cf. (3.40)). Working with λ and δ rather than with λ and ε turns out to be more convenient in this regime.

For $\delta = 0$ and $\lambda > 0$, the projection of the flow for System (3.86) is as in Figure 3.3. In

region \mathcal{R}_3 , however, we are also interested in covering a small neighbourhood of $\lambda = 0$, which gives again the singular dynamics shown in Figure 3.4. In (u, w) -space, the singular solution for $\lambda = 0$ consists of $[0, 1] \times \{-1\}$ and $[0, 1] \times \{1\}$, *i.e.*, the singular solution approaches the degenerate line of equilibria $(0, w)$ forward/backwards in x (see Figure 3.19).

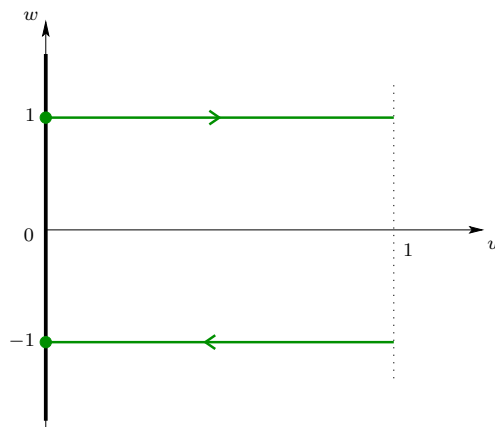


Figure 3.19: Singular solution of System (3.86) for $(\delta = 0, \lambda = 0)$ in (u, w) -space (in green).

This solution is of type II (cf. Figure 3.7(b)). The solid black line represents the degenerate line of equilibria $(0, w)$.

To analyze the dynamics close to this manifold, we have to introduce a blow up of $(u, \lambda) = (0, 0)$. For the blow-up involving λ we append the trivial equation $\lambda' = 0$ to (3.86):

$$u' = u^4 w, \tag{3.87a}$$

$$w' = \lambda(u^2 - \delta^4 \lambda^2), \tag{3.87b}$$

$$\xi' = u^4, \tag{3.87c}$$

$$\lambda' = 0, \tag{3.87d}$$

$$\delta' = 0. \tag{3.87e}$$

The blow-up is

$$u = r\bar{u}, \quad \lambda = r\bar{\lambda}, \tag{3.88}$$

where $(\bar{u}, \bar{\lambda}) \in S^1$, *i.e.*, $\bar{u}^2 + \bar{\lambda}^2 = 1$. We define the chart corresponding to $\bar{u} = 1$ as κ_1 . The

analysis in this chart turns out to be sufficient to prove Proposition 3.4.6. In chart κ_1 the blow-up transformation (3.88) reads

$$u = r_1, \quad \lambda = r_1 \lambda_1. \quad (3.89)$$

In chart κ_1 , System (3.87) is described by

$$r_1' = r_1 w, \quad (3.90a)$$

$$w' = \lambda_1(1 - \delta^4 \lambda_1^2), \quad (3.90b)$$

$$\xi' = r_1, \quad (3.90c)$$

$$\lambda_1' = -\lambda_1 w, \quad (3.90d)$$

$$\delta' = 0, \quad (3.90e)$$

where δ is the small regular perturbation parameter. We can analyze the existence of solutions of System (3.90) for every $\lambda \in [0, 1]$ using the shooting argument based on symmetry outlined in Section 3.2. To this aim, we consider a set of initial conditions at $(r_1, \xi) = (1, -1)$:

$$\mathcal{V}_\lambda = \{ (1, w_0, -1, \lambda, \delta) \mid w_0 \in I \}, \quad (3.91)$$

where I is a neighbourhood of $w = -1$. We remark that the initial value λ of λ_1 results from the fact that $\lambda = r_1 \lambda_1$ (cf. (3.89)) and the initial value of r_1 is 1. We can introduce w as the independent variable in System (3.90), whence

$$\frac{dr_1}{dw} = \frac{r_1 w}{\lambda_1(1 - \delta^4 \lambda_1^2)}, \quad (3.92a)$$

$$\frac{d\xi}{dw} = \frac{r_1}{\lambda_1(1 - \delta^4 \lambda_1^2)}, \quad (3.92b)$$

$$\frac{d\lambda_1}{dw} = -\frac{w}{1 - \delta^4 \lambda_1^2}, \quad (3.92c)$$

$$\frac{d\delta}{dw} = 0, \quad (3.92d)$$

with the initial conditions

$$r_1(w_0) = 1, \quad \xi(w_0) = -1, \quad \delta(w_0) = 0, \quad \lambda_1(w_0) = \lambda. \quad (3.93)$$

We follow \mathcal{V}_λ by the flow given by System (3.92), (3.93) up to the hyperplane $\{w = 0\}$ (see Figure 3.20). There, we obtain a point $(r_1^{\text{out}}, 0, \xi^{\text{out}}, \lambda_1^{\text{out}}, \delta)$ in $(r_1, w, \xi, \lambda_1, \delta)$ -space. Our

shooting argument implies that we have to solve the equation

$$\xi^{\text{out}}(w_0, \lambda, \delta) = 0. \quad (3.94)$$

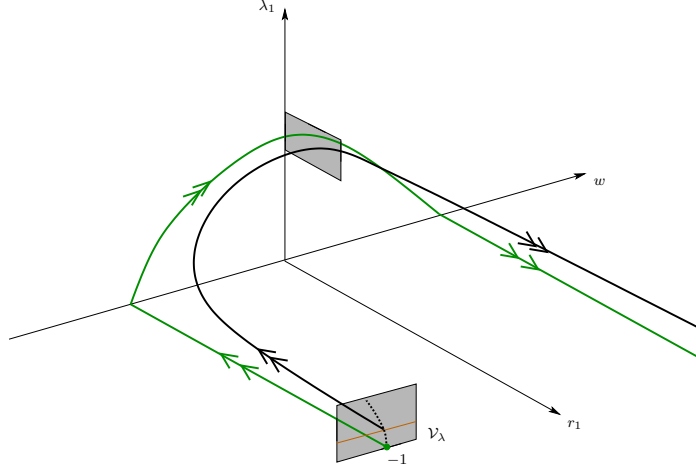


Figure 3.20: Dynamics of System (3.90) in (r_1, w, λ_1) -space. The gray section at $r_1 = 0$ corresponds to \mathcal{V}_λ (cf. (3.91)), which is flown up to $\{w = 0\}$. The green orbit corresponds to the singular solution for $\lambda = 0$, *i.e.*, a singular solution of type II, satisfying $w = -1$ at $\xi = -1$. The black orbit corresponds to a solution of System (3.90) with initial conditions in \mathcal{V}_λ for a fixed value of $\lambda > 0$ and $\delta = 0$. This solution is of type III. The dashed curve contained in \mathcal{V}_λ corresponds to the set of $w_0 = w_0(\lambda)$ solving Equation (3.96). This set is defined by Equation (3.97) for $\delta = 0$. The orange line indicates \mathcal{V}_λ for fixed $\lambda > 0$.

At this point we split \mathcal{R}_3 into two subregions and we apply two separate arguments to prove the existence of the bifurcation curve in region \mathcal{R}_3 . For $\lambda \geq \tilde{\lambda}$ with $\tilde{\lambda}$ fixed and positive and $\delta = 0$, Equations (3.92), (3.93) can be solved explicitly and solutions $w_0 = w_0(\lambda)$ of Equation (3.94) are proved to exist for $\lambda \leq \lambda^*$. At $\lambda = \lambda^*$, transversality breaks down, as Equation (3.94) does not admit a solution for $\lambda > \lambda^*$. The corresponding singular solutions are of type III (cf. Definition 3.4.1). Thanks to the regularity of Equation (3.94) with respect to δ , these $\delta = 0$ solutions perturb regularly to solutions of the boundary value problem for δ small and positive, in particular for $\delta \leq \frac{1}{\sqrt{\lambda_3}}$ with λ_3 large, cf. (3.40).

Individual solutions for λ close to λ^* do not perturb regularly. However, the structurally stable saddle-node bifurcation as a whole will persist as a regular perturbation giving rise to a slightly perturbed value $\lambda^*(\delta)$ for the perturbed saddle-node point. Since this regular perturbation is not our main concern we do not consider it in more detail.

The second subregion of \mathcal{R}_3 , which includes the overlap with region \mathcal{R}_2 , corresponds to a small neighbourhood of $(\lambda, \delta) = (0, 0)$ given by

$$(\lambda, \delta) \in \left[0, \tilde{\lambda}\right] \times \left[0, \frac{1}{\sqrt{\lambda_3}}\right]. \quad (3.95)$$

To study the bifurcation curve in this region, we solve Equations (3.92) with initial values (3.93) by expanding around $(w_0, \lambda, \delta) = (-1, 0, 0)$ and by using the fact that the equations can be solved explicitly for $\delta = 0$. A computation with Mathematica gives the following expanded form of Equation (3.94):

$$w_0 + 1 - (4 + 3w_0) \lambda \ln \lambda + \frac{1}{288} (1 + w_0) \delta^8 \ln \lambda + \text{h.o.t.} = 0. \quad (3.96)$$

Equation (3.96) shows again logarithmic terms due to a resonance phenomenon realized in chart κ_1 between the eigenvalues $-1, 0$ (double), and 1 of the linearization of Equation (3.90) about the steady state $(0, -1, -1, 0)$. We note that for $\lambda = 0$ Equation (3.96) becomes the trivial equation $w_0 + 1 = 0$, which is solved for $w_0 = -1$ independently from δ . These singular solutions correspond to type II solutions, shown as the part of the green curve in the blown-up bifurcation diagram in Figure 3.9 corresponding to $\bar{\varepsilon}$ small. In line with this observation, Equation (3.96) is identical to Equation (3.81) up to $\mathcal{O}(\delta^2\lambda)$ terms after the rescaling of w in (3.21). For $\delta = 0$ and $\lambda > 0$, on the other hand, we match with the branch obtained in the part of region \mathcal{R}_3 corresponding to $\lambda \geq \tilde{\lambda}$.

Solving Equation (3.96) for w_0 gives

$$w_0 = -1 + \lambda \ln \lambda + \lambda \mathcal{O}(\delta^8) + \mathcal{O}(\lambda^2). \quad (3.97)$$

This equation is regular in δ , as expected.

The results obtained in these two subregions prove existence and uniqueness of a curve of solutions of the boundary value problem (3.23), (3.18) in \mathcal{R}_3 as stated in Proposition 3.4.6.

Region \mathcal{R}_3 in (λ, δ) -space corresponds to

$$[0, 1] \times \left[0, \frac{1}{\sqrt{\lambda_3}}\right] \setminus [0, \varepsilon\lambda_3] \times \left[\frac{1}{\sqrt{\lambda_2}}, \frac{1}{\sqrt{\lambda_3}}\right]. \quad (3.98)$$

In (λ, δ) -space, \mathcal{R}_2 covers the area

$$[0, \varepsilon\lambda_2] \times \left[\frac{1}{\sqrt{\lambda_2}}, \delta_1 \right], \quad (3.99)$$

where $\delta_1 < \frac{2}{\sqrt{3}}$ is defined in Proposition 3.4.2.

Hence, in this space regions \mathcal{R}_3 and \mathcal{R}_2 overlap in the rectangle

$$[\varepsilon\lambda_3, \varepsilon\lambda_2] \times \left[\frac{1}{\sqrt{\lambda_2}}, \frac{1}{\sqrt{\lambda_3}} \right] \quad (3.100)$$

(see Figure 3.21), which is the area where the transition between the two regions occurs.

This finishes the proof of Proposition 3.4.6. \square

Theorem 3.1.1 is hence proved.

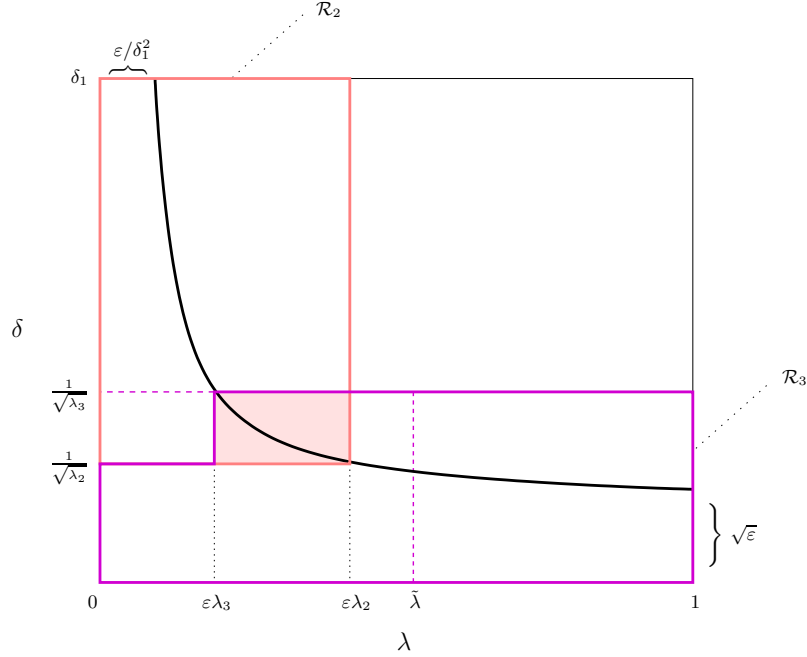


Figure 3.21: Regions \mathcal{R}_2 (pink) and \mathcal{R}_3 (magenta) in (λ, δ) parameter space (cf. (3.98) and (3.99)). The dashed vertical magenta line at $\lambda = \tilde{\lambda}$ delimits the two subregions considered in the proof of Proposition 3.4.6. The dashed horizontal magenta line at $\delta = \frac{1}{\sqrt{\lambda_3}}$ indicates that the argument applied in the second part of the proof of Proposition 3.4.6 is valid in the whole rectangle in (3.95), but region \mathcal{R}_3 excludes the area $[0, \varepsilon\lambda_3] \times \left[\frac{1}{\sqrt{\lambda_2}}, \frac{1}{\sqrt{\lambda_3}}\right]$ by construction (cf. (3.40)). Regions \mathcal{R}_2 and \mathcal{R}_3 overlap in the light pink shaded rectangle given by (3.100). The black curve corresponds to $\delta^2\lambda = \varepsilon$, for given $0 < \varepsilon \ll 1$.

3.5 Logarithmic switchbacks

In Lindsay’s work [54], logarithmic terms in ε , as well as fractional powers of ε , arise in the asymptotic expansions of solutions to Equation (3.5) as “switchback” terms that need to be included during matching in order to ensure the consistency of these expansions [56]. In this section, we provide a geometric interpretation of these logarithmic terms, hence establishing a connection between our dynamical systems approach and the method of matched asymptotic expansions. That connection has already been observed in various

classical singular perturbation problems, such as in Lagerstrom's model equation for low Reynolds number flow [49, 48, 67, 68] and in the Evans function for degenerate shock waves [70]. As described more generally in [66], a geometric singular perturbation analysis can show how the occurrence of these terms is caused by a resonance phenomenon in the blown-up vector field.

3.5.1 Dynamics in chart K_1

The occurrence of logarithmic switchback is necessarily studied in chart K_1 , as the small parameter ε has to appear as a dynamic variable for resonances to be possible between eigenvalues of the linearization about an appropriately chosen steady state, namely P_1^\mp (cf. Equation (3.60)). Hence, we reiterate the definition of the corresponding vector field in that chart, cf. Equation (3.35):

$$\begin{aligned} r_1' &= r_1 w_1, \\ w_1' &= \varepsilon_1(1 - \varepsilon_1^2), \\ \xi_1' &= \delta r_1, \\ \varepsilon_1' &= -\varepsilon_1 w_1. \end{aligned}$$

In particular, we intend to describe the transition under the flow of (3.35) past the resonant saddle points at P_1^\mp . We recall that the ξ_1 -value in the definition of $P_1^\mp = (0, \mp \frac{2}{\sqrt{3}}, \xi_1^\mp, 0)$ is $\xi_1^\mp = \pm \frac{\sqrt{3}}{2} \delta \mp 1$ (cf. Equation (3.60)). Finally, we emphasize that, due to the symmetry properties of the corresponding vector field, it again suffices to restrict to the transition past P_1^- only.

Normal form transformation

In a first step, we perform a sequence of near-identity transformations in a neighbourhood of P_1^- that will allow us to derive the normal form for Equation (3.35). To that end, we shift P_1^- to the origin, introducing the new variables \tilde{w}_1 and $\tilde{\xi}_1$ via $w_1 = -\frac{2}{\sqrt{3}} + \tilde{w}_1$ and $\xi_1 = \xi_1^- + \tilde{\xi}_1$. Then, we divide out a positive factor of $\frac{2}{\sqrt{3}} - \tilde{w}_1 (= -w_1)$ from the right-hand sides in the resulting equations, which corresponds to a transformation of the independent

variable that leaves the phase portrait unchanged:

$$r_1' = -r_1, \quad (3.101a)$$

$$\tilde{w}_1' = \frac{\varepsilon_1(1 - \varepsilon_1^2)}{\frac{2}{\sqrt{3}} - \tilde{w}_1}, \quad (3.101b)$$

$$\tilde{\xi}_1' = \delta \frac{r_1}{\frac{2}{\sqrt{3}} - \tilde{w}_1}, \quad (3.101c)$$

$$\varepsilon_1' = \varepsilon_1. \quad (3.101d)$$

The eigenvalues of the linearization of (3.101) about the origin are now -1 , 0 (double), and 1 , in accordance with the fact that there must be potential for resonance (for more details on the topic, the reader is referred to [66]).

Next, we expand

$$\left(\frac{2}{\sqrt{3}} - \tilde{w}_1\right)^{-1} = \frac{\sqrt{3}}{2} \left(1 - \frac{\sqrt{3}}{2} \tilde{w}_1\right)^{-1} = \frac{\sqrt{3}}{2} \left(1 + \frac{\sqrt{3}}{2} \tilde{w}_1 + \frac{3}{4} \tilde{w}_1^2 + \mathcal{O}(w_1^3)\right)$$

in (3.101b) and (3.101c), whence

$$\begin{aligned} \tilde{w}_1' &= \frac{\sqrt{3}}{2} \varepsilon_1 \left[1 + \frac{\sqrt{3}}{2} \tilde{w}_1 + \frac{3}{4} \tilde{w}_1^2 - \varepsilon_1^2\right] + \mathcal{O}(4), \\ \tilde{\xi}_1' &= \frac{\sqrt{3}}{2} \delta r_1 \left[1 + \frac{\sqrt{3}}{2} \tilde{w}_1 + \frac{3}{4} \tilde{w}_1^2\right] + \mathcal{O}(4). \end{aligned}$$

Since none of the terms in the \tilde{w}_1 -equation above are resonant, they can be removed by a sequence of near-identity transformations. For instance, setting $\tilde{w}_1 = \hat{w}_1 + \frac{\sqrt{3}}{2} \varepsilon_1$, we may eliminate the linear ε_1 -term from that equation, whence

$$\hat{w}_1' = \frac{3}{4} \varepsilon_1 \hat{w}_1 + \frac{3\sqrt{3}}{8} \varepsilon_1^2 + \frac{3\sqrt{3}}{8} \hat{w}_1^2 \varepsilon_1 + \frac{9}{8} \hat{w}_1 \varepsilon_1^2 - \frac{7\sqrt{3}}{32} \varepsilon_1^3 + \mathcal{O}(4).$$

Similarly, we can eliminate the linear r_1 -terms in the $\tilde{\xi}_1$ -equation by introducing

$$\tilde{\xi}_1 = \hat{\xi}_1 - \frac{\sqrt{3}}{2} \delta r_1.$$

The equation for $\hat{\xi}_1$ then reads

$$\hat{\xi}_1' = \frac{3}{4} \delta r_1 \hat{w}_1 + \frac{3\sqrt{3}}{8} \delta \varepsilon + \frac{3\sqrt{3}}{8} \delta r_1 \hat{w}_1^2 + \frac{9}{8} \delta \varepsilon \hat{w}_1 + \frac{9\sqrt{3}}{32} \delta \varepsilon \varepsilon_1 + \mathcal{O}(4).$$

The term $\frac{3\sqrt{3}}{8} \delta \varepsilon$ in the above equation is now resonant, as $(-1) + 1 = 0$ for the eigenvalues corresponding to the monomial $r_1 \varepsilon_1$ therein. Hence, that term cannot be eliminated in

general. (Here, we note that any factor of ε contributes a quadratic term to the asymptotics when considered in $(r_1, \hat{w}_1, \hat{\xi}_1, \varepsilon_1)$ -coordinates, as $\varepsilon = r_1 \varepsilon_1$.)

A final sequence of near-identity transformations allows us to eliminate any second-order terms from (3.101), as well. Specifically, introducing W_1 and Ξ_1 such that

$$\begin{aligned}\hat{w}_1 &= W_1 + \frac{3}{4}W_1\varepsilon_1 + \frac{3\sqrt{3}}{16}\varepsilon_1^2, \\ \hat{\xi}_1 &= \Xi_1 - \frac{3}{4}\delta r_1 W_1,\end{aligned}$$

we finally have

$$r_1' = -r_1, \tag{3.102a}$$

$$W_1' = \frac{3\sqrt{3}}{8}W_1^2\varepsilon_1 + \frac{27}{16}W_1\varepsilon_1^2 - \frac{5\sqrt{3}}{64}\varepsilon_1^3 + \mathcal{O}(4), \tag{3.102b}$$

$$\Xi_1' = \frac{3\sqrt{3}}{8}\delta\varepsilon + \frac{27}{16}\delta\varepsilon W_1 + \frac{3\sqrt{3}}{8}\delta r_1 W_1^2 + \frac{27\sqrt{3}}{64}\delta\varepsilon\varepsilon_1 + \mathcal{O}(4), \tag{3.102c}$$

$$\varepsilon_1' = \varepsilon_1. \tag{3.102d}$$

Remark 18. The truncation of Equation (3.102b) which is obtained by disregarding $\mathcal{O}(4)$ -terms is a standard Riccati equation [3] which can be solved in terms of special (Kummer) functions.

Expansion for ξ_1

In this subsection, we calculate an expansion for ξ_1 – or, rather, for the value ξ_1^{out} thereof in the section Σ_1^{out} , as defined in (3.32b). As indicated already in Section 3.4.1, that expansion is distinguished by the presence of logarithmic (“switchback”) terms that arise in the transition from Σ_1^{in} to Σ_1^{out} under the flow of Equation (3.35). In the process, we will refine the approximation for ξ_1^{out} that was derived in the proof of Propositions 3.4.2; recall Equation (3.70).

Lemma 3.5.1. *Consider the point $V_1^- = (1, w, -1, \varepsilon) \in \mathcal{V}_{1\varepsilon}^-$, with w in a small neighbourhood of $w_0^- = -\frac{2}{\sqrt{3}}$, and denote the orbit of Equation (3.35) initiating in V_1^- by γ_1 . Then, γ_1 intersects the section Σ_1^{out} in a point $(\frac{\varepsilon}{\sigma}, w_1^{\text{out}}, \xi_1^{\text{out}}, \delta)$, with*

$$\xi_1^{\text{out}} = -1 + \frac{\sqrt{3}}{2}\delta - \frac{3\sqrt{3}}{8}\delta\varepsilon \ln \varepsilon + \mathcal{O}(\delta\varepsilon). \tag{3.103}$$

Proof. Equations (3.102a) and (3.102d) can be solved explicitly for r_1 and ε_1 , which gives

$$r_1(\tilde{x}) = \rho e^{-\tilde{x}} \quad \text{and} \quad \varepsilon_1(\tilde{x}) = \frac{\varepsilon}{\rho} e^{\tilde{x}}; \quad (3.104)$$

here, \tilde{x} denotes the rescaled independent variable that was introduced in the derivation of (3.102). Hence, the transition ‘time’ \tilde{X} between the sections Σ_1^{in} and Σ_1^{out} under the flow of Equation (3.102) is given by

$$\tilde{X} = \ln \frac{\rho \delta}{\varepsilon}. \quad (3.105)$$

For sake of simplicity, we will henceforth only consider terms of up to order 2 in Equations (3.102b) and (3.102c), which gives

$$W_1' = 0 \quad \text{and} \quad \Xi_1' = \frac{3\sqrt{3}}{8} \delta \quad (3.106)$$

to that order. Hence, solving Equation (3.106) for W_1 and Ξ_1 in forward time gives

$$W_1 \equiv W_0 \quad \text{and} \quad \Xi_1 = \Xi_0 + \frac{3\sqrt{3}}{8} \delta \varepsilon \tilde{x}, \quad (3.107)$$

where $W_0 (= W_1(0))$ and $\Xi_0 (= \Xi_1(0))$ are constants that remain to be determined.

Undoing the above sequence of near-identity transformations – i.e., reverting to the ‘shifted’ variable $\tilde{\xi}_1$ – we obtain

$$\tilde{\xi}_1 = \Xi_1 - \frac{\sqrt{3}}{2} \delta r_1 - \frac{3}{4} \delta r_1 W_1 = \Xi_0 + \frac{3\sqrt{3}}{8} \delta \varepsilon \tilde{x} - \frac{\sqrt{3}}{2} \delta r_1 - \frac{3}{4} \delta r_1 W_1. \quad (3.108)$$

Hence, we also need to undo the transformation for W_1 . Solving Equation (3.102b) for W_1 , we find $W_1 \equiv \text{constant} = W_0$. Inverting the successive transformations for the variable w_1 , we have

$$w_1 = -\frac{2}{\sqrt{3}} + \left(1 + \frac{3}{4} \varepsilon_1\right) W_1 + \frac{\sqrt{3}}{2} \varepsilon_1 + \frac{3\sqrt{3}}{16} \varepsilon_1^2. \quad (3.109)$$

Since $w_1 \rightarrow -\frac{2}{\sqrt{3}}$ in the singular limit as $\varepsilon_1 \rightarrow 0$, it follows that $W_0 = 0$ to the order considered here. In fact, expanding the expression for $w_1(\varepsilon_1)$ in Equation (3.68) and retracing the above sequence of normal form transformations $w_1 \mapsto \tilde{w}_1 \mapsto \hat{w}_1 \mapsto W_1$, we may infer from (3.107) that $W_0 = \tilde{w}_0 + \mathcal{O}(\varepsilon)$, where we have written $w_0 = -\frac{2}{\sqrt{3}} + \tilde{w}_0$ in (3.68). As $\tilde{w}_0 = \mathcal{O}(\varepsilon)$, by the proof of Proposition 3.4.2, we may conclude that $W_1 (\equiv W_0) = \mathcal{O}(\varepsilon)$.

Next, substituting into (3.108) and noting that $\Xi_0 = \tilde{\xi}_0 + \frac{\sqrt{3}}{2}\delta\rho + \mathcal{O}(\delta\varepsilon)$ due to $r_1 = \rho$ in Σ_1^{in} , we obtain

$$\tilde{\xi}_1 = \tilde{\xi}_0 + \frac{\sqrt{3}}{2}\delta(\rho - r_1) + \frac{3\sqrt{3}}{8}\delta\varepsilon\tilde{x} + \mathcal{O}(\delta\varepsilon). \quad (3.110)$$

Reverting to the original variable $\xi = \xi_1^- + \tilde{\xi}_1$, we then conclude that in Σ_1^{out} ,

$$\xi_1^{\text{out}} = \xi_1(\tilde{X}) = \xi_0 + \frac{\sqrt{3}}{2}\delta\rho - \frac{3\sqrt{3}}{8}\delta\varepsilon\ln\varepsilon + \mathcal{O}(\delta\varepsilon). \quad (3.111)$$

Here, we emphasize that the error estimate in (3.111) is again due to the fact that $W_1 = \mathcal{O}(\varepsilon)$ throughout.

It remains to approximate ξ_0 . To that end, we consider Equation (3.101c), rewritten with r_1 as the independent variable: solving

$$\frac{d\tilde{\xi}_1}{dr_1} = \frac{d\xi_1}{dr_1} = -\frac{\delta}{\frac{2}{\sqrt{3}} - \tilde{w}_1} = -\frac{\sqrt{3}}{2}\delta[1 + \mathcal{O}(\tilde{w}_1)]$$

with $\xi_1(1) = -1$ and noting that $\tilde{w}_1 = \mathcal{O}(\varepsilon)$, by Equation (3.107), we find

$$\xi_1(r_1) = -1 - \frac{\sqrt{3}}{2}\delta(r_1 - 1) + \mathcal{O}(\delta\varepsilon)$$

and, hence, $\xi_0 = \xi_1(\rho) = -1 - \frac{\sqrt{3}}{2}\delta(\rho - 1) + \mathcal{O}(\delta\varepsilon)$ which, in combination with (3.111), yields Equation (3.103), as claimed. \square

Remark 19. The independence of Equation (3.101c), in combination with the structure of the above sequence of normal form transformations $\tilde{w}_1 \mapsto \hat{w}_1 \mapsto W_1$ – which depends on ε_1 only – implies that no resonances will occur in the corresponding expansion for w_1^{out} . In fact, such an expansion can immediately be derived from (3.109).

Remark 20. We emphasize that the results obtained in Lemma (3.5.1) perfectly agree with Lindsay's, as can be shown by converting the variables involved. The quantity ξ_1^{out} corresponds in fact to the point $-x_c$ in [54], where $\lambda_{0c} = \frac{3}{4}$ as $m = 4$ in our case:

$$-x_c = -1 + \varepsilon^{1/2}\bar{x}_c = -1 + \frac{\sqrt{3}}{2}\delta - \frac{3\sqrt{3}}{8}\sqrt{\frac{\varepsilon}{\lambda}}\varepsilon\ln\varepsilon + \mathcal{O}(\delta\varepsilon). \quad (3.112)$$

3.5.2 Dynamics in chart K_2

In this subsection, we continue the expansion for ξ_1^{out} in Equation (3.103) into chart K_2 . To that end, we recall the definition of the governing equations in that chart; cf. (3.37):

$$\begin{aligned} u_2' &= u_2^4 w_2, \\ w_2' &= u_2^2 - 1, \\ \xi_2' &= \delta r_2 u_2^4, \\ r_2' &= 0. \end{aligned}$$

Our aim is to show that the expansion in (3.103), when interpreted as an initial condition for (3.37) in Σ_1^{out} , can be matched to a corresponding expansion that is valid throughout chart K_2 . By symmetry, it again suffices to restrict to the scenario considered before, with negative w_2 .

Expansion for ξ_2

We make the following Ansatz for the variable ξ_2 , which is now interpreted as a function $\xi_2(u_2, r_2) \equiv \xi_2(u_2, w_2(u_2), r_2)$ of (u_2, r_2) . (Here, we recall the explicit expression

$$w_2(u_2) = -\sqrt{\frac{4}{3} - \frac{2}{u_2} + \frac{2}{3u_2^3}}$$

for w_2 quoted in Equation (3.47), which corresponds to the stable foliation $\mathcal{F}_2^s(Q_2)$ of the slow manifold $\mathcal{S}_2^{r_2}$ in chart K_2 .) We postulate the following series expansion for ξ_2 in powers of r_2 , with u_2 -dependent coefficients $a_j(u_2)$:

$$\xi_2(u_2, r_2) = \sum_{j=0}^{\infty} a_j(u_2) r_2^j. \quad (3.113)$$

The coefficients a_j can be determined as solution of a recursive system of ordinary differential equations, as follows: rewriting (3.37c) with u_2 as the independent variable, substituting for $w_2(u_2)$, by (3.47), and expanding about $u_2 = \infty$, we find

$$\begin{aligned} \frac{d\xi_2}{du_2} &= \sum_{j=0}^{\infty} \frac{da_j}{du_2} r_2^j \stackrel{!}{=} \delta r_2 \frac{1}{w_2(u_2)} = -\delta r_2 \frac{1}{\sqrt{\frac{4}{3} - \frac{2}{u_2} + \frac{2}{3u_2^3}}} \\ &= -\delta r_2 \left[\frac{\sqrt{3}}{2} + \frac{3\sqrt{3}}{8} \frac{1}{u_2} + \frac{19\sqrt{3}}{64} \frac{1}{u_2^2} + \mathcal{O}(u_2^{-3}) \right]. \end{aligned}$$

Comparing coefficients of like powers in r_2 , we find that, to the order in u_2 considered here,

$$\mathcal{O}(r_2): \quad \frac{da_1}{du_2} = -\delta \left[\frac{\sqrt{3}}{2} + \frac{3\sqrt{3}}{8} \frac{1}{u_2} + \frac{19\sqrt{3}}{64} \frac{1}{u_2^2} + \mathcal{O}(u_2^{-3}) \right], \quad (3.114a)$$

$$\mathcal{O}(r_2^j), \quad j \neq 1: \quad \frac{da_j}{du_2} = 0 \quad (3.114b)$$

Solving, we obtain

$$a_1(u_2) = A_1 - \frac{\sqrt{3}}{2} \delta u_2 - \frac{3\sqrt{3}}{8} \delta \ln u_2 + \frac{19\sqrt{3}}{64} \frac{\delta}{u_2} + \mathcal{O}(u_2^{-2}), \quad (3.115a)$$

$$a_j(u_2) = A_j \quad (j \neq 1), \quad (3.115b)$$

where A_j are coefficients that are to be determined by matching with the previously derived expansion for ξ_1^{out} . In sum, we find

$$\xi_2(u_2, \varepsilon) = A_1 \varepsilon - \frac{\sqrt{3}}{2} \delta \varepsilon u_2 - \frac{3\sqrt{3}}{8} \delta \varepsilon \ln u_2 + \frac{19\sqrt{3}}{64} \frac{\delta \varepsilon}{u_2} + \sum_{\substack{j=0 \\ j \neq 1}}^{\infty} A_j \varepsilon^j. \quad (3.116)$$

In particular, evaluating (3.116) in Σ_2^{in} , i.e., at $u_2 = \sigma^{-1}$, we obtain

$$\xi_2^{\text{in}} = A_0 + A_1 \varepsilon - \frac{\sqrt{3}}{2} \frac{\delta \varepsilon}{\sigma} + \frac{3\sqrt{3}}{8} \delta \varepsilon \ln \sigma + \frac{19\sqrt{3}}{64} \delta \varepsilon \sigma + \sum_{j=2}^{\infty} A_j \varepsilon^j. \quad (3.117)$$

A direct comparison of the above expression with (3.103) yields

$$\begin{aligned} A_0 &= -1 + \frac{\sqrt{3}}{2} \delta, \\ A_1 - \frac{\sqrt{3}}{2} \frac{\delta}{\sigma} + \frac{3\sqrt{3}}{8} \delta \ln \sigma + \frac{19\sqrt{3}}{64} \delta \sigma &= -\frac{3\sqrt{3}}{8} \delta \ln \varepsilon + \tilde{A}_1 \delta, \end{aligned}$$

where \tilde{A}_1 now cannot be determined to the order considered here. This in particular implies $A_1 = -\frac{3\sqrt{3}}{8} \delta \ln \varepsilon$.

The fact that A_1 in (3.117) has to contain an $\ln \varepsilon$ -term in order for that expansion to match the one in (3.103) is due to the resonances found in chart K_1 . The inclusion of such a term *a posteriori* is akin to the logarithmic switchback that is performed classically, in asymptotic matching. We emphasize that no logarithmic terms (in r_2) may appear in the series in (3.113), as that expansion is valid in chart K_2 , where no resonances occur, and that it must hence be regular in r_2 . A more comprehensive study of the phenomenon from

a geometric point of view would require us to transform Equation (3.113) to chart K_1 , whence

$$\xi_1(r_1, \varepsilon_1) = \sum_{j=0}^{\infty} a_j(\varepsilon_1^{-1})(r_1 \varepsilon_1)^j =: \sum_{j=0}^{\infty} \tilde{a}_j(\varepsilon_1) r_1^j, \quad \text{with } \tilde{a}_j(\varepsilon_1) = a_j(\varepsilon_1^{-1}) \varepsilon_1^j. \quad (3.118)$$

In a second step, and motivated by the fact that a_j can be seen to depend on ε_1 and $\ln \varepsilon_1$ when rewritten in the coordinates of K_1 , cf. (3.116), we would then rewrite (3.118) – considered as a double expansion in (r_1, ε_1) – as a series with respect to the basis $(\varepsilon_1, \ln \varepsilon_1)$, with r_1 -dependent coefficients b_j . Substitution into the governing equations in chart K_1 , as given in Equation (3.35), then yields a recursive system of ODEs for $\{b_j\}_{j=0}^{\infty}$ which can be solved to any desired order. Details can be found in [68], where an analogous procedure was performed in the context of the Lagerstrom model problem for low-Reynolds-number flow.

3.6 Discussion and Outlook

In this chapter, we have investigated stationary solutions of a second-order parabolic PDE that arises in the modelling of Micro-Electro Mechanical Systems (MEMS). In particular, we have unveiled the complex structure of the bifurcation diagram that arises after regularization of the underlying canonical model under the assumption that the regularizing parameter is sufficiently small; recall Figure 3.2(a). In the process, we have proven that the additional branch which appears in the bifurcation diagram of the regularized model derives from a singular structure that had not, to date, been elucidated in the relevant literature [54]. Applying tools from dynamical systems theory and, in particular, geometric singular perturbation theory and the blow-up technique, we have considered separately three principal regions in the bifurcation diagram; cf. Figure 3.8. Combination of the resulting local asymptotics has then allowed us to describe in detail the global dynamics of the boundary value problem defined by Equations (3.23), (3.18).

One of the most interesting features of the regularized model considered here is the presence of a highly singular saddle-node bifurcation point. While Lindsay *et al.* [54] were able to derive a formal leading-order asymptotic expansion in the regularization parameter

at that point, the coefficients therein had remained undetermined thus far. Our approach, on the other hand, allows us to obtain the fold point as the minimum in an appropriately defined bifurcation equation and then explicitly determine the coefficients in the expansion. As confirmation, a comparison with the numerical data obtained with the continuation package AUTO has been performed, showing very good agreement with our analytical results.

Finally, the asymptotic expansion proved in [54] for the solutions to the steady-state problem exhibits logarithmic switchback terms. While there their presence was justified by means of a matching procedure, here we have been able to reveal their nature as a natural consequence of a resonance phenomenon in the eigenvalues of chart K_1 .

The procedure applied here to the second-order model could be similarly applied to the fourth-order model arising in the beam case (3.4) and comprehensively studied in [54, 55, 52]. Our aim in the future is to establish analogous results in this case as well, as the singular nature of the bifurcation diagram presents some similarities, while new features can be again possibly enlightened by means of geometric singular perturbation theory and the blow up method.

Bibliography

- [1] R. Abeyaratne, K. Bhattacharya, and J.K. Knowles. Strain-energy functions with multiple local minima: modeling phase transformations using finite thermoelasticity. In *Nonlinear elasticity: theory and applications*, volume 283 of *London Math. Soc. Lecture Note Ser.*, pages 433–490. Cambridge Univ. Press, Cambridge, 2001.
- [2] R. Abeyaratne and J.K. Knowles. *Evolution of phase transitions: a continuum theory*. Cambridge University Press, 2006.
- [3] M. Abramowitz and I.A. Stegun. *Handbook of mathematical functions: with formulas, graphs, and mathematical tables*, volume 55. Courier Corporation, 1964.
- [4] M.J. Álvarez, A. Ferragut, and X. Jarque. A survey on the blow up technique. *International Journal of Bifurcation and Chaos*, 21(11):3103–3118, 2011.
- [5] J.M. Ball. Mathematical models of martensitic microstructure. *Materials Science and Engineering: A*, 378(1):61–69, 2004.
- [6] J.M. Ball and R.D. James. Fine phase mixtures as minimizers of energy. *Arch. Rational Mech. Anal.*, 100(1):13–52, 1987.
- [7] K. Bhattacharya. Comparison of the geometrically nonlinear and linear theories of martensitic transformation. *Continuum Mechanics and Thermodynamics*, 5(3):205–242, 1993.
- [8] K. Bhattacharya. *Microstructure of martensite: why it forms and how it gives rise to the shape-memory effect*, volume 2. Oxford University Press, 2003.

- [9] P. Bonckaert, P. De Maesschalck, and F. Dumortier. Well adapted normal linearization in singular perturbation problems. *J. Dynam. Differential Equations*, 23(1):115–139, 2011.
- [10] M. Brunella and M. Miari. Topological equivalence of a plane vector field with its principal part defined through Newton polyhedra. *J. Differential Equations*, 85(2):338–366, 1990.
- [11] A.D. Bruno. *Local methods in nonlinear differential equations*. Springer Series in Soviet Mathematics. Springer-Verlag, Berlin, 1989. Part I. The local method of nonlinear analysis of differential equations. Part II. The sets of analyticity of a normalizing transformation, Translated from the Russian by William Hovingh and Courtney S. Coleman, With an introduction by Stephen Wiggins.
- [12] P. Carter and B. Sandstede. Fast pulses with oscillatory tails in the FitzHugh-Nagumo system. *SIAM J. Math. Anal.*, 47(5):3393–3441, 2015.
- [13] A.R. Champneys, V. Kirk, E. Knobloch, B.E. Oldeman, and J. Sneyd. When Shil’nikov meets Hopf in excitable systems. *SIAM J. Appl. Dyn. Syst.*, 6(4):663–693, 2007.
- [14] B. Dacorogna. *Introduction to the calculus of variations*. Imperial College Press, London, third edition, 2015.
- [15] M. Desroches, T.J. Kaper, and M. Krupa. Mixed-mode bursting oscillations: dynamics created by a slow passage through spike-adding canard explosion in a square-wave burster. 23:046106, 2013.
- [16] M. Desroches, B. Krauskopf, and H.M. Osinga. Numerical continuation of canard orbits in slow-fast dynamical systems. 23(3):739–765, 2010.
- [17] N. Doble and D.R. Williams. The application of MEMS technology for adaptive optics in vision science. *IEEE Journal of Selected Topics in Quantum Electronics*, 10(3):629–635, 2004.

- [18] E. Doedel. AUTO: a program for the automatic bifurcation analysis of autonomous systems. In *Proceedings of the Tenth Manitoba Conference on Numerical Mathematics and Computing, Vol. I (Winnipeg, Man., 1980)*, volume 30, pages 265–284, 1981.
- [19] G. Dolzmann. *Variational methods for crystalline microstructure-analysis and computation*, volume 1803. Springer Science & Business Media, 2003.
- [20] F. Dumortier. Techniques in the theory of local bifurcations: Blow-up, normal forms, nilpotent bifurcations, singular perturbations. In *Bifurcations and periodic orbits of vector fields*, pages 19–73. Springer, 1993.
- [21] F. Dumortier and R. Roussarie. *Canard Cycles and Center Manifolds*, volume 121 of *Memoirs Amer. Math. Soc.* 1996.
- [22] N. Fenichel. Geometric singular perturbation theory for ordinary differential equations. *J. Differential Equations*, 31(1):53–98, 1979.
- [23] R. FitzHugh. Mathematical models of threshold phenomena in the nerve membrane. *The bulletin of mathematical biophysics*, 17(4):257–278, 1955.
- [24] V. Gelfreich and L. Lerman. Almost invariant elliptic manifold in a singularly perturbed Hamiltonian system. *Nonlinearity*, 15(2):447–457, 2002.
- [25] A. Giuliani and S. Müller. Striped periodic minimizers of a two-dimensional model for martensitic phase transitions. *Comm. Math. Phys.*, 309(2):313–339, 2012.
- [26] M. Grinfeld and G.J. Lord. Bifurcations in the regularized ericksen bar model. *Journal of Elasticity*, 90(2):161–173, 2008.
- [27] J. Guckenheimer and C. Kuehn. Computing slow manifolds of saddle type. *SIAM J. Appl. Dyn. Syst.*, 8(3):854–879, 2009.
- [28] J. Guckenheimer and C. Kuehn. Homoclinic orbits of the fitzhugh-nagumo equation: The singular limit. *DCDS-S*, 2(4):851–872, 2009.
- [29] J. Guckenheimer and C. Kuehn. Homoclinic orbits of the fitzhugh-nagumo equation: Bifurcations in the full system. *SIAM J. Appl. Dyn. Syst.*, 9:138–153, 2010.

- [30] J. Guckenheimer and D. LaMar. Periodic orbit continuation in multiple time scale systems. In *Understanding Complex Systems: Numerical continuation methods for dynamical systems*, pages 253–267. 2007.
- [31] J. Guckenheimer and P. Meerkamp. Bifurcation analysis of singular Hopf bifurcation in \mathbb{R}^3 . *SIAM J. Appl. Dyn. Syst.*, 11(4):1325–1359, 2012.
- [32] Y. Guo, Z. Pan, and M.J. Ward. Touchdown and pull-in voltage behavior of a MEMS device with varying dielectric properties. *SIAM Journal on Applied Mathematics*, 66(1):309–338, 2005.
- [33] T.J. Healey and U. Miller. Two-phase equilibria in the anti-plane shear of an elastic solid with interfacial effects via global bifurcation. In *Proceedings of the Royal Society of London A: Mathematical, Physical and Engineering Sciences*, volume 463, pages 1117–1134. The Royal Society, 2007.
- [34] B.D. Iverson and S.V. Garimella. Recent advances in microscale pumping technologies: a review and evaluation. *Microfluidics and Nanofluidics*, 5(2):145–174, 2008.
- [35] C.K.R.T. Jones. Geometric singular perturbation theory. In *Dynamical systems (Montecatini Terme, 1994)*, volume 1609 of *Lecture Notes in Math.*, pages 44–118. Springer, Berlin, 1995.
- [36] C.K.R.T. Jones and N. Kopell. Tracking invariant manifolds with differential forms in singularly perturbed systems. *J. Differential Equations*, 108(1):64–88, 1994.
- [37] C.K.R.T. Jones, N. Kopell, and R. Langer. Construction of the FitzHugh-Nagumo pulse using differential forms. In *Multiple-Time-Scale Dynamical Systems*, pages 101–113. Springer, 2001.
- [38] A.G. Khachaturyan. *Theory of structural transformations in solids*. Courier Corporation, 2013.
- [39] A.G. Khachaturyan and G. Shatalov. Theory of macroscopic periodicity for a phase transition in the solid state. *Soviet Phys. JETP*, 29(3):557–561, 1969.

- [40] R.V. Kohn and S. Müller. Surface energy and microstructure in coherent phase transitions. *Comm. Pure Appl. Math.*, 47(4):405–435, 1994.
- [41] I. Kosiuk and P. Szmolyan. Scaling in singular perturbation problems: blowing-up a relaxation oscillator. *SIAM J. Appl. Dyn. Syst.*, 10(4):1307–1343, 2011.
- [42] K.U. Kristiansen. Computation of saddle-type slow manifolds using iterative methods. *SIAM J. Appl. Dyn. Syst.*, 14(2):1189–1227, 2015.
- [43] M. Krupa, B. Sandstede, and P. Szmolyan. Fast and slow waves in the FitzHugh-Nagumo equation. *J. Differential Equat.*, 133:49–97, 1997.
- [44] M. Krupa and P. Szmolyan. Extending geometric singular perturbation theory to nonhyperbolic points—fold and canard points in two dimensions. *SIAM journal on mathematical analysis*, 33(2):286–314, 2001.
- [45] M. Krupa and P. Szmolyan. Geometric analysis of the singularly perturbed planar fold. In *Multiple-time-scale dynamical systems (Minneapolis, MN, 1997)*, volume 122 of *IMA Vol. Math. Appl.*, pages 89–116. Springer, New York, 2001.
- [46] C. Kuehn. *Multiple time scale dynamics*, volume 191 of *Applied Mathematical Sciences*. Springer, Cham, 2015.
- [47] C. Kuehn and P. Szmolyan. Multiscale geometry of the Olsen model and non-classical relaxation oscillations. *J. Nonlinear Sci.*, 25(3):583–629, 2015.
- [48] P.A. Lagerstrom. *Matched asymptotic expansions: ideas and techniques*, volume 76. Springer Science & Business Media, 1988.
- [49] P.A. Lagerstrom and D.A. Reinelt. Note on logarithmic switchback terms in regular and singular perturbation expansions. *SIAM Journal on Applied Mathematics*, 44(3):451–462, 1984.
- [50] F. Lin and Y. Yang. Nonlinear non-local elliptic equation modelling electrostatic actuation. In *Proceedings of the Royal Society of London A: Mathematical, Physical and Engineering Sciences*, volume 463, pages 1323–1337. The Royal Society, 2007.

- [51] A.E. Lindsay. An asymptotic study of blow up multiplicity in fourth order parabolic partial differential equations. *Discrete & Continuous Dynamical Systems-Series B*, 19(1), 2014.
- [52] A.E. Lindsay. Regularized model of post-touchdown configurations in electrostatic MEMS: bistability analysis. *Journal of Engineering Mathematics*, 99(1):65–77, 2016.
- [53] A.E. Lindsay and J. Lega. Multiple quenching solutions of a fourth order parabolic PDE with a singular nonlinearity modeling a MEMS capacitor. *SIAM Journal on Applied Mathematics*, 72(3):935–958, 2012.
- [54] A.E. Lindsay, J. Lega, and K.B. Glasner. Regularized model of post-touchdown configurations in electrostatic MEMS: equilibrium analysis. *Physica D: Nonlinear Phenomena*, 280:95–108, 2014.
- [55] A.E. Lindsay, J. Lega, and K.B. Glasner. Regularized model of post-touchdown configurations in electrostatic MEMS: interface dynamics. *IMA Journal of Applied Mathematics*, page hxv011, 2015.
- [56] A.E. Lindsay and M.J. Ward. Asymptotics of some nonlinear eigenvalue problems modelling a MEMS capacitor. Part II: multiple solutions and singular asymptotics. *European Journal of Applied Mathematics*, 22(02):83–123, 2011.
- [57] A.E. Lindsay, M.J. Ward, et al. Asymptotics of some nonlinear eigenvalue problems for a MEMS capacitor. Part I: Fold point asymptotics. *Methods Appl. Anal*, 15(3):297–325, 2008.
- [58] S. Müller. Singular perturbations as a selection criterion for periodic minimizing sequences. *Calc. Var. Partial Differential Equations*, 1(2):169–204, 1993.
- [59] S. Müller. Variational models for microstructure and phase transitions. In *Calculus of variations and geometric evolution problems (Cetraro, 1996)*, volume 1713 of *Lecture Notes in Math.*, pages 85–210. Springer, Berlin, 1999.
- [60] J. Nagumo, S. Arimoto, and S. Yoshizawa. An active pulse transmission line simulating nerve axon. *Proceedings of the IRE*, 50(10):2061–2070, 1962.

- [61] D. Panazzolo. Resolution of singularities of real-analytic vector fields in dimension three. *Acta Math.*, 197(2):167–289, 2006.
- [62] P. Pedregal. *Variational methods in nonlinear elasticity*. Society for Industrial and Applied Mathematics (SIAM), Philadelphia, PA, 2000.
- [63] J.A. Pelesko. Mathematical modeling of electrostatic MEMS with tailored dielectric properties. *SIAM Journal on Applied Mathematics*, 62(3):888–908, 2002.
- [64] J.A. Pelesko and D.H. Bernstein. *Modeling Mems and Nems*. Chapman Hall and CRC press, 2002.
- [65] M. Pitteri and G. Zanzotto. *Continuum models for phase transitions and twinning in crystals*, volume 19 of *Applied Mathematics (Boca Raton)*. Chapman & Hall/CRC, Boca Raton, FL, 2003.
- [66] N. Popović. A geometric analysis of logarithmic switchback phenomena. In *Journal of Physics: Conference Series*, volume 22, page 164. IOP Publishing, 2005.
- [67] N. Popović and P. Szmolyan. A geometric analysis of the Lagerstrom model problem. *Journal of Differential Equations*, 199(2):290–325, 2004.
- [68] N. Popović and P. Szmolyan. Rigorous asymptotic expansions for Lagerstrom’s model equation—a geometric approach. *Nonlinear Analysis: Theory, Methods & Applications*, 59(4):531–565, 2004.
- [69] A.L. Roitburd. Martensitic transformation as a typical phase transformation in solids. *Solid state physics*, 33:317–390, 1978.
- [70] B. Sandstede and A. Scheel. Evans function and blow-up methods in critical eigenvalue problems. *Discrete and Continuous Dynamical Systems*, 10(2004), 2004.
- [71] S. Schecter. Exchange lemmas 1: Deng’s lemma. *Journal of Differential Equations*, 245(2):392–410, 2008.
- [72] S. Schecter. Exchange lemmas 2: General exchange lemma. *Journal of Differential Equations*, 245(2):411–441, 2008.

- [73] C. Soto-Treviño. A geometric method for periodic orbits in singularly-perturbed systems. In *Multiple-time-scale dynamical systems (Minneapolis, MN, 1997)*, volume 122 of *IMA Vol. Math. Appl.*, pages 141–202. Springer, New York, 2001.
- [74] A.N. Tikhonov. Systems of differential equations containing small parameters in the derivatives. *Matematicheskii sbornik*, 73(3):575–586, 1952.
- [75] L. Truskinovsky and G. Zanzotto. Finite-scale microstructures and metastability in one-dimensional elasticity. *Meccanica*, 30(5):577–589, 1995.
- [76] L. Truskinovsky and G. Zanzotto. Ericksen’s bar revisited: Energy wiggles. *Journal of the Mechanics and Physics of Solids*, 44(8):1371–1408, 1996.
- [77] NC. Tsai and CY. Sue. Review of MEMS-based drug delivery and dosing systems. *Sensors and Actuators A: Physical*, 134(2):555–564, 2007.
- [78] K.T. Tsaneva-Atanasova, H.M. Osinga, T. Riess, and A. Sherman. Full system bifurcation analysis of endocrine bursting models. *J. Theor. Biol.*, 264(4):1133–1146, 2010.
- [79] A. Vainchtein, T. Healey, P. Rosakis, and L. Truskinovsky. The role of the spinodal region in one-dimensional martensitic phase transitions. *Physica D: Nonlinear Phenomena*, 115(1):29–48, 1998.
- [80] S. Van Gils, M. Krupa, and P. Szmolyan. Asymptotic expansions using blow-up. *Zeitschrift für angewandte Mathematik und Physik ZAMP*, 56(3):369–397, 2005.
- [81] B. Watson, J. Friend, and L. Yeo. Piezoelectric ultrasonic micro/milli-scale actuators. *Sensors and Actuators A: Physical*, 152(2):219–233, 2009.
- [82] S. Wiggins. *Introduction to applied nonlinear dynamical systems and chaos*, volume 2. Springer Science & Business Media, 2003.
- [83] N.K. Yip. Structure of stable solutions of a one-dimensional variational problem. *ESAIM: Control, Optimisation and Calculus of Variations*, 12(4):721–751, 2006.

Curriculum Vitae

Annalisa Iuorio

Personal information

Date of Birth: 28.04.1989

Place of Birth: Naples, Italy

Citizenship: Italian

Work Address: TU Wien, Institute for Analysis and Scientific Computing (E101)
Wiedner Hauptstraße 8-10, 1040 Vienna, Austria

Scientific interests

Multiple time-scale systems; geometric singular perturbation theory; mathematical biology; PDE analysis; numerical simulations.

Employment

Since 03/2017: **TU Wien, Vienna, Austria**

Scientific Manager of the Doctoral School “*Dissipation and Dispersion in Nonlinear PDEs*”

01/2014–06/2017: **TU Wien, Vienna, Austria**

Project Assistant

Education

- 01/2014–01/2018 **TU Wien, Vienna, Austria**
(expected) Ph.D in Technical Mathematics
Supervisor: Prof. Peter Szmolyan
- 09/2016–12/2016 **University of Edinburgh, Edinburgh, UK**
Research collaboration with Prof. Nikola Popović
- 04/2011–05/2013 **University of Naples Federico II**
Laurea Magistrale (M.Sc.) in Mathematics
Supervisors: Prof. Addolorata Marasco, Prof. Francesco Gian-
nino
- 09/2007–03/2011 **University of Naples Federico II**
Laurea (B.Sc.) in Mathematics
Supervisor: Prof. Maria Longobardi
-

Publications (articles, proceedings, and preprints)

5. A. Iuorio, N. Popović and P. Szmolyan. *Singular perturbation analysis of a regularized MEMS model*. To submit, 2017.
4. A. Iuorio and S. Melchionna. *Long-time behavior of a nonlocal Cahn-Hilliard equation with reaction*. Submitted, preprint available at arXiv:1706.05996, 2017.
3. A. Iuorio, C. Kuehn, and P. Szmolyan. *Geometry and numerical continuation of multiscale orbits in a nonconvex variational problem*. Submitted, preprint available at arXiv:1701.08153v1, 2017.
2. A. Marasco, A. Iuorio, F. Carteni, G. Bonanomi, D.M. Tartakovsky, S. Mazzoleni, and F. Giannino. *Vegetation pattern formation due to interactions between water availability and toxicity in plant-soil feedback*. Bull. Math. Biol., 76(11):2866–2883, 2014.

Bibliography

1. A. Marasco, A. Iuorio, F. Cartenì, G. Bonanomi, F. Giannino, and S. Mazzoleni. *Water limitation and negative plant-soil feedback explain vegetation patterns along rainfall gradient*. *Procedia Environ. Sci.*, 19: 139–147, 2013
-

Additional information

- Languages: Italian (mother tongue), English, German.
- Main software skills: Microsoft Windows (ECDL License), L^AT_EX, Mathematica, Matlab, AUTO, Python.

Wien, am Datum

Name des Autors